DESIGN AND LIFE-CYCLE ASSESSMENT OF GABION BARRIERS FOR ROCKFALL MITIGATION USING NUMERICAL MODELING

Final Report

PROJECT SPR 831

Oregon Department of Transportation

DESIGN AND LIFE-CYCLE ASSESSMENT OF GABION BARRIERS FOR ROCKFALL MITIGATION USING NUMERICAL MODELING

Final Report

PROJECT SPR 831

by

Jeff Knowles, Ph.D., Postdoctoral Researcher
T. Matthew Evans, Ph.D., Professor
Oregon State University
101 Kearney Hall, Corvallis, OR 97331

Yifei Ma, Ph.D., Assistant Professor
Lawrence Technological University
21000 W 10 Mile Road, Southfield, MI 48075

for

Oregon Department of Transportation
Research Section
555 13th Street NE, Suite 1
Salem OR 97301

and

Federal Highway Administration
1200 New Jersey Avenue SE
Washington, DC 20590

June 2023

Technical Report Documentation Page

1. Report No. FHWA-OR-RD-23-11	2. Government Accession No.	3. Recipient's Catalog No.
4. Title and Subtitle Design and Life-Cycle Assessment of Gabion Barriers for Rockfall Mitigation using Numerical Modeling		5. Report Date June 2023 6. Performing Organization Code
7. Author(s) Jeff Knowles, Ph.D., 0000-0003-1453-9923 T. Matthew Evans, Ph.D., 0000-0002-8457-7602 Yifei Ma, Ph.D., 0000-0003-3902-6120		8. Performing Organization Report No.
9. Performing Organization Name and Address Oregon Department of Transportation Research Section 555 13th Street NE, Suite 1 Salem, OR 97301		10. Work Unit No. (TRAIS) 11. Contract or Grant No.
12. Sponsoring Agency Name and Address Oregon Dept. of Transportation Research Section 555 13th Street NE, Suite 1 Salem, OR 97301 Federal Highway Admin. 1200 New Jersey Avenue SE Washington, DC 20590		13. Type of Report and Period Covered Final Report 14. Sponsoring Agency Code
15. Supplementary Notes		

16. Abstract

A Graphical User Interface (GUI) software is developed to perform numerical simulations in which gabion barriers are impacted by boulders of various geometries and initial momentum values. The results generated from this tool are used to develop design standards and life-cycle analysis procedures.

17. Key Words Gabion, DEM, Geotechnical	18. Distribution Statement Copies available from NTIS, and online at www.oregon.gov/ODOT/TD/TP_RES/		
19. Security Classification (of this report) Unclassified	20. Security Classification (of this page) Unclassified	21. No. of Pages 85	22. Price

Technical Report Form DOT F 1700.7 (8-72) Reproduction of completed page authorized Printed on recycled paper

SI* (MODERN METRIC) CONVERSION FACTORS

APPROXIMATE CONVERSIONS TO SI UNITS

Symbol	When You Know	Multiply By	To Find	Symbol
		LENGTH		
in	inches	25.4	millimeters	mm
ft	feet	0.305	meters	m
yd	yards	0.914	meters	m
mi	miles	1.61	kilometers	km
		AREA		
in^2	square inches	645.2	millimeters squared	mm^2
ft^2	square feet	0.093	meters squared	m^2
yd^2	square yards	0.836	meters squared	m^2
ac	acres	0.405	hectares	ha
mi^2	square miles	2.59	kilometers squared	km^2
		VOLUME		
fl oz	fluid ounces	29.57	milliliters	ml
gal	gallons	3.785	liters	L
ft^3	cubic feet	0.028	meters cubed	m^3
yd^3	cubic yards	0.765	meters cubed	m^3
~NOTE: Volumes greater than 1000 L shall be shown in m^3.				
		MASS		
oz	ounces	28.35	grams	g
lb	pounds	0.454	kilograms	kg
T	short tons (2000 lb)	0.907	megagrams	Mg
		TEMPERATURE (exact)		
°F	Fahrenheit	(F-32)/1.8	Celsius	°C

APPROXIMATE CONVERSIONS FROM SI UNITS

Symbol	When You Know	Multiply By	To Find	Symbol
		LENGTH		
mm	millimeters	0.039	inches	in
m	meters	3.28	feet	ft
m	meters	1.09	yards	yd
km	kilometers	0.621	miles	mi
		AREA		
mm^2	millimeters squared	0.0016	square inches	in^2
m^2	meters squared	10.764	square feet	ft^2
m^2	meters squared	1.196	square yards	yd^2
ha	hectares	2.47	acres	ac
km^2	kilometers squared	0.386	square miles	mi^2
		VOLUME		
ml	milliliters	0.034	fluid ounces	fl oz
L	liters	0.264	gallons	gal
m^3	meters cubed	35.315	cubic feet	ft^3
m^3	meters cubed	1.308	cubic yards	yd^3
		MASS		
g	grams	0.035	ounces	oz
kg	kilograms	2.205	pounds	lb
Mg	megagrams	1.102	short tons (2000 lb)	T
		TEMPERATURE (exact)		
°C	Celsius	1.8C+32	Fahrenheit	°F

*SI is the symbol for the International System of Measurement

ACKNOWLEDGEMENTS

This project is sponsored by the Oregon Department of Transportation (ODOT). The funding opportunity is greatly acknowledged. The authors thank Kira Glover-Cutter, Heather Livingston and Curran Mohney from ODOT for their encouragement and support during the execution of the project. The authors also thank the Technical Advisory Committee (TAC) members – Sophie Brown, Thomas Braibish, Michael Zimmerman, Tim Pfeiffer, and Kira Glover-Cutter – for their guidance, assistance, experience, and professional comments during the preparation of this project report.

DISCLAIMER

TABLE OF CONTENTS

LIST OF TABLES

LIST OF FIGURES

1.0 INTRODUCTION

The following document provides a summary of numerical results and developments generated from a discrete element method (DEM) model developed using the open-source software *Yade* (Smilauer et al., 2015). A graphical user interface (GUI) has been programmed in Python to facilitate a simple and user-friendly environment for generating and running gabion barrier simulations. These two programs have been combined to create a new software, titled *Gabions and Boulder Impacts* (*GabBI*). Details for working with *GabBI* as an investigatory tool for damage prediction and life-cycle analysis are outlined in the User's Manual (Appendix A). Possible design standards are also presented with the goal of building barriers which are structurally sound, yet cost-effective. Therefore, the research plan was partitioned into incremental stages to determine the basic module unit size and design based on susceptibility to deformation, overturning, and wire rupture when subjected to a range of boulder impact scenarios. Through these experiments, another damage parameter considered was the radius of influence, which is a measure of how much a local impact event can affect the neighboring vicinity in terms of movement and wire rupture. By focusing on just a portion of the barrier domain, we were able to run more efficient simulations that capture the salient features of boulder impact without having to use a superfluous number of particles. A statistical component is also included in the analysis to assist in determining time intervals for maintenance and replacement. The limitations of the numerical model and ranges of acceptable values for stability and computational efficiency are discussed as well. The organization of the report is outlined in Table 1.1.

Table 1.1: Items Outlined in the Work Plan to be Included in Final Report.

Requirement	Section(s)
Parametric Study on Damage and Failure Patterns	Section 3.1 & 3.2
Effects of Rock Shape and Number for various Energy Levels	Section 3.3
Life-cycle analysis of gabion barrier (statistical + GabBI coupled approach)	Section 4
Possible design guidelines for gabion barriers	Section 5.3
User's Manual for developed numerical software GabBI	Appendix A

2.0 MODEL DETAILS

2.1 OVERVIEW

After receiving input from the user, *GabBI* creates a scene consisting of gabions and boulders in *Yade*. The gabions consist of a wire mesh basket filled with either angular or spherical rock. The boulders may also be either spherical or polyhedral in geometry. The material properties, constitutive contact laws, inertial properties, and strength parameters of the different components of the model are discussed below.

2.2 GABIONS

The wires of the gabion baskets are made from a cohesive frictional material, specifically the `cohFrictMat` Material Class in *Yade*, and are assigned an angle of interface friction of $\phi' = 35^o$ between the wire-rockfill and wire-ground interfaces. The wire is assigned a Poisson's ratio of $\nu = 0.3$, a density of $\rho = 624\ lb/ft^3$, and a Young's modulus of $E = 7.25 \times 10^6\ psi$ which are typical values for steel. The normal and shear cohesion, which dictate the rupture of the wire basket, are both set equal to $7.25 \times 10^5\ psi$, which are larger than typical values of the ultimate tensile strength for wire, but are necessary to reproduce results consistent with laboratory results reported in the literature (Ng et al., 2016; Peila et al., 2007) because of the cohesive-frictional model used for the wires (i.e., "real" steel is a pure Tresca material). A moment rotation law is also assigned to the wire so that bending may occur between adjacent pairs of grid nodes, as opposed to a rigid brittle behavior. The wire mesh for the gabions is available in a welded pattern (Figure 2.1) and a hexagonal pattern (Figure 2.2). Note that for the double-twisted hexagonal wire pattern that the double-twisted grid connections are assigned a stiffness of twice that of the singular wire to account for the extra cross-sectional area.

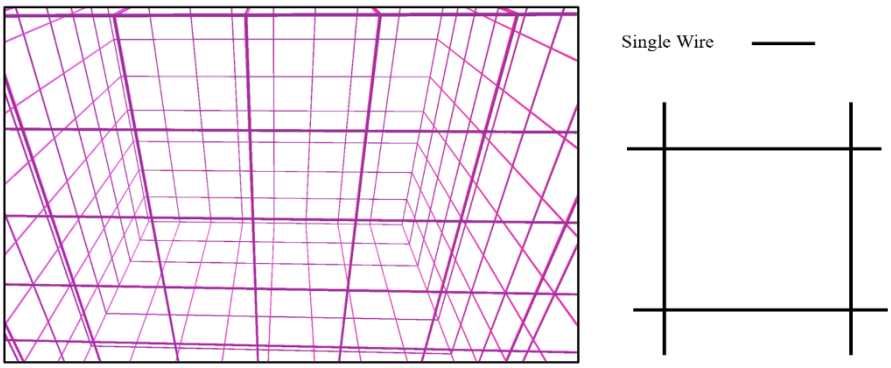

Figure 2.1: Welded wire pattern for gabion basket.

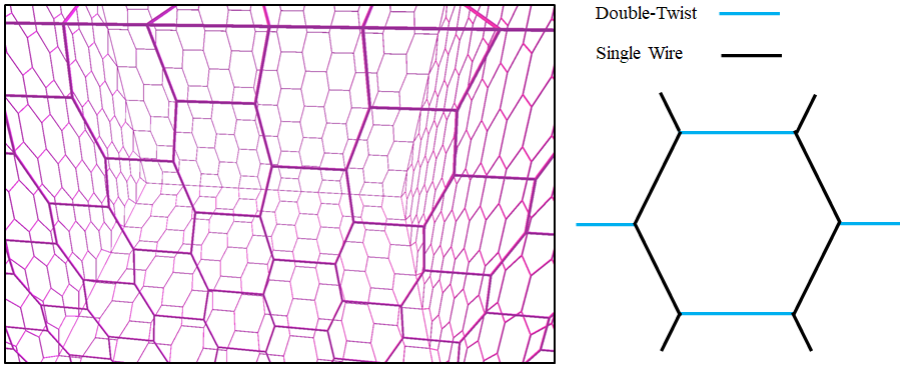

Figure 2.2: Hexagonal wire pattern for gabion basket.

The rockfill is also derived from the `cohFrictMat` class in *Yade*, however these particles are composed of a combination of grid nodes (vertices), grid connections (edges + internal support), and pfacets (faces). These polyhedral bodies are generated from a Delaunay triangulation (Maur, 2002) which operates on a cloud of vertices and returns a convex topology. The inertial properties of the polyhedrons are computed by partitioning the polyhedrons into tetrahedrons and summing over the volumes to find the total mass and inertia tensor of the body. A grid node is then placed at the centroid of the polyhedron with the computed inertial values. We refer to this method as the Polyhedral Reinforced Interior Shell Method (PRISM), which is illustrated in Figure 2.3. For the rockfill, it was observed that the motion was primarily translational, as opposed to rotational, so the "exact aspherical" option in *Yade* was not used for the contents of the gabion barrier, resulting in increased computational efficiency. Furthermore, a strut is placed at every other grid node between the vertices and the centroid of the polyhedron. This reduces the number of bodies in the simulation (fewer grid connections) while maintaining sufficiently rigid internal supports. A detailed summary of the PRISM approach is provided in Appendix B. Note that the average length scale for the rockfill particles is 0.75 ft, but may be slightly adjusted, depending on the dimensions of the gabion barrier, so that the fill fits within the bounds of the wire basket. The material properties for the rockfill are as follows: modulus of elasticity is $1.45 \times 10^7\ psi$, an angle of friction of 40°, a density of 178 lb/ft^3, and a normal and shear cohesion of $1.45 \times 10^{16}\ psi$ (note that the particles themselves are not cohesive, but they are comprised of particles that rely upon cohesive forces to resist fracture).

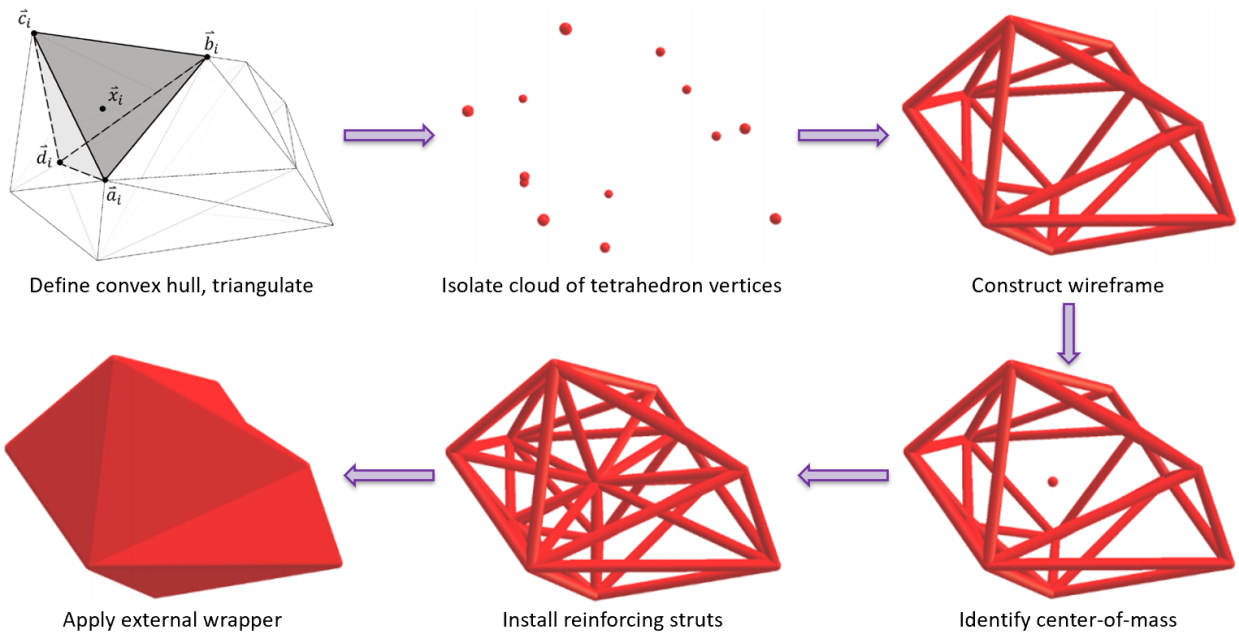

Figure 2.3: Definition sketch for generating polyhedral boulders through the PRISM method.

2.3 BOULDERS

Boulders are also generated from the PRISM method, however, the "exact aspherical" option is selected for the boulders so that proper initial values of angular momentum may be assigned to the bodies. Higher values of internal stiffness are also assigned to ensure rigid body motion. The material properties for the boulders are as follows: modulus of elasticity is $1.45 \times 10^7\ psi$, an angle of friction of 40°, a density of 178 lb/ft^3, and a normal and shear cohesion of $1.45 \times 10^{16}\ psi$ (note that the particles themselves are not cohesive, but they are comprised of particles that rely upon cohesive forces to resist fracture).

2.4 MODEL LIMITATIONS

One of the model limitations that was not considered in the experiments was rock crushing. As reported by Ng et al. (2016), the effects of crushing can create a densification (added mass) effect which increases the magnitude of the force for successive boulder impacts. The PRISM particle model at this level of development is not capable of handling crushing effects, and therefore were not included in the *GabBI* software. However, the magnitude of the force is still on the same level of magnitude of experimental results presented in Ng et al. (2016) for a given range of initial boulder velocities and radii.

Another limitation is that *Yade* does not always conserve angular momentum during impacts between aspherical bodies as a consequence of an internal inconsistency within the DEM software associated with the `cohFrictMat` material class. However, the dynamics of the problem are dominated by translational motion, as opposed to rotational motion, suggesting that errors in angular momentum do not significantly hinder the more salient features of the

simulations. Furthermore, the moment of inertia tensor and total mass assigned to the polyhedral bodies are calculated exactly from analytic formulas. Therefore, the inertial properties are accurate, but resulting torques during collision may carry a certain degree of error.

Note that when assigning dimensions and geometry to the gabion wire mesh that some rounding is required to create a consistent and uniform wire pattern that avoids particle overlap. Specifically, the wire diameter, and the gabion's length, width, and height in the virtual model are exactly the same as the values entered by the user. However, to create a uniform pattern for the welded or hexagonal wire geometry, the dimensions of the openings between adjacent wires may be rounded so that the appropriate integer number of wires will be rendered.

When creating polyhedral boulders, it is important to ensure that the boulder dimensions are not too small for a given edge radius. If the vertices of a polyhedron are too close together, then there is the possibility for potential overlap of grid nodes (vertices) and grid connections (edges) which may result in physically and numerically meaningless results. As a worst-case-scenario, the model may become unstable and some or all of the particles attain unmeasurable energies (`NaN` values) so that the objects in the model will seemingly disappear. Furthermore, the model may be unstable for higher energy impacts and may then require a smaller time step for stability.

Note that the intended purpose of *GabBI* is to simulate gabion barriers with dimensions ranging up to nine or twelve feet in length, width, and height. While larger barriers may be readily simulated, the limitation is tied to the computational cost associated with domains consisting of a large number of particles. The numerical model allows for simple regular barrier geometries aligned with a standard $x - y - z$ coordinate system.

As a general comment, the data on gabions exposed to boulder impacts is quite scarce as this is a rather unexplored topic. Thus, calibrating model results is challenging because, so few measurements have been made from physical experiments. Furthermore, the experiments which have been performed often involve a gabion sandwiched against a solid barrier or some other mesh, making a fair comparison even more challenging. See for example, Lambert et al. (2014), Ng et al. (2016), and Simac et al. (1997). Therefore, it should be noted that further work should be done with regards to calibrating the model to generate results comparable to physical experiment.

3.0 PARAMETRIC ANALYSIS OF GABION DAMAGE

Numerical experiments were conducted to model boulders impacting gabion barriers. The structures were made progressively larger to determine the smallest allowable barrier dimensions that still ensured structural stability. As part of this process, numerical stability was tested by monitoring the performance of the model under different impact velocities and boulder radii. Results suggest that for a time step of 1 μs (i.e., 10^{-6} s), the largest velocity and boulder weight are 50 ft/s and 2400 lb., respectively. Boulder diameters ranging from 0.5 feet to 1.5 feet were used for the spherical-boulder trials. These values were determined from data, reports, and a memo provided by ODOT (Cornforth Consultants Inc., 2015; McNamara and Bauer, personal communication, 2019), allowing us to infer the length scales from past rockfall events. The initial boulder velocities ranged from 5 ft/s to 50 ft/s. This interval is based on elevation data inferred from ODOT Columbia River survey notes (ODOT, 2019) and is based on the conservative assumption that all the initial potential energy of a dislodged rock, originating from some given height, has 100% of its potential energy converted to translational horizontal kinetic energy near the end of its trajectory. The simulation cases are summarized in Table 3.1.

Table 3.1: Gabion Simulation Cases for Spherical Boulders

Case Name	Boulder Radius (ft.)	Boulder Velocity (ft/s)	Rows	Columns	Stacks	Wire Diameter (in.)
SAG-I	0.25	5	1	1	1	0.087
SAG-II	0.25	20	1	1	1	0.087
SAG-III	0.25	50	1	1	1	0.087
SAG-IV	0.50	5	1	1	1	0.087
SAG-V	0.50	10	1	1	1	0.087
SAG-VI	0.50	20	1	1	1	0.087
SAG-VII	0.50	50	1	1	1	0.087
SBG-I	0.25	30	1	3	1	0.087
SBG-II	0.25	50	1	3	1	0.120
SBG-III	0.50	30	1	3	1	0.120
SBG-IV	0.25	10	2	3	1	0.120
SBG-V	0.25	30	2	3	1	0.120
SBG-VI	0.25	40	2	3	1	0.120
SBG-VII	0.50	40	2	3	1	0.120
SBG-VIII	0.75	10	2	3	1	0.120
SBG-IX	0.25	10	2	3	2	0.120
SBG-X	0.25	50	2	3	2	0.120
SBG-XI	0.50	10	2	3	2	0.120
SBG-XII	0.50	30	2	3	2	0.120
SBG-XIII	0.75	30	2	3	2	0.120
SBG-XIV	1.0	30	2	3	2	0.120
SBG-XV	1.5	30	2	3	2	0.120
SBG-XVI	1.5	30	3	3	2	0.120

3.1 STAND-ALONE GABIONS

3.1.1 Introduction

Individual gabion units were impacted with progressively larger initial energies to determine the resulting damage from the numerical simulations. These stand-alone gabion units have dimensions of $3' \times 3' \times 3'$ with angular fill and are not bound or fastened to any adjacent gabion baskets and represent a scenario where sliding resistance is minimal and therefore deformation and displacement are predicted to be relatively significant for a given impact loading. The wire diameter during this phase of experiments was chosen to be 0.087 in., which corresponds to the standard lacing wire diameter used by the Maccaferri company. The standard mesh diameter is 0.120 in., but the former smaller diameter is used initially to determine the performance of a thinner wire which is anticipated to give more conservative results. This section is prudent in classifying the different types of damage and failure modes that may be incurred during such boulder-impact events.

3.1.2 Results and Damage Patterns for Stand-Alone Gabion Units

Numerical simulations were performed in *GabBI* in which a spherical boulder impacted a single stand-alone gabion (SAG) unit with dimensions of $3' \times 3' \times 3'$ and a welded wire pattern with a diameter of 0.087 in. and 3.25-in. openings. Different combinations of boulder radii and velocity were used to determine the possible resulting damage patterns that occur after a certain number of impacts. One of the goals of this overall investigation is to find a gabion barrier design which is structurally and economically sound. Therefore, the plan of action requires us to start at smaller scales and then gradually progress up to larger and more stable barriers while ensuring that the structure has not been over-designed in terms of movement or wire rupture.

The first case examined was a stand-alone gabion unit subjected to consecutive spherical boulder impacts with a radius of 0.25 ft and an initial velocity of 5 ft/s as shown in Figure 3.1. A relatively small projectile was used in this simulation in consideration of examining the effects of concentrated loads. Stress is defined as force per unit area, so we wanted to investigate if a smaller force may still be able to cause significant damage if acting over a relatively small area. Numerical simulation results of the gabion basket after repeated impacts are illustrated in Figure 3.2, where we see how the damage of the gabion has progressed after zero, two, four, six, eight, and twelve impacts. Note that "zero impacts" corresponds to the initial condition of the gabion barrier. Consecutive impacts are performed by restoring the boulder to its initial position and velocity after one of the following two criteria has been satisfied: (i) the boulder has rebounded off the gabion unit (see Appendix D for how this is calculated in terms of the vector dot-product); or (ii) no less than 95% of the total kinetic energy in the system has been dissipated.

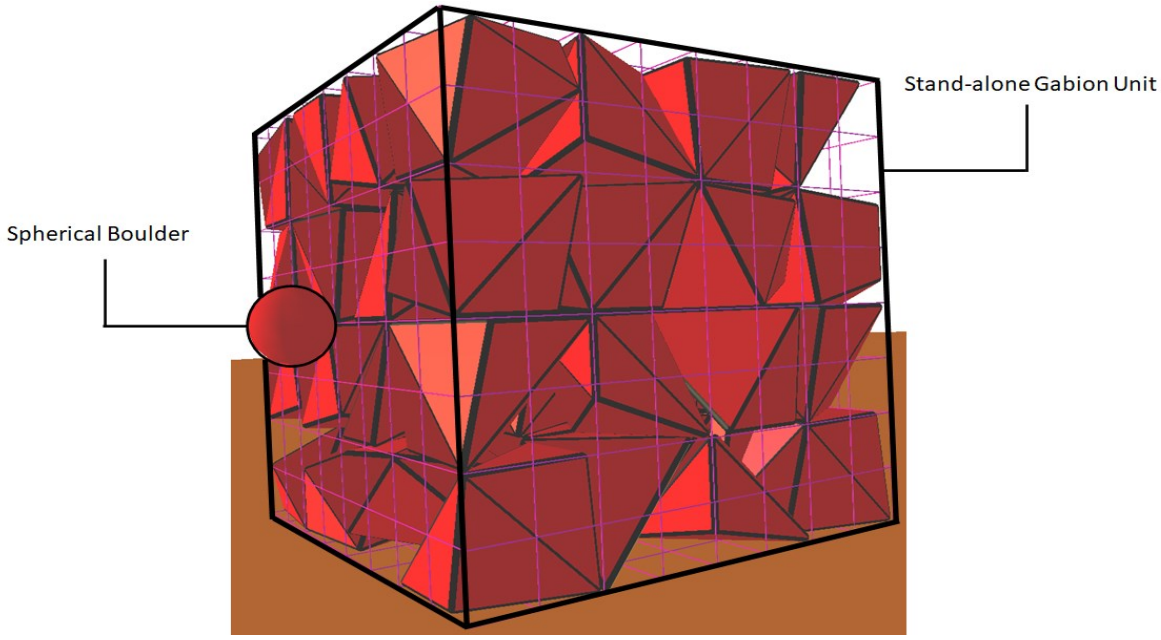

Figure 3.1: Initial conditions for boulder radius of 0.25 ft with velocity of 5 ft/s impacting a single gabion unit with dimensions: $3' \times 3' \times 3'$.

Figure 3.2 shows that the contents of the gabion have been disturbed and rearranged because of the sequential boulder impacts, and there is some minor wire deformation without wire rupture.

Information pertaining to the deformation and movement of the gabion was also recorded during the simulations. One of the features of *GabBI* is that it can keep track of the position of grid nodes on the wire basket portion of the gabion. Therefore, a set of inquiry points can be assigned which measure the position of the grid nodes relative to their initial location. Figure 3.3 depicts where query points have been placed on the surface of the gabion basket and Table 3.2 provides a list of the numerical coordinate values. Note that the front left toe of the gabion is located at the origin of our coordinate system. The maximum displacement measured during the simulation was approximately 0.17 ft, which corresponds to query point 2. Query point 5 experiences a maximum deformation of approximately 0.15 ft.

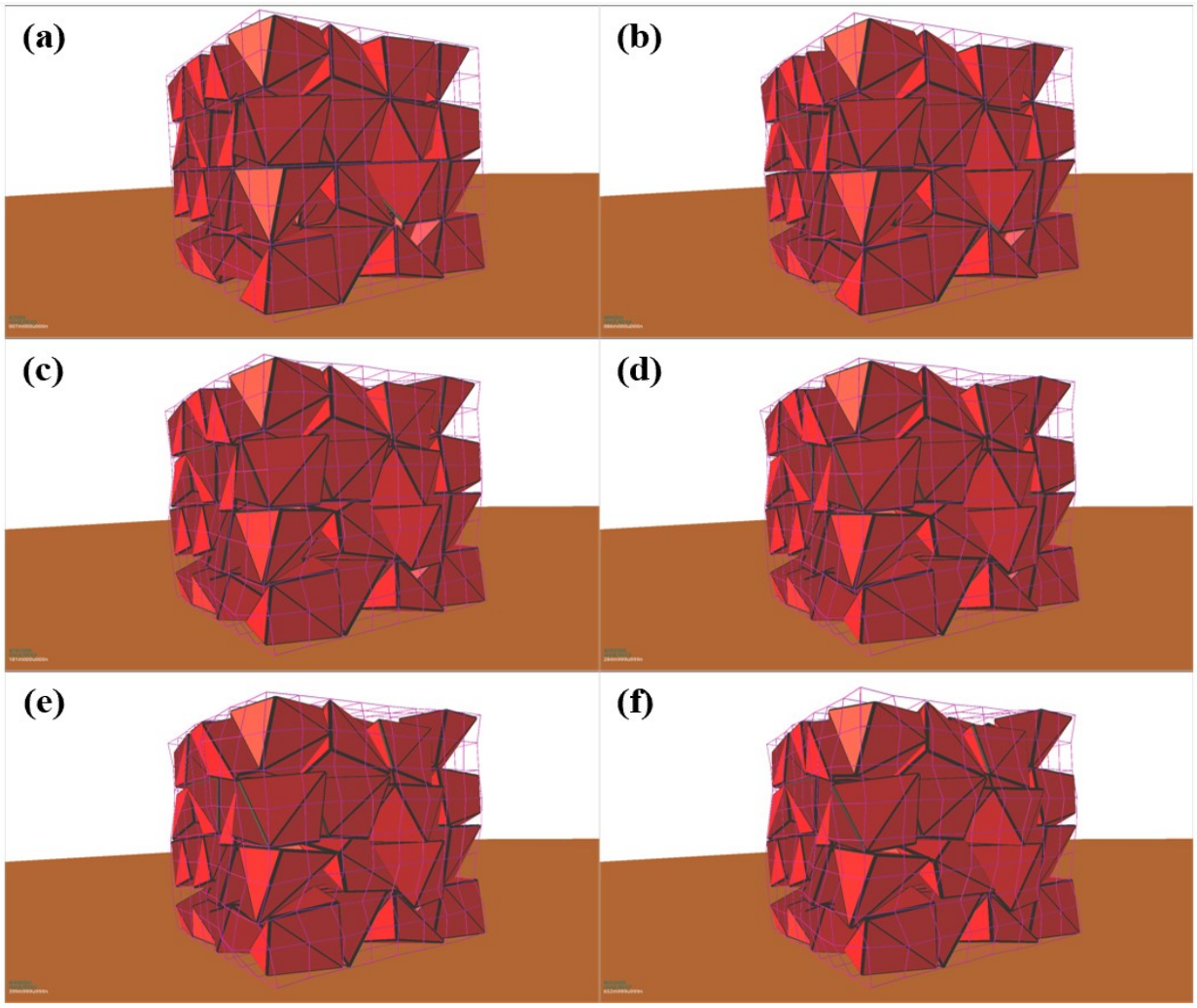

Figure 3.2: Case SAG-I: Boulder radius of 0.25 ft with initial velocity of 5 ft/s after (a) 0 impacts; (b) 2 impacts; (c) 4 impacts; (d) 6 impacts; (e) 8 impacts; (f) 12 impacts.

Another round of impacts was performed on a separate gabion unit using a boulder with a radius of 0.25 ft with an initial velocity of 20 ft/s. An ensemble of images of the gabion after successive impacts is displayed in Figure 3.4. The signs of deformation are more pronounced in this case (Case SAG-II), compared with Case SAG-I, however no wire rupture is observed after the ten consecutive impacts. Query points 2 and 5 both sustained deformation values of about 0.82 ft.

Query points 1, 3, and 4 were all displaced an approximate equal distance of 0.4 ft., suggesting that these points were moving in unison. Therefore, the observation implies, as seen in Figure 3.4(d), (e), and (f), that not only was deformation present, but minor sliding was as well.

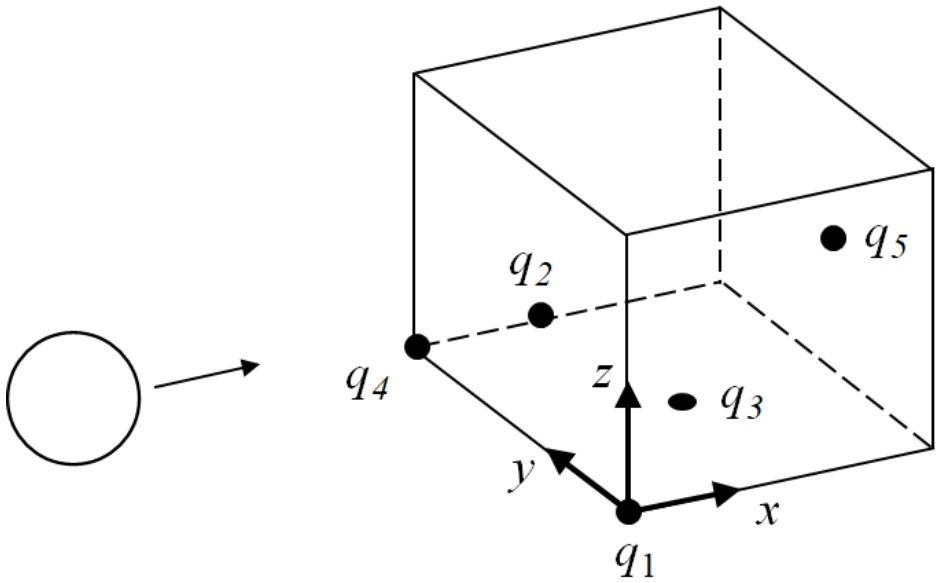

Figure 3.3: Definition sketch for displacement query points on stand-alone gabion unit (rows = 1; columns = 1; stacks = 1).

Table 3.2: List of Query Points for Gabion Movement (rows = 1; columns = 1; stacks = 1)

Query Point	Label on Figure 3.3	Coordinates (ft.)
Query 1	q_1	(0, 0, 0)
Query 2	q_2	(0, 1.5, 0)
Query 3	q_3	(1.5, 1.5, 0)
Query 4	q_4	(0, 3, 0)
Query 5	q_5	(3, 1.5, 1.5)

Significant deformation and some wire rupture were observed for the case with an initial boulder velocity of 50 ft/s with a radius of 0.25 ft (SAG-III). Figure 3.5 displays the movement and damage done to the gabion unit after five impacts, after which the simulation was terminated due to the fact that the gabion was considered to have failed by excessive deformation as a result of the incurred impacts. Figure 3.6 shows the areas over which wire rupture has occurred. It is assumed that if the size of the perforations in the wire basket are on the order of the length scale of the rockfill then it is possible for the gravel to spill out from the barrier.

The boulder the radius is increased to a size of 0.50 ft., but with an initial velocity of 5 ft/s. The deformation that the gabion incurs after seven impacts is displayed in Figure 3.7. The gabion deforms in a shearing fashion, but no wire rupture is observed. Sliding is also minimal during this simulation. Overall, the gabion is not considered to be failing as it shows negligible displacement, moderate deformation, and no signs of rupture.

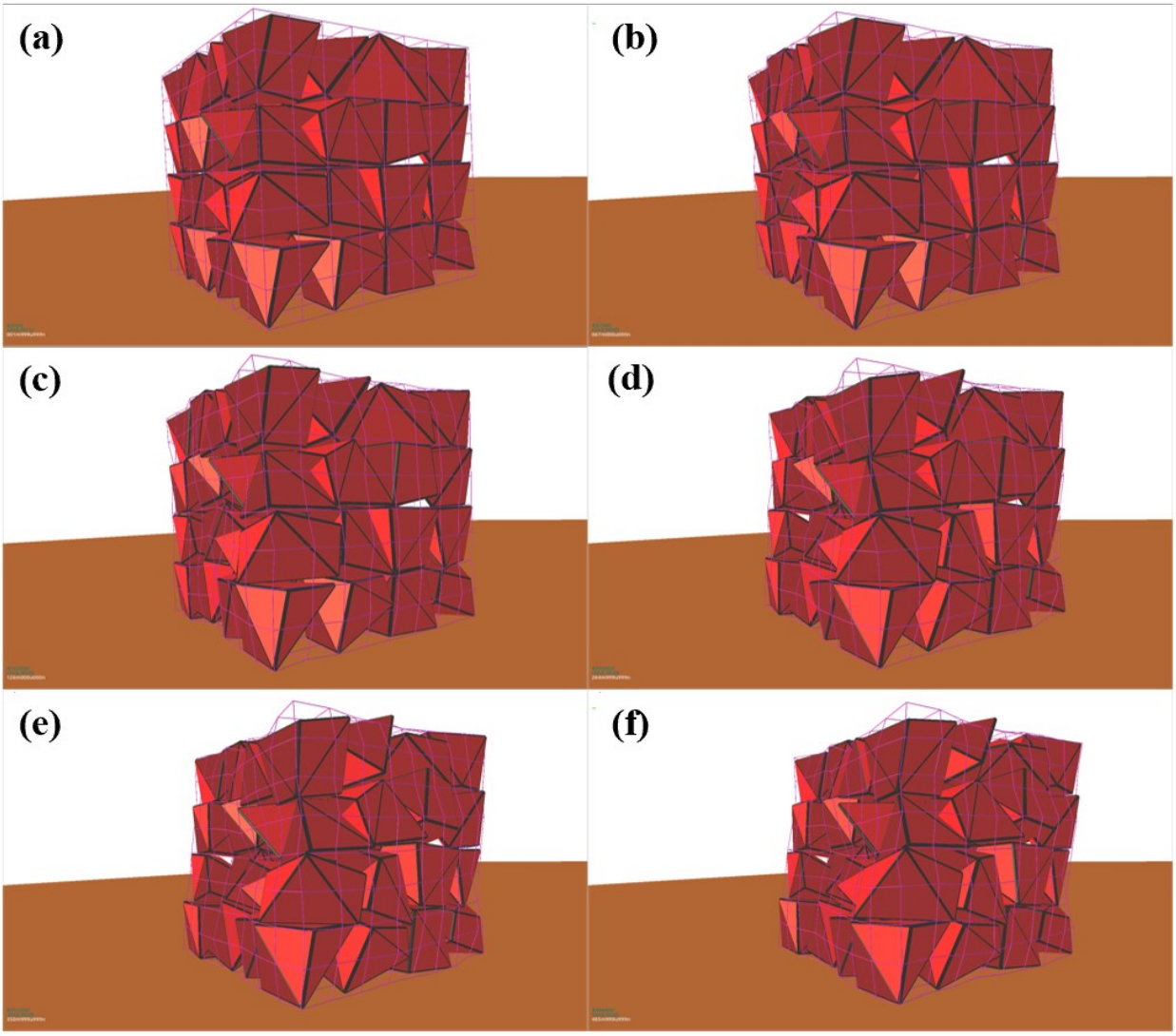

Figure 3.4: Case SAG-II: Boulder radius of 0.25 ft with initial velocity of 20 ft/s after (a) 0 impacts; (b) 2 impacts; (c) 4 impacts; (d) 6 impacts; (e) 8 impacts; (f) 10 impacts.

In Figure 3.8, results are shown for a boulder of radius 0.5 ft., with an initial velocity of 10 ft/s, impacting a gabion unit nine consecutive times. The gabion experiences significant deformation and displacement during the first seven impacts. By the end of the simulation, the entire gabion unit moves approximately a total of two feet. After the eighth impact, moderate to significant wire rupture can be observed near the bottom middle portion of the basket as seen in Figure 3.8(c) and (d). The final condition of the gabion suggests that it has failed, not only due to wire damage, but also excessive displacement. This verifies that single gabion units, when subjected to boulder impacts of this level of momentum, are not sufficient to provide adequate protection during a rockfall event of minor volume initiated from a moderate height. This directly validates the requirement of larger barriers with fastenings made to adjacent gabion units, requiring further investigation of the damage severity, in terms of wire rupture, under higher-momentum impacts. Therefore, we investigate boulder impacts for a radius of 0.5 ft. with initial velocities of 20 and 50 ft/s, which are presented in Figure 3.9 and Figure 3.10.

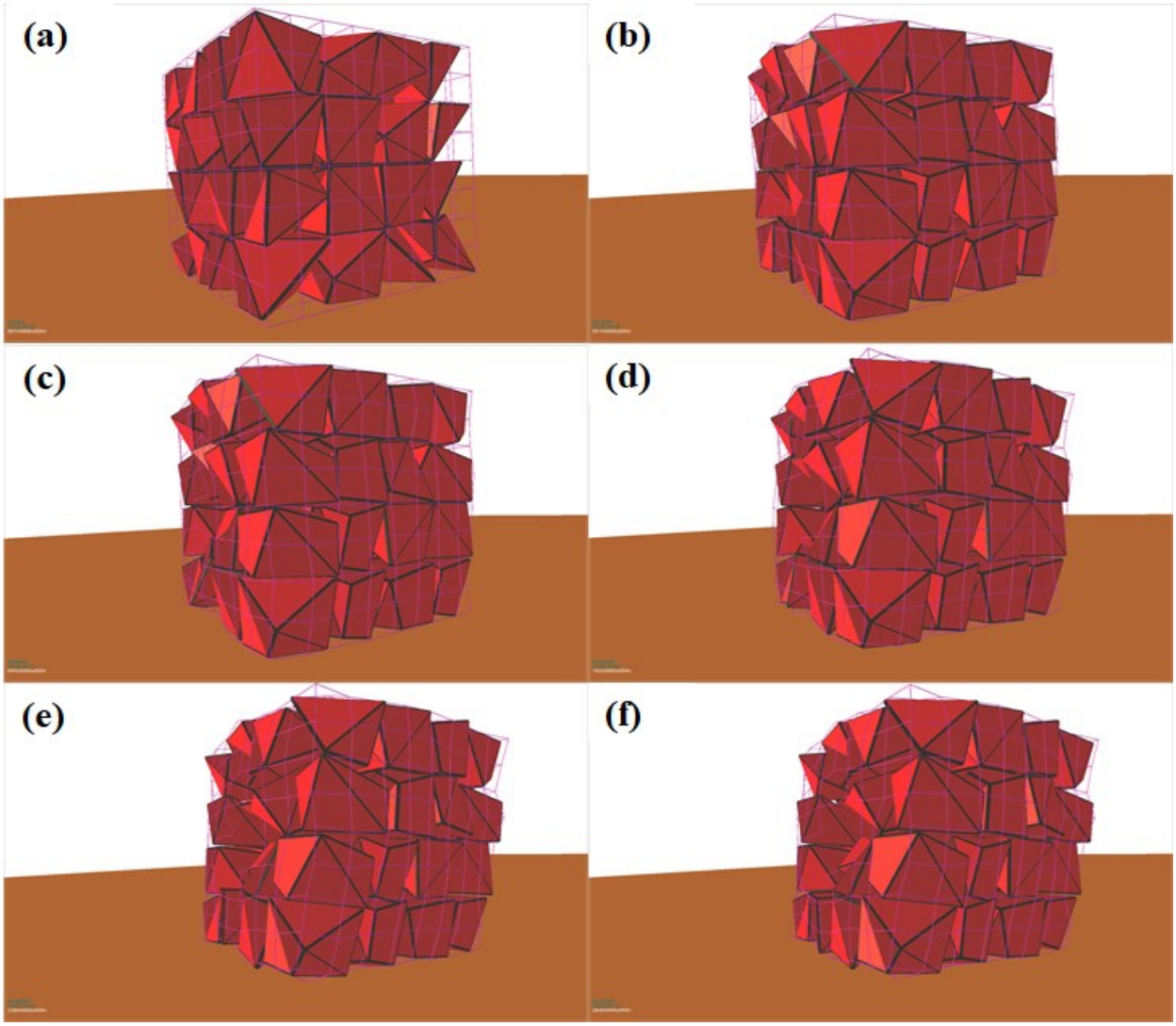

Figure 3.5: Case SAG-III: Boulder radius of 0.25 ft with initial velocity of 50 ft/s after (a) 0 impacts; (b) 1 impact; (c) 2 impacts; (d) 3 impacts; (e) 4 impacts; (f) 5 impacts.

In the case of boulder-gabion impact with a spherical boulder of radius 0.5 ft and velocity 20 ft/s, minor wire rupture occurs at multiple places on the face of the gabion after one impact. Figure 3.9(c) gives a global view of the gabion unit, where the white dots locate where rupture has happened, whereas Figure 3.9(d) gives an enhanced view of the damage where ruptures occur. Note that displacement is also significant after a single impact, resulting in a 1-ft movement of the basket in x-direction.

Next, a numerical experiment with a boulder of 0.5 ft in radius and an initial velocity of 50 ft/s is performed. After one impact, a devastating amount of damage is done to the gabion unit, as shown in Figure 3.10. Significant wire ruptures (i.e., openings greater than the length scale of the rockfill) are present, and the gabion unit displaces approximately 4 feet as a result of the impact. The final state of the gabion is considered to be completely failed.

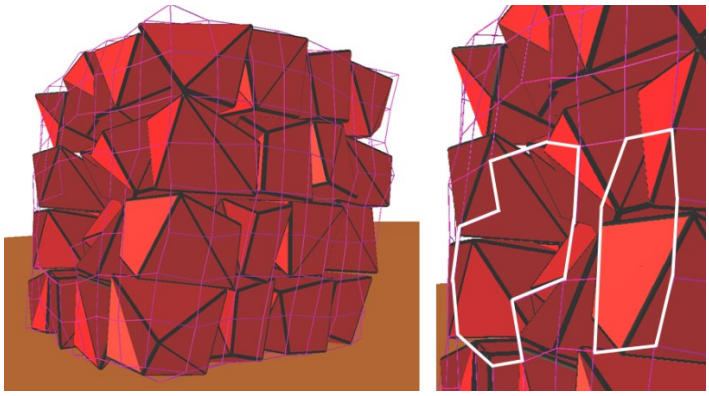

Figure 3.6: Case SAG-III: Boulder radius of 0.25 ft with initial velocity of 50 ft/s after 5 impacts (close-up of wire rupture).

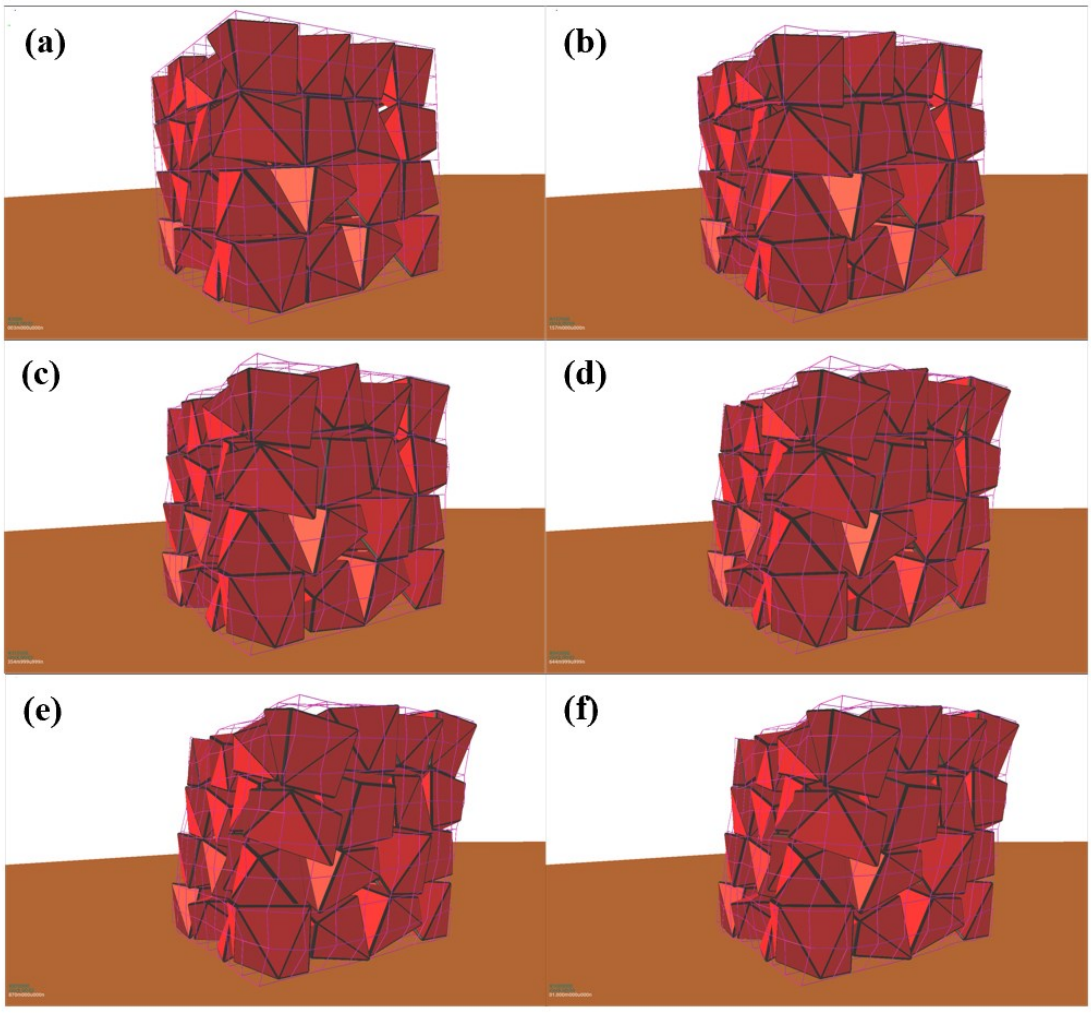

Figure 3.7: Case SAG-IV: Boulder radius of 0.50 ft with initial velocity of 5 ft/s after (a) 0 impacts; (b) 1 impact; (c) 2 impacts; (d) 4 impacts; (e) 6 impacts; (f) 7 impacts.

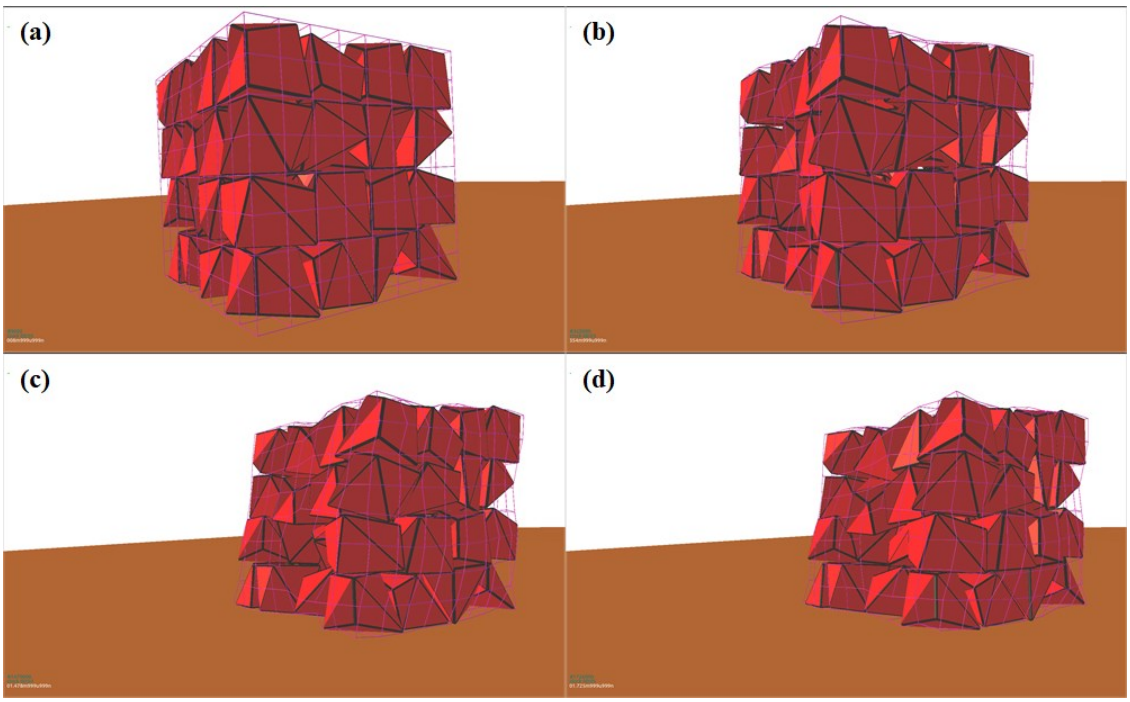

Figure 3.8: Case SAG-V: Boulder radius of 0.5 ft with initial velocity of 10 ft/s after (a) 0 impacts; (b) 1 impact; (c) 8 impacts; (d) 9 impacts.

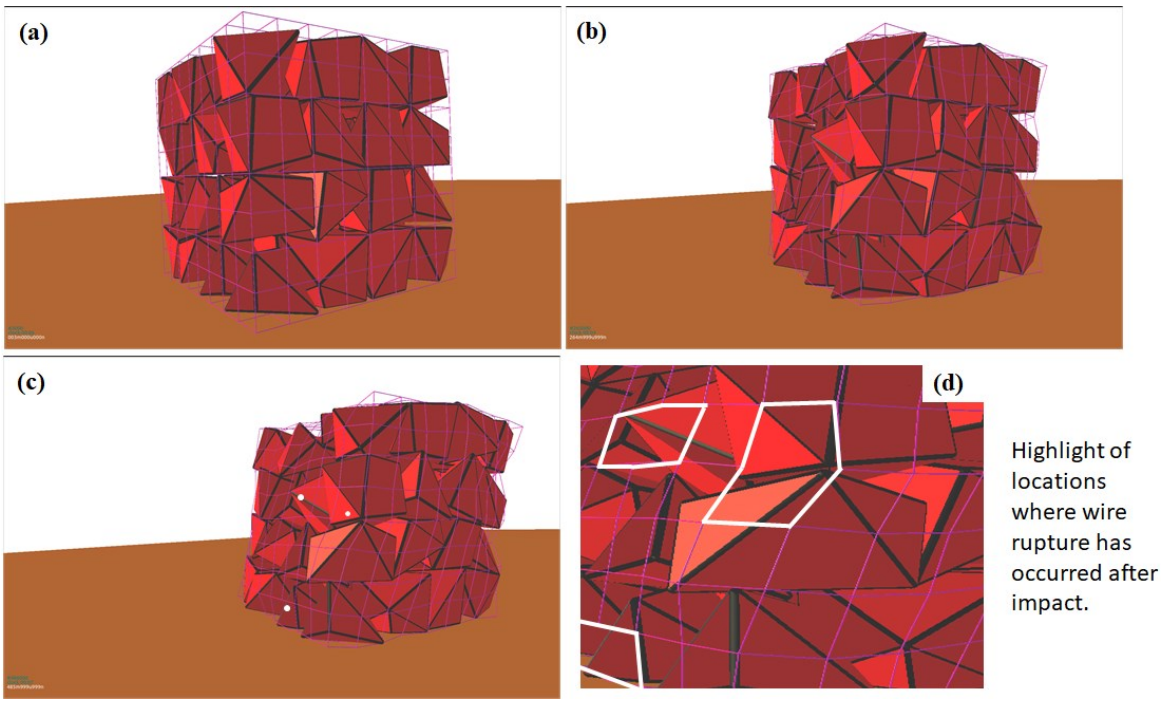

Figure 3.9: Case SAG-VI: Boulder radius of 0.50 ft with initial velocity of 20 ft/s after (a) 0 impacts; (b) 1 impact; (c) 2 impacts (white dots locate the rupture; (d) highlight of locations where wire rupture has occurred.

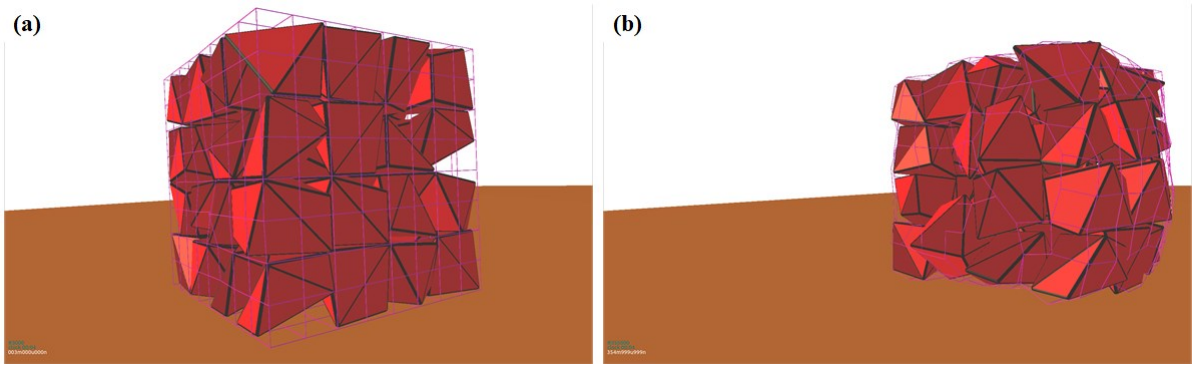

Figure 3.10: Case SAG-VII: Boulder radius of 0.50 ft with initial velocity of 50 ft/s after (a) 0 impacts; (b) 1 impact.

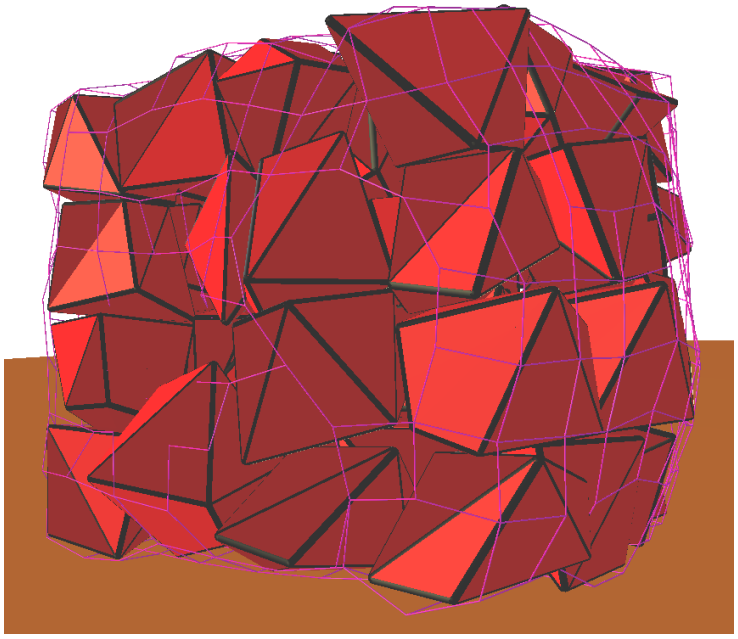

Figure 3.11: Case SAG-VII: Significant wire rupture after one impact from boulder with radius of 0.50 ft and initial velocity of 50 ft/s.

3.2 GABION BARRIERS

It was observed that stand-alone gabions can experience significant movement from the impact of a boulder with a radius of 0.5 ft and an initial velocity of 10 ft/s. Therefore, adjacent gabion units are fastened together to create a gabion barrier to increase the resistance from similar rockfall events. These configurations will be referred to as a series of bound gabions (SBG). The goal in this section is to observe various damage patterns and to determine how many impacts, and at what energy levels, will lead to failure of the gabion barrier. Each gabion unit in the barrier has dimensions of $3' \times 3' \times 3'$ with a wire diameter of 0.120 in. and an opening spacing of 3.25 in. in a welded pattern. The proceeding sections are organized by the number of rows, columns, and stacks (R, C, S, see Figure 3.12) of gabion units that are bound together. To track

the movement and deformation of the gabion barriers, five query points are located on the surface of the wire basket, as shown in Figure 3.12. A list of the query points is presented in Table 3.3. Figure 3.13 shows the typical boulder-barrier configuration for the numerical simulations in this section of the report.

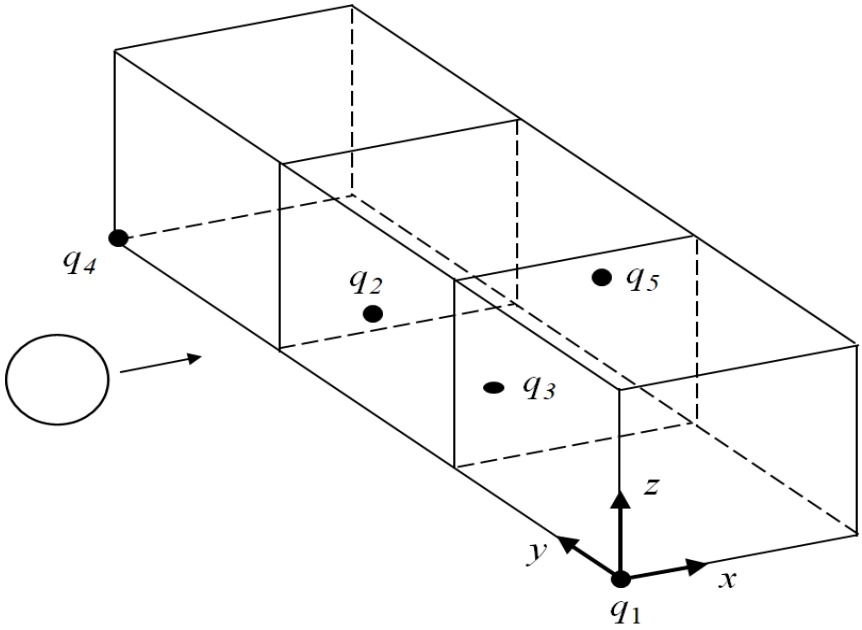

Figure 3.12: Definition sketch for displacement query points on gabion barrier with dimensions: $3' \times 3' \times 3'$ (rows = 1; columns = 3; stacks = 1).

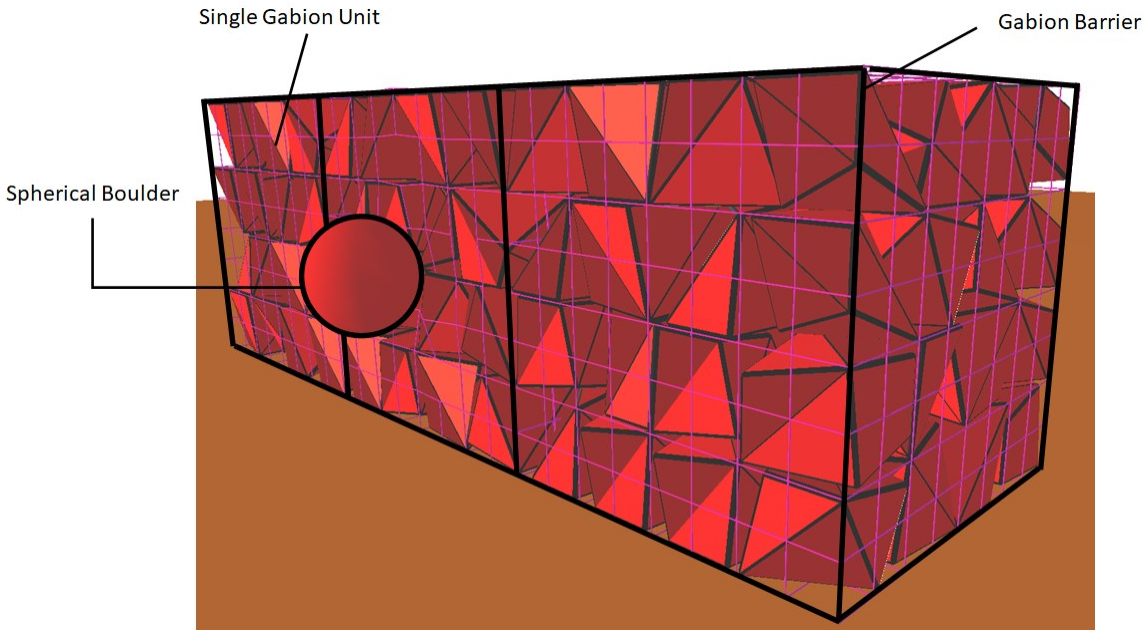

Figure 3.13: Initial conditions for boulder radius of 0.5 ft impacting a gabion barrier constructed from three gabion units with dimensions: $3' \times 3' \times 3'$ (rows = 1; columns = 3; stacks = 1).

Table 3.3: List of Query Points for Gabion Movement (rows = 1; columns = 3; stacks = 1)

Query Point	Label on Figure 3.12	Coordinates (ft.)
Query 1	q_1	(0, 0, 0)
Query 2	q_2	(0, 4.5, 1.5)
Query 3	q_3	(1.5, 4.5, 0)
Query 4	q_4	(0, 9, 0)
Query 5	q_5	(3, 4.5, 1.5)

3.2.1 Test Barrier 1 $(R, C, S) = (1, 3, 1)$

A barrier constructed of three fastened $3' \times 3' \times 3'$ gabion units is subjected to boulder impacts for various boulder sizes and velocities. The initial velocity of the boulder is oriented in a direction transverse to the longitudinal orientation of the barrier. Observations from the numerical simulations are presented after a various number of impacts to keep track of the damage and movement of the barrier.

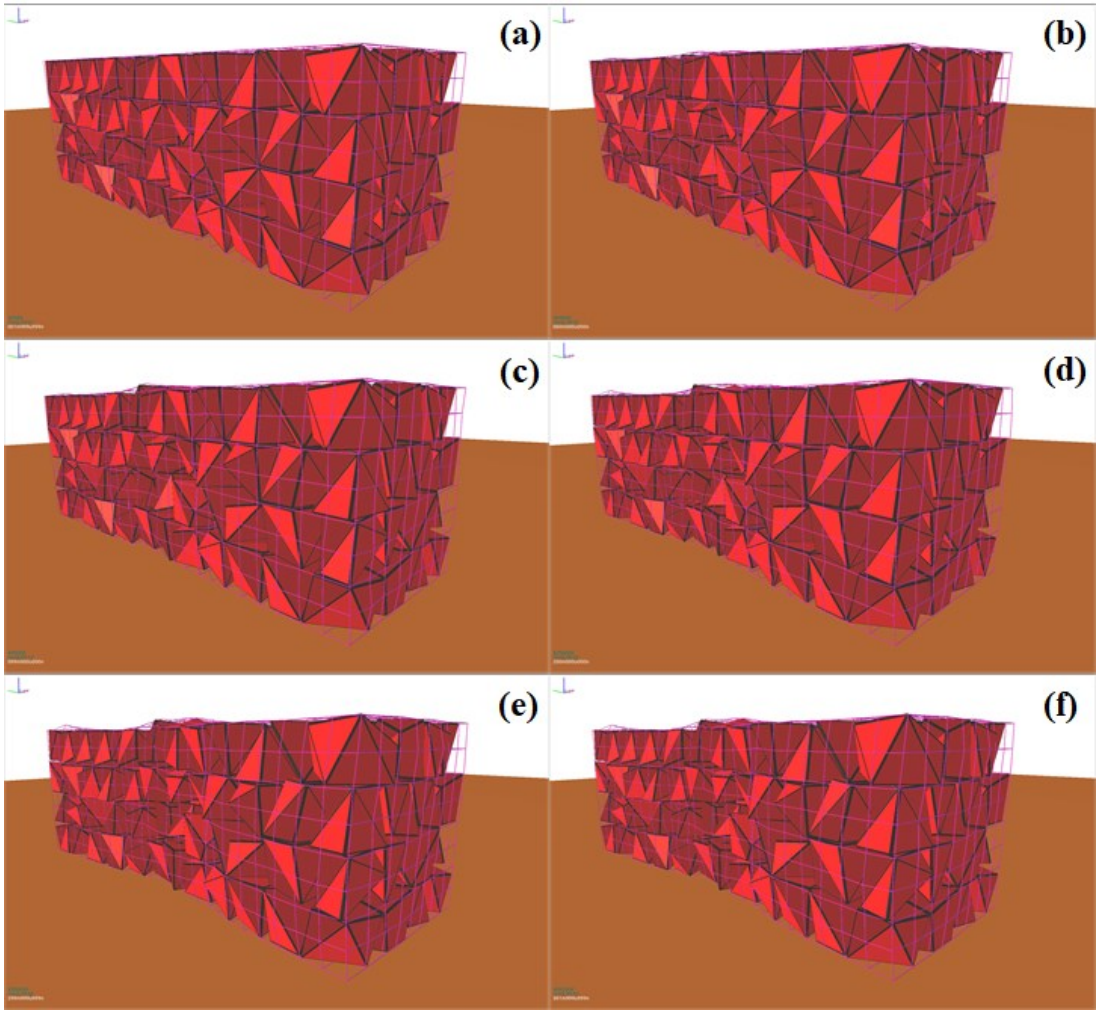

Figure 3.14: Case SBG-I: Boulder radius of 0.25 ft with initial velocity of 30 ft/s (front) after (a) 0 impacts; (b) 2 impacts; (c) 4 impacts; (d) 6 impacts; (e) 8 impacts; (f) 10 impacts.

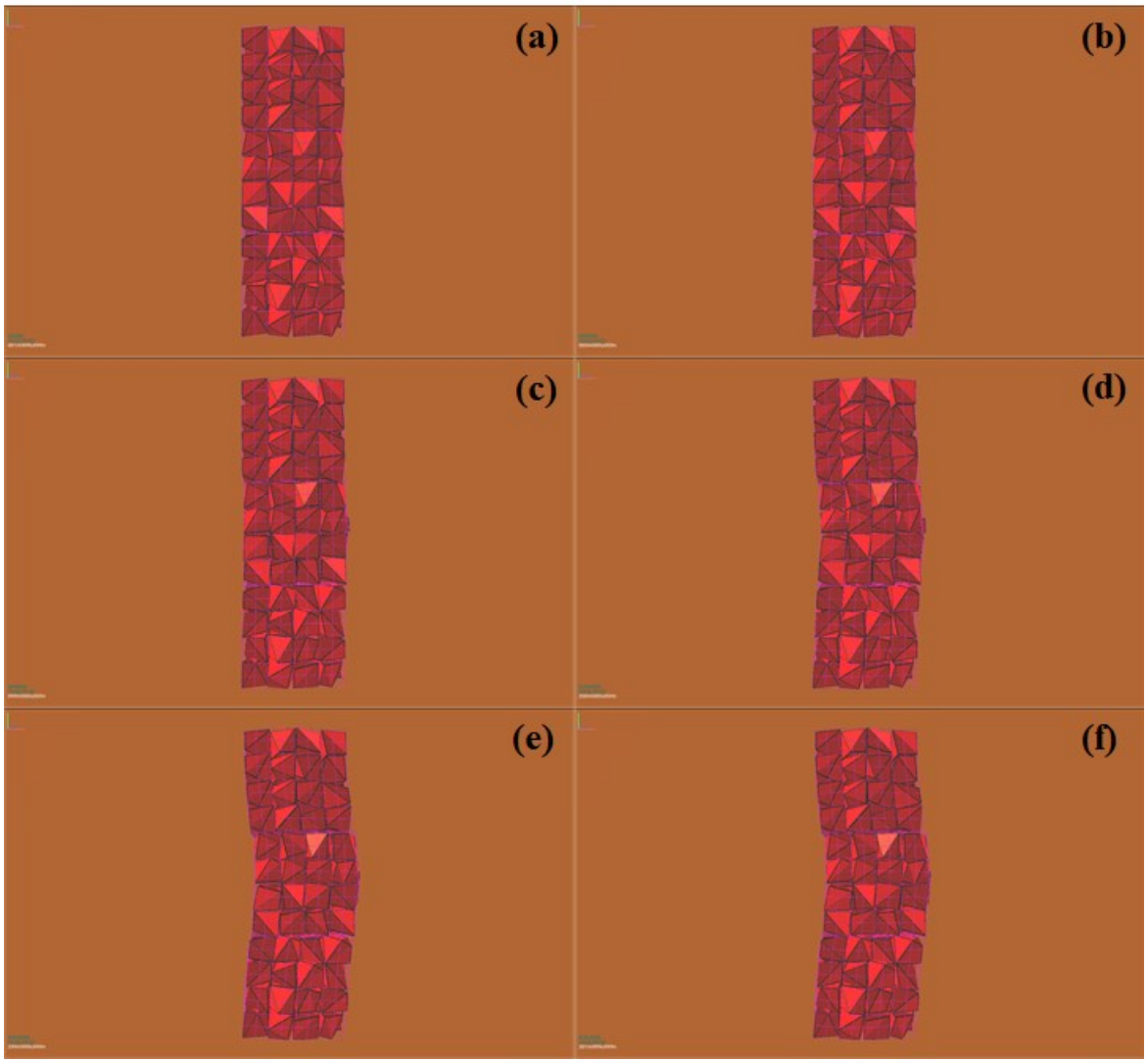

Figure 3.15: Case SBG-I: Boulder radius of 0.25 ft with initial velocity of 30 ft/s (plan view) after (a) 0 impacts; (b) 2 impacts; (c) 4 impacts; (d) 6 impacts; (e) 8 impacts; (f) 10 impacts.

Numerical experiments were conducted for a boulder radius of 0.25 ft for various velocities. Figure 3.14 and Figure 3.15 show the front and plan view of the barrier after being subjected to consecutive impacts at velocities of 30 ft/s. Minor wire rupture is observed after the eighth impact with moderate deformation. The barrier does not appear to fail after the tenth impact, but the deformation of the middle front and back faces (q_2 and q_5 from Figure 3.12) experience a total displacement of approximately 0.8 feet. Query points q_1 and q_4 experience a displacement of approximately 0.05 feet, suggesting that the radius of influence for this given boulder impact is less than 4.5 feet because the displacement at the ends is negligible (about 1% of the width of the gabion unit).

The initial boulder velocity is then increased to 50 ft/s. Front and plan view images of the results are presented in Figure 3.16. The barrier is determined to have failed after the fourth impact (Figure 3.16(e) and (f)) because the area of wire rupture is significant enough to allow for the

contents of the gabion to disperse from the interior of the wire basket. Note that connections between adjacent gabion units in a gabion barrier are generated by virtual interactions to model the lacing wires. If relative sliding motion exists between adjacent gabions, then it is assumed that the fastening has failed. For impacts of greater momentum, and given boulder radius, this may imply that there is a smaller global radius of influence, as the adjacent gabion units no longer move with the primary impacted gabion unit due to the failure of the fastening (numerically modeled through virtual force interactions).

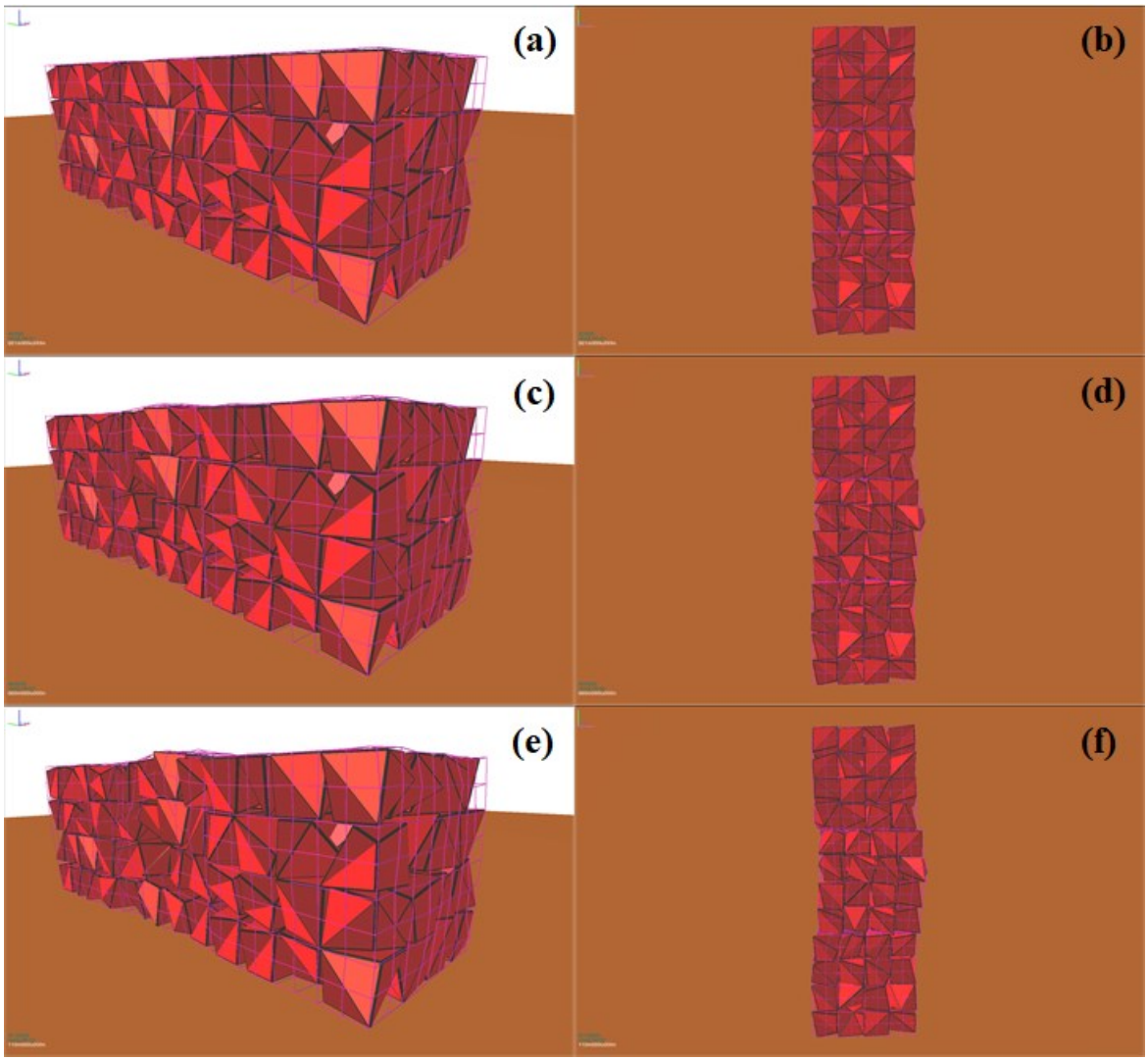

Figure 3.16: Case SBG-II: Boulder radius of 0.25 ft with initial velocity of 50 ft/s (front) after (a) 0 impacts; (c) 2 impacts; (e) 4 impacts.

However, the local displacement may then be larger because the surrounding gabion units are no longer able to provide resistance after the bonds in the lacing wire fail.

As determined from the numerical simulations from Case SBG-II, a boulder with a radius of 0.25 ft and initial velocity of 50 ft/s can lead to gabion failure after four impacts. In the following set of experiments, the boulder radius is increased to 0.50 ft and a range of velocities are explored to

determine the performance and failure characteristics of the gabion barrier. The boulder radius is increased to 0.50 ft to explore the effects of the size of the projectile intercepted by a gabion barrier. Results are presented in Figure 3.17 and Figure 3.18 for the front and plan view perspectives of the barrier, for boulder impacts with an initial velocity of 30 ft/s. The gabion barrier has been determined to fail after one impact as a consequence of displacement and wire rupture. Figure 3.18 displays the significant wire rupture which has occurred, leaving an opening greater than the average rockfill length scale, allowing the contents to have the potential to spill out from the wire cage.

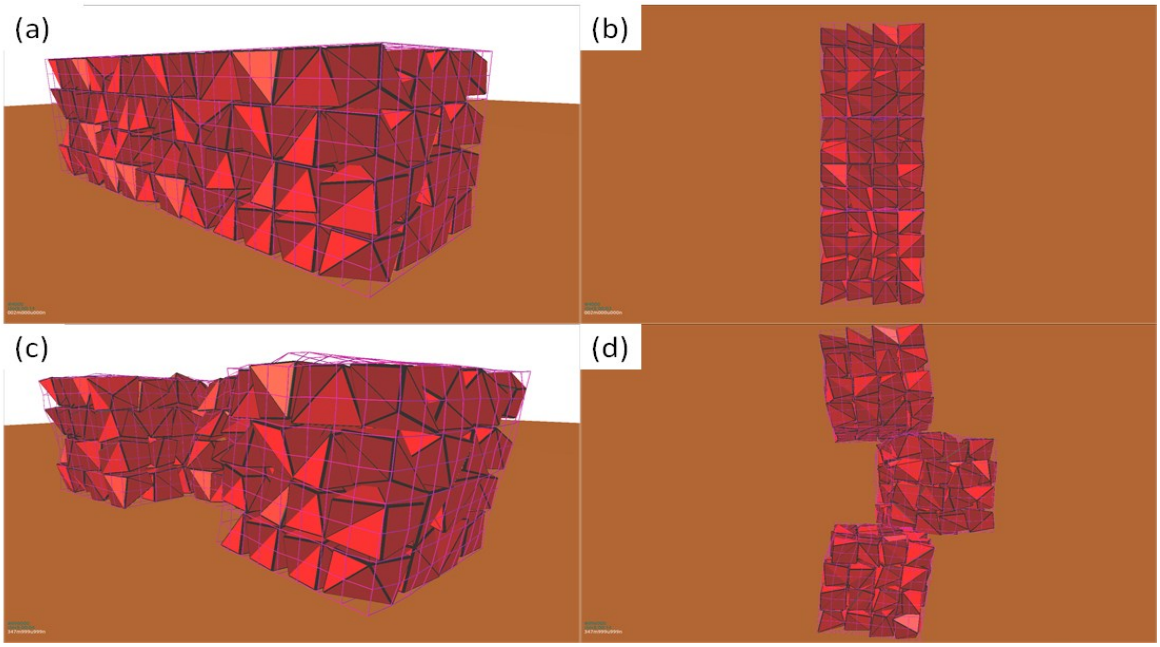

Figure 3.17: Case SBG-III: Boulder radius of 0.50 ft with initial velocity of 30 ft/s after (a-b) 0 impacts; (c-d) 1 impact.

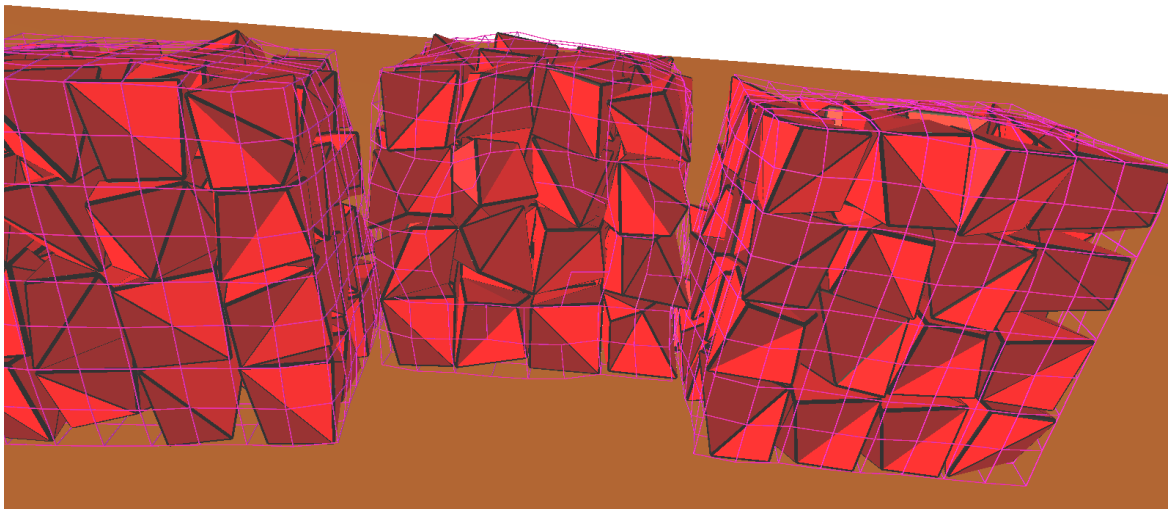

Figure 3.18: Case SBG-III: Boulder radius of 0.50 ft with initial velocity of 30 ft/s after one impact (front view).

The displacement failure mode observed in Figure 3.17 and Figure 3.18 will be referred to as dislodgement. Dislodgement is defined as the separation of an individual gabion unit from its neighboring gabions. This process occurs when impact from a boulder is capable of breaking the lacing bonds along the perimeter of the shared faces between the adjacent gabions. The impacted gabion unit translates independently from the other gabions but may result in slight rotation of the adjacent gabion units as a result of the torque generated before the virtual forces break. Note that an experiment for an initial velocity of 40 ft/s was also conducted, but results were qualitatively similar in terms of damage patterns but were of a greater scale in response to the larger initial momentum. Overall, it is clear from the experiment involving a spherical boulder with a radius of 0.50 ft with an initial velocity of 30 ft/s, that a single row of gabions does not provide adequate structural support against a rockfall event of this intensity. Therefore, the next phase in the investigatory process is to test the performance of a barrier consisting of two rows and three columns of gabions.

3.2.2 Test Barrier 2 $(R, C, S) = (2, 3, 1)$

The second test barrier is presented schematically in Figure 3.19 and query points are presented in Table 3.4. The area of the base of the gabion barrier in the experiments is doubled by creating two rows of three columns of gabion units. This allows testing changes in the barrier stability for larger volumes of rockfill. A numerical simulation was carried out involving a boulder with a radius of 0.25 ft and initial velocity of 10 ft/s. Images of the front and plan view of the barrier for successive impacts are summarized in Figure 3.20 and Figure 3.21, respectively. The overall damage and movement after the ten impacts is negligible, suggesting that two rows of adjacently bound gabions are sufficient to protect against boulder impacts of this size and energy.

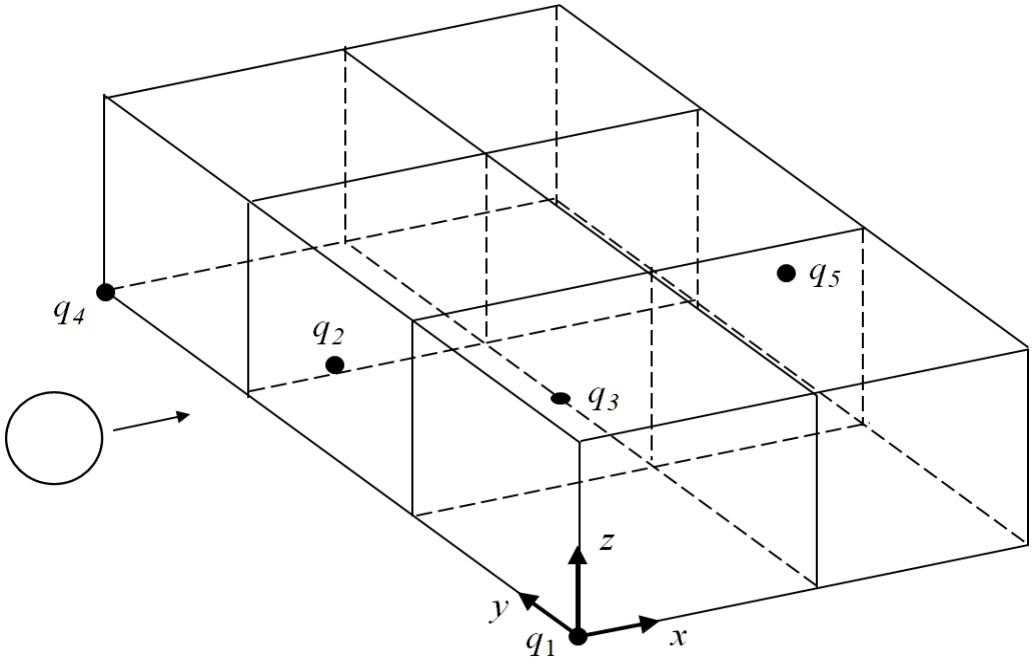

Figure 3.19: Definition sketch for displacement query points on gabion barrier with dimensions: $3' \times 3' \times 3'$ (rows = 2; columns = 3; stacks = 1).

Table 3.4: List of Query Points for Gabion Movement (rows = 2; columns = 3; stacks = 1)

Query Point	Label on Figure 3.3	Coordinates (ft.)
Query 1	q_1	(0, 0, 0)
Query 2	q_2	(0, 4.5, 1.5)
Query 3	q_3	(3, 4.5, 0)
Query 4	q_4	(0, 9, 0)
Query 5	q_5	(6, 4.5, 1.5)

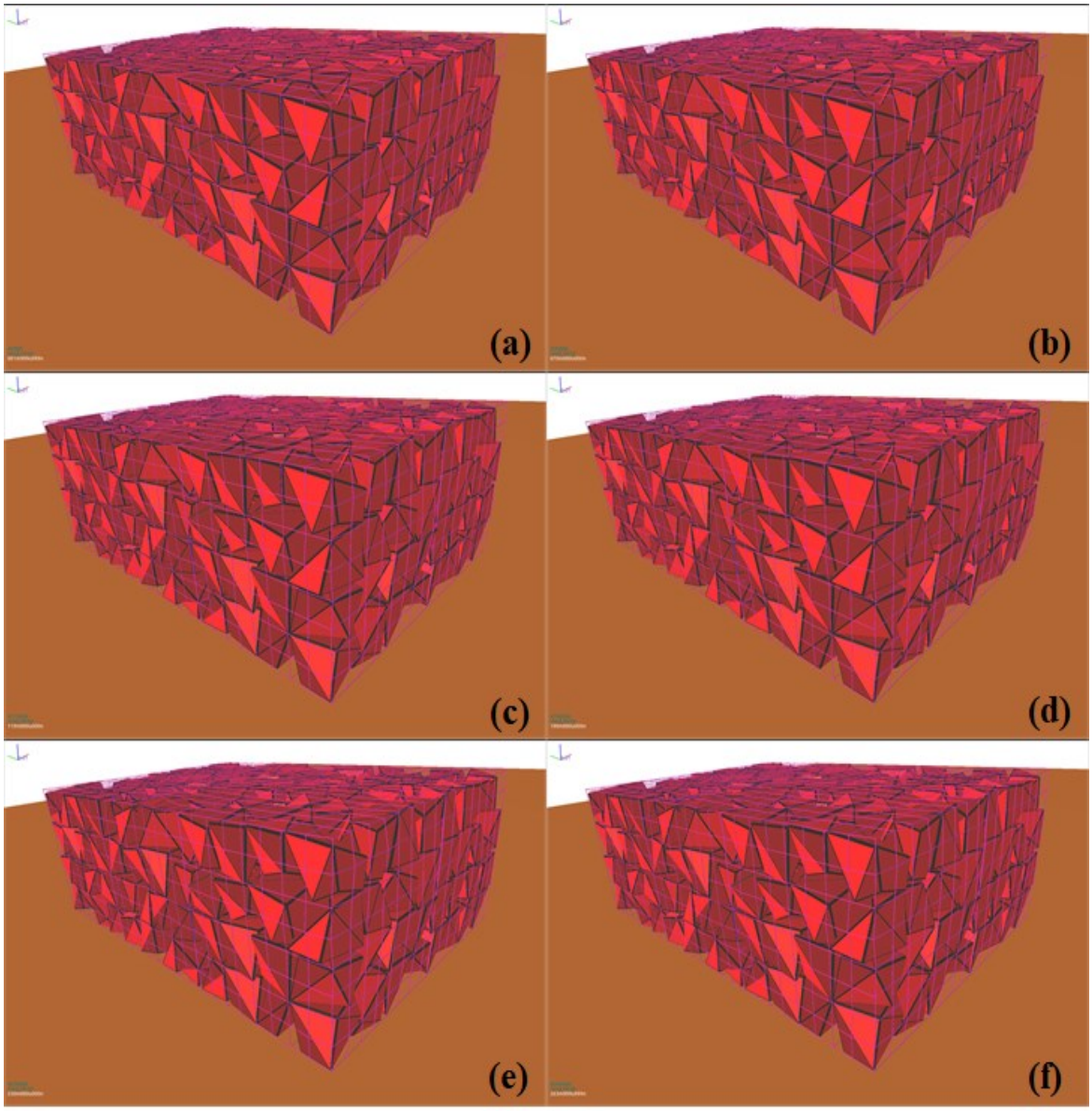

Figure 3.20: Case SBG-IV: Boulder radius of 0.25 ft with initial velocity of 10 ft/s after (front) (a) 0 impacts; (b) 2 impacts; (c) 4 impacts; (d) 6 impacts; (e) 8 impacts; (f) 10 impacts.

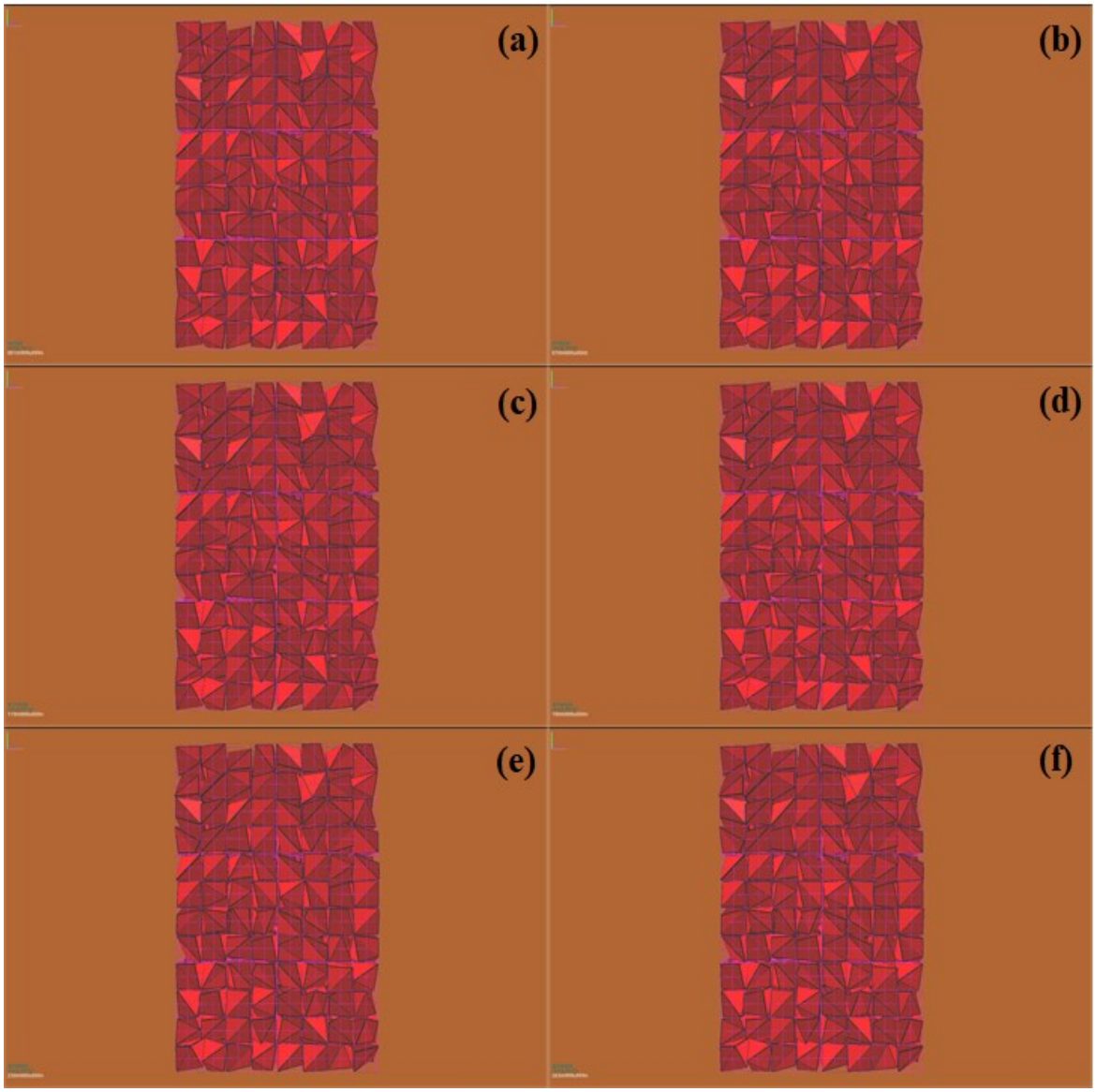

Figure 3.21: Case SBG-IV: Boulder radius of 0.25 ft with initial velocity of 10 ft/s after (plan) (a) 0 impacts; (b) 2 impacts; (c) 4 impacts; (d) 6 impacts; (e) 8 impacts; (f) 10 impacts.

A second simulation was then performed where the velocity of the boulder (radius = 0.25 ft) was increased to 30 ft/s for four sequential impacts. Moderate wire rupture was observed after the fourth impact, but negligible movement was detected throughout the simulation. Figure 3.22 and Figure 3.23 display the frontal and plan view images of the gabion barrier after various impacts have been sustained. The deformations for query points q_2 and q_5 by the end of the simulation were approximately 0.1 ft. The overall deformation of the structure was minor, but in terms of wire rupture it appears that this gabion configuration can fail after four consecutive impacts for the given radius and velocity.

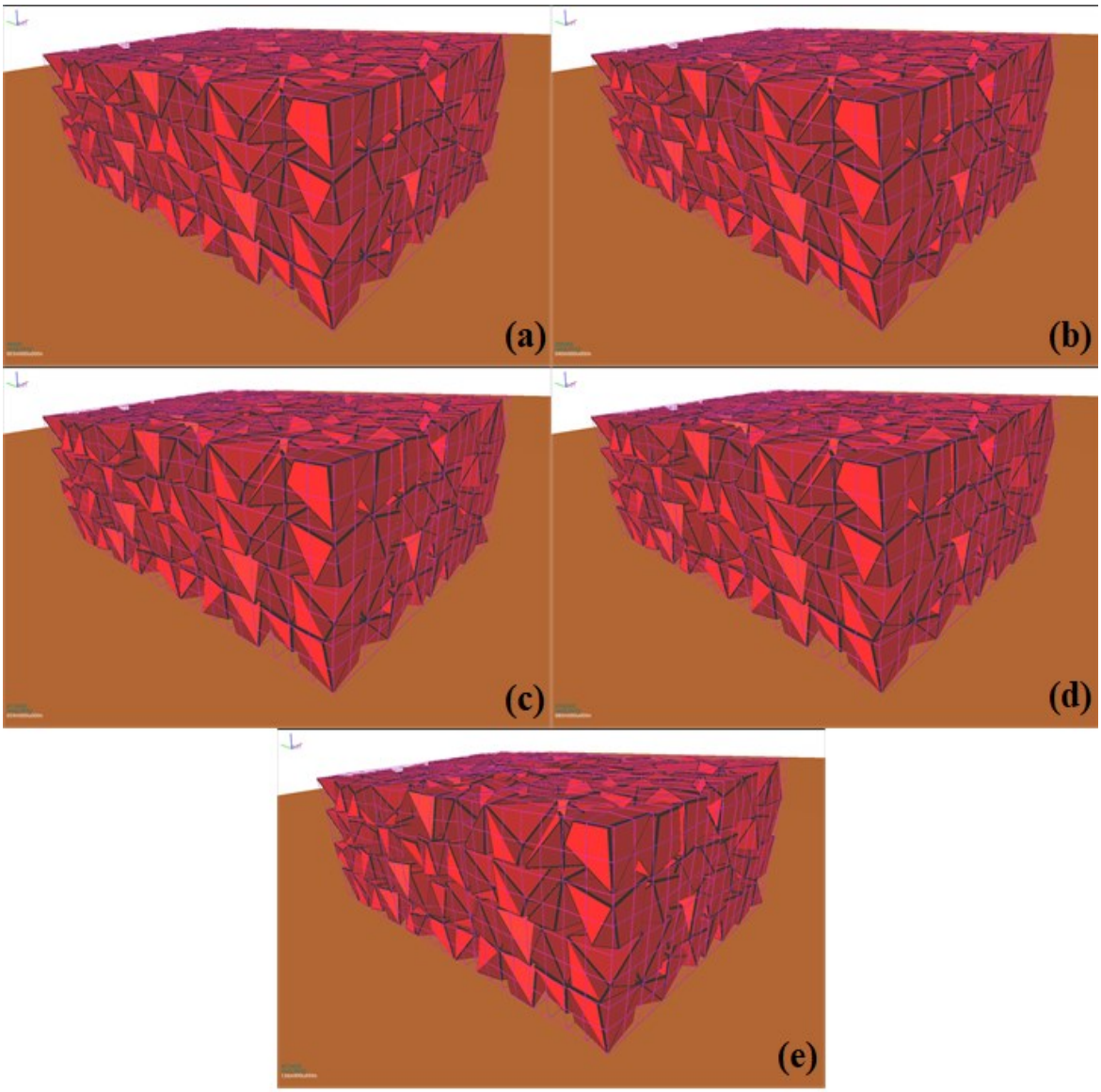

Figure 3.22: Case SBG-V: Boulder radius of 0.25 ft with initial velocity of 30 ft/s after (front) (a) 0 impacts; (b) 1 impacts; (c) 2 impacts; (d) 3 impacts; (e) 4 impacts.

For the next round of impacts, the boulder radius was kept at 0.25 ft, but the velocity was increased to 40 ft/s. After six consecutive impacts, enough damage was accumulated to lead to major wire rupture. Images of the wire damage are presented in Figure 3.24(c) and (d), whereas Figure 3.25 shows the plan view of minor displacement or deformation of the gabion barrier.

Figure 3.26 and Figure 3.27 show the front and plan views, respectively, of a gabion barrier for eight consecutive impacts from a spherical boulder (radius = 0.5 ft) with an initial velocity of 40 ft/s. The wire basket experiences moderate wire rupture and the overall structure deforms and displaces a moderate amount as well (total displacement of query point q_2 is recorded to be approximately 2.5 ft). Sliding is also significant (query points q_1 and q_4 experience

displacements of 1.5 ft and 2.2 ft, respectively) which suggests that the radius of influence for this impact is greater than 4.5 ft (i.e., half the length of the barrier).

In the next set of impacts the radius of the boulder is increased to 0.75 ft but the initial velocity is reduced to 10 ft/s. The state of the gabion barrier after consecutive impacts is presented in Figure 3.28 and Figure 3.29. There is moderate deformation after the ten impacts, but no signs of wire rupture can be observed from the simulation results.

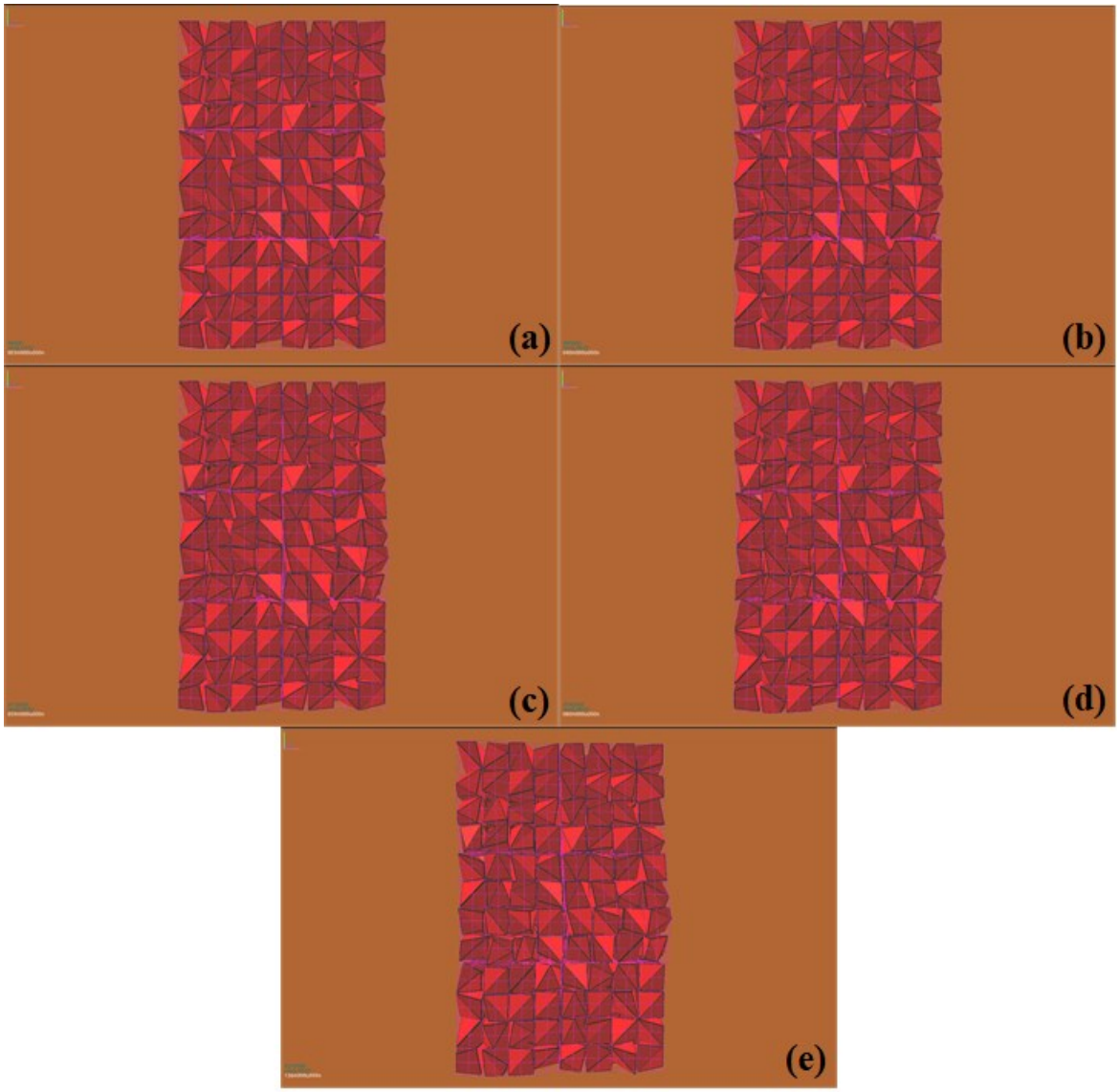

Figure 3.23: Case SBG-V: Boulder radius of 0.25 ft with initial velocity of 30 ft/s after (plan) (a) 0 impacts; (b) 1 impacts; (c) 2 impacts; (d) 3 impacts; (e) 4 impacts.

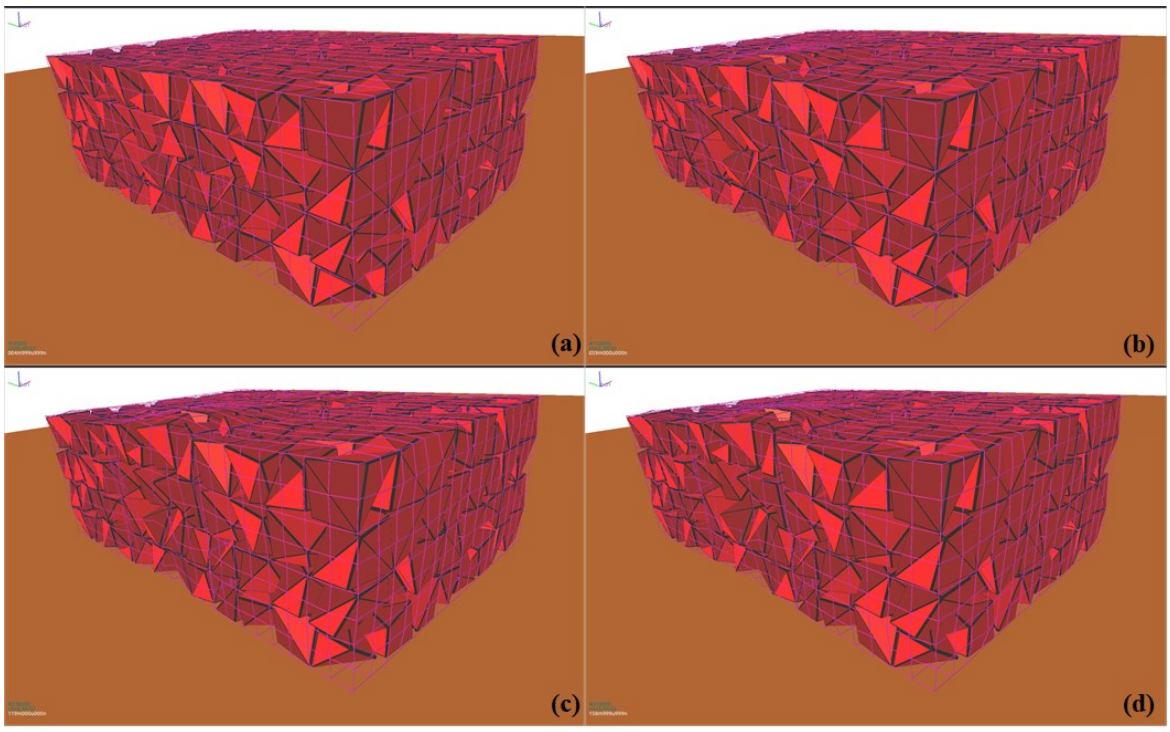

Figure 3.24: Case SBG-VI: Boulder radius of 0.25 ft with initial velocity of 40 ft/s after (front) (a) 0 impacts; (b) 2 impacts; (c) 4 impacts; (d) 6 impacts.

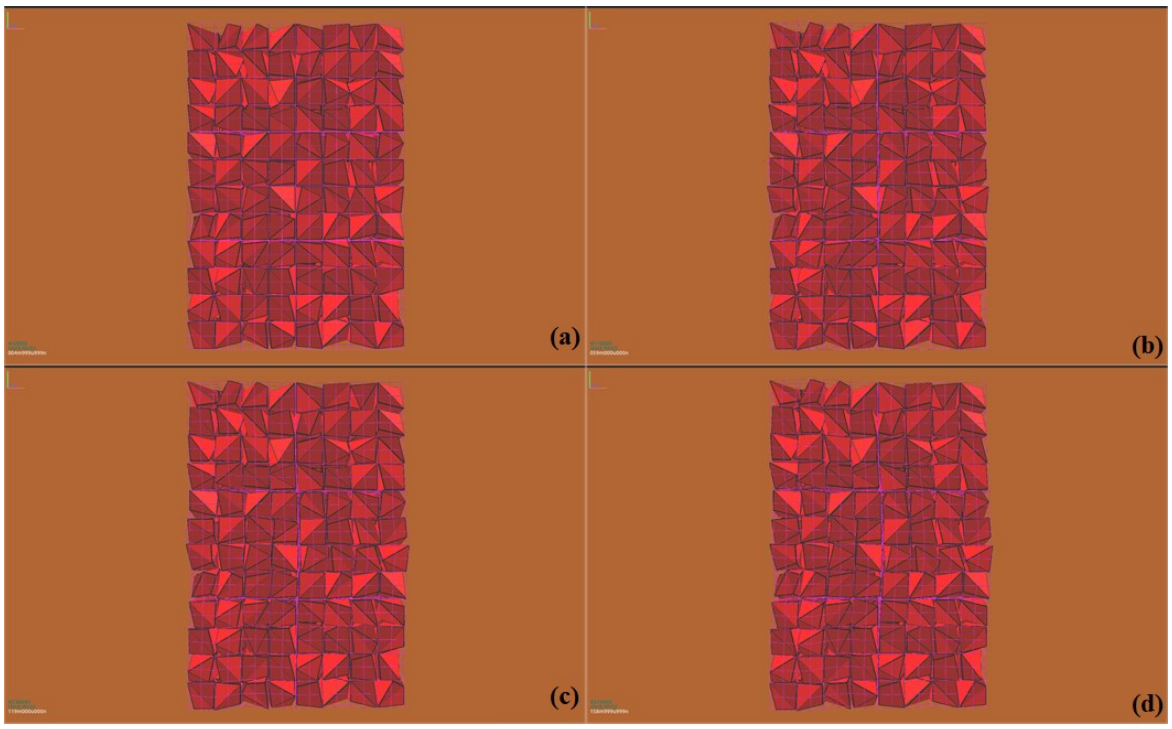

Figure 3.25: Case SBG-VI: Boulder radius of 0.25 ft with initial velocity of 40 ft/s after (plan) (a) 0 impacts; (b) 2 impacts; (c) 4 impacts; (d) 6 impacts.

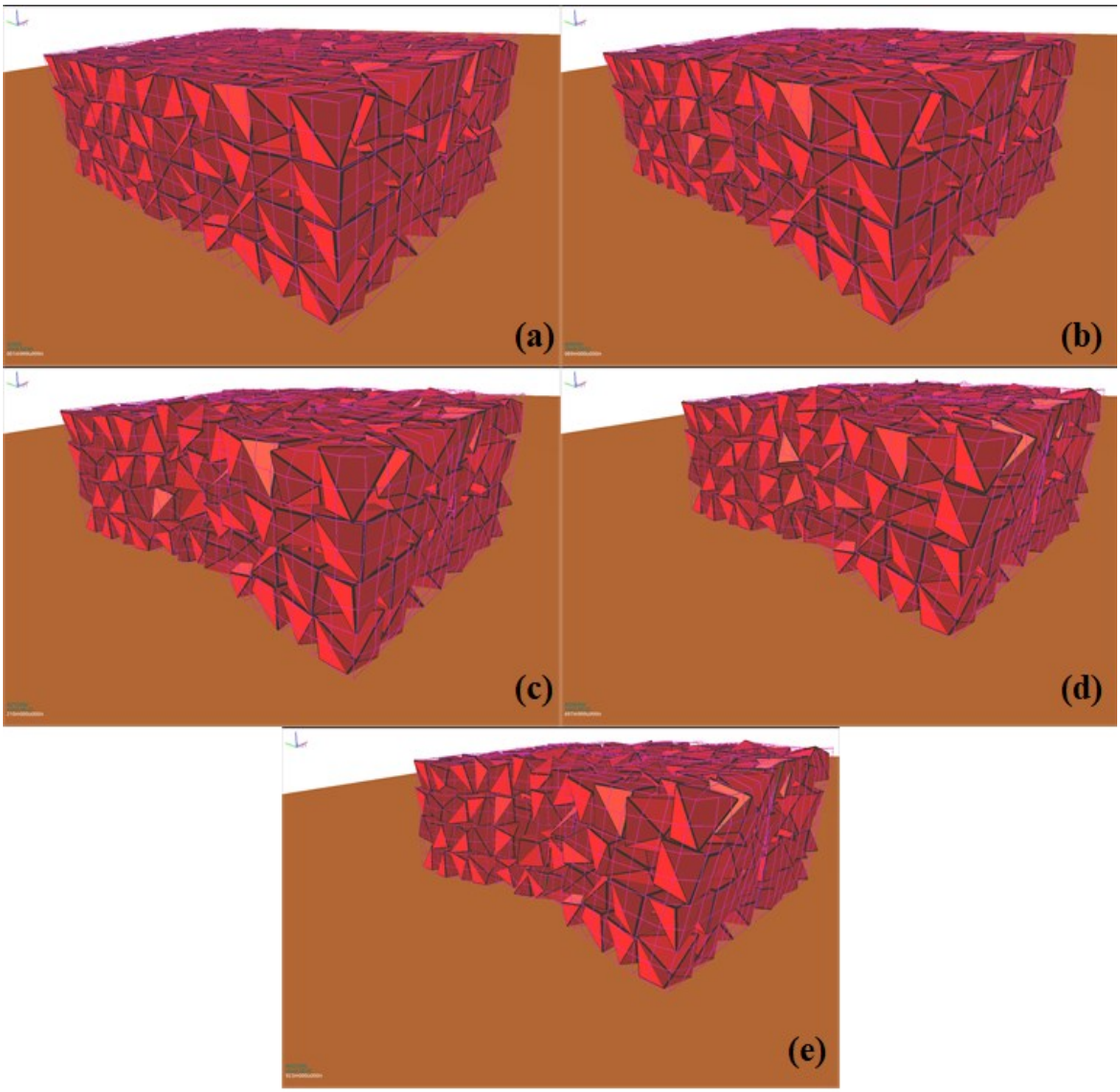

Figure 3.26: Case SBG-VII: Boulder radius of 0.5 ft with initial velocity of 40 ft/s after (front) (a) 0 impacts; (b) 2 impacts; (c) 4 impacts; (d) 6 impacts; (e) 8 impacts.

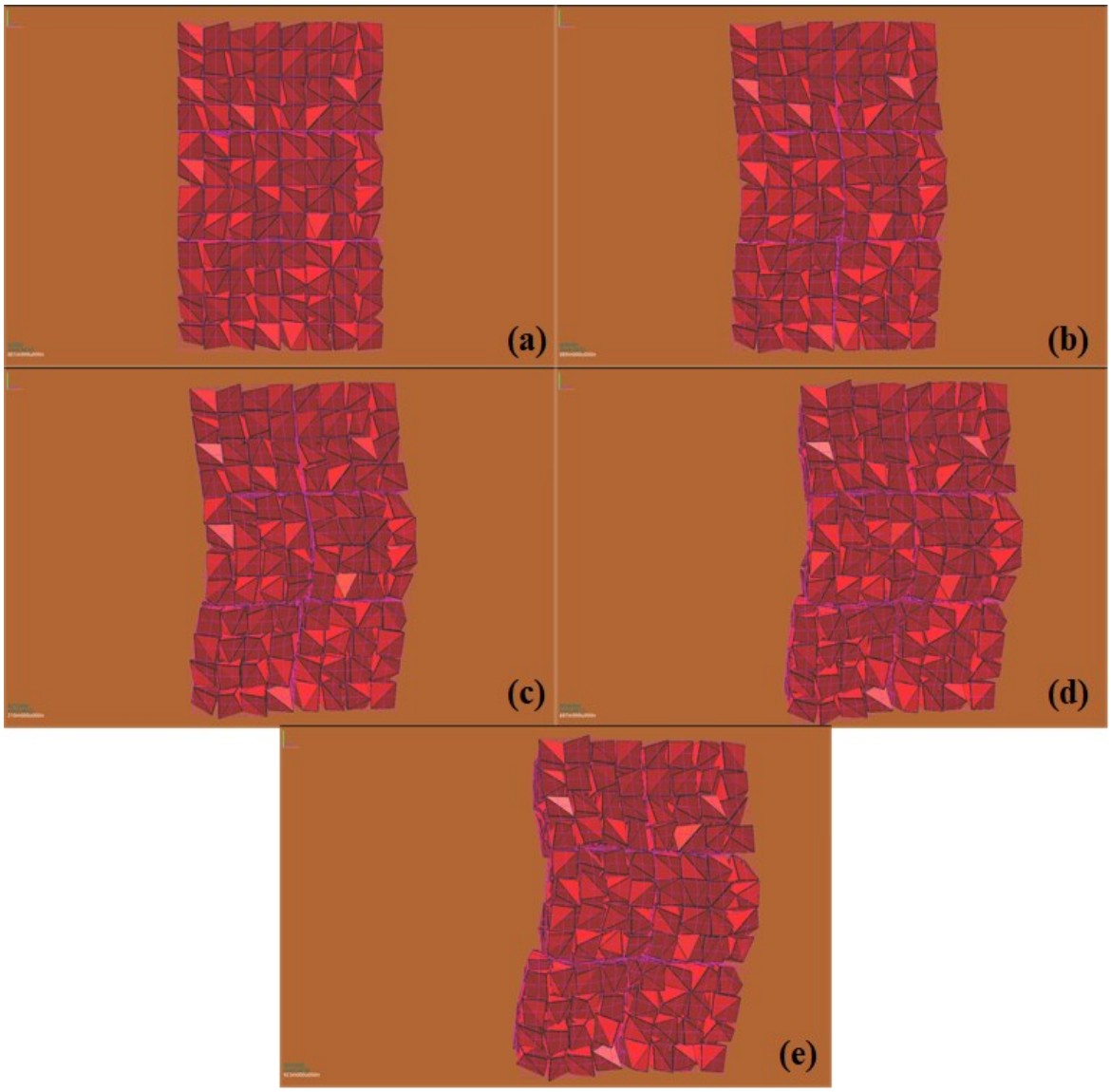

Figure 3.27: Case SBG-VII: Boulder radius of 0.5 ft with initial velocity of 40 ft/s after (plan) (a) 0 impacts; (b) 2 impacts; (c) 4 impacts; (d) 6 impacts; (e) 8 impacts.

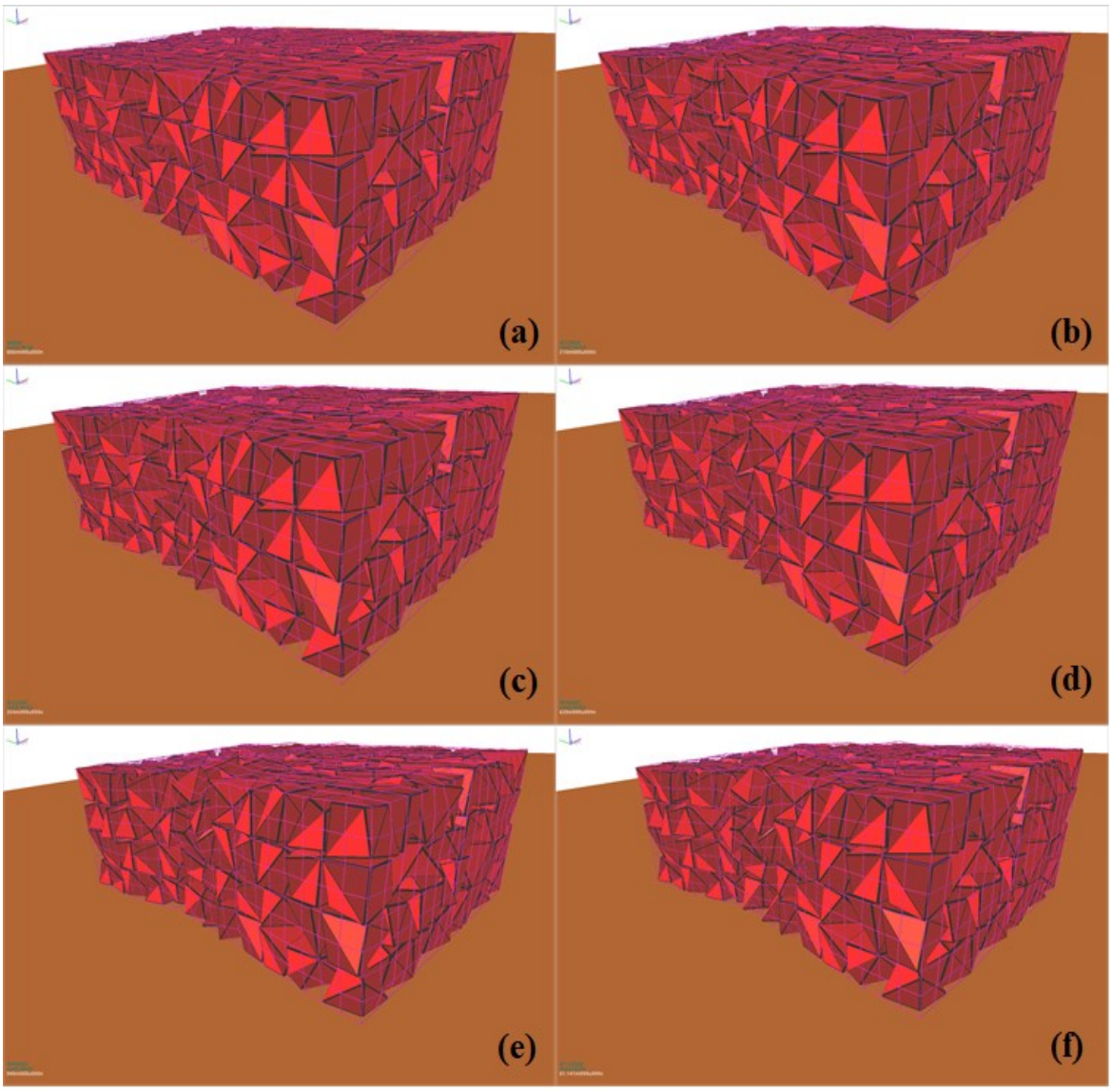

Figure 3.28: Case SBG-VIII: Boulder radius of 0.75 ft with initial velocity of 10 ft/s after (front) (a) 0 impacts; (b) 2 impacts; (c) 4 impacts; (d) 6 impacts; (e) 8 impacts; (f) 10 impacts.

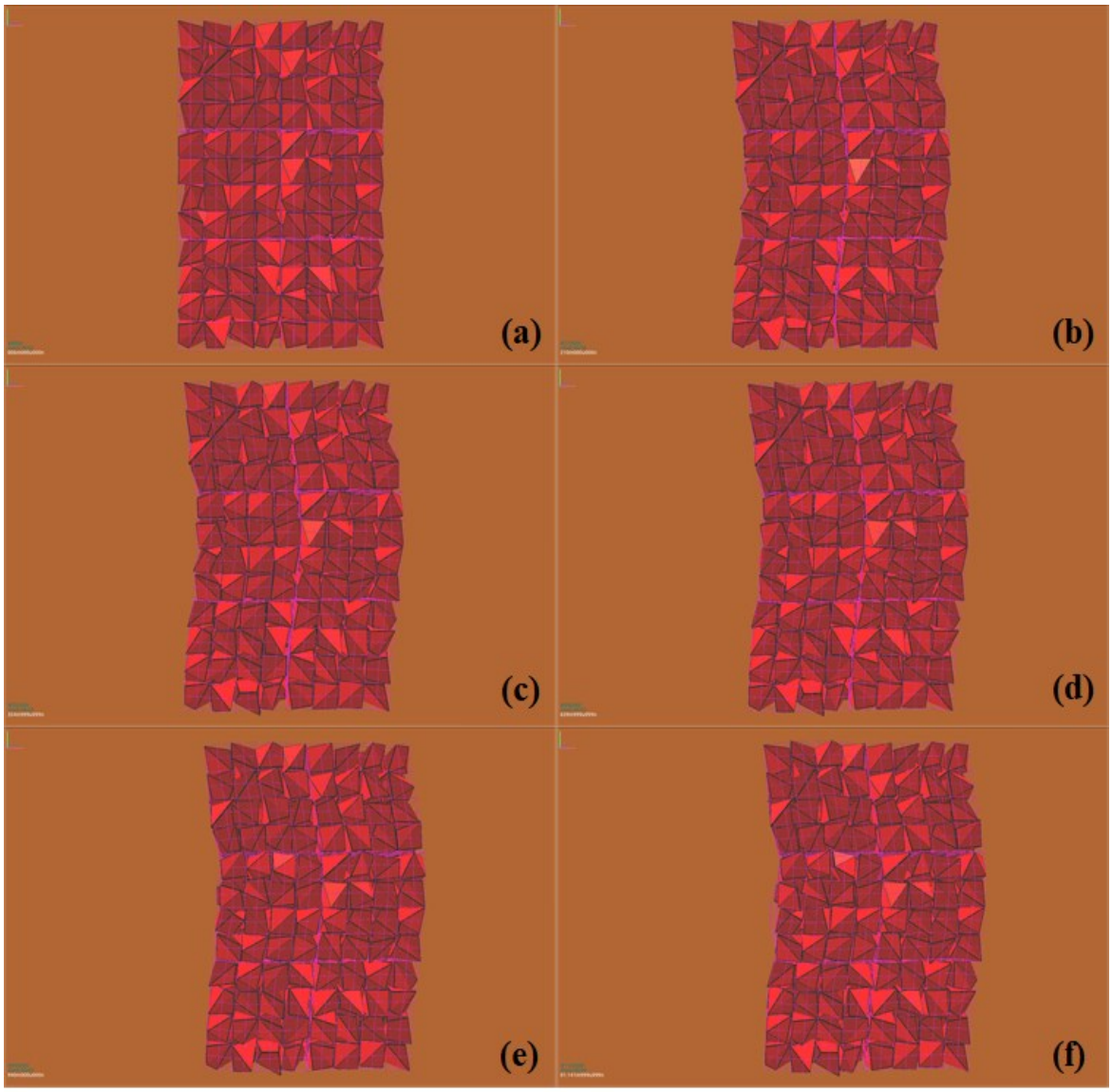

Figure 3.29: Case SBG-VIII: Boulder radius of 0.75 ft with initial velocity of 10 ft/s after (plan) (a) 0 impacts; (b) 2 impacts; (c) 4 impacts; (d) 6 impacts; (e) 8 impacts; (f) 10 impacts.

3.2.3 Test Barrier 3 $(R, C, S) = (2, 3, 2)$

In this set of experiments, the dimensions of the base (columns and rows) stay the same but we double the height to provide more weight, and therefore increase the sliding resistance as well as inertia of the barrier. Spherical boulders of different size and velocity are used to impact the barrier. The barrier is presented in Figure 3.30 and shown schematically in Figure 3.31. Query points are tabulated in Table 3.5.

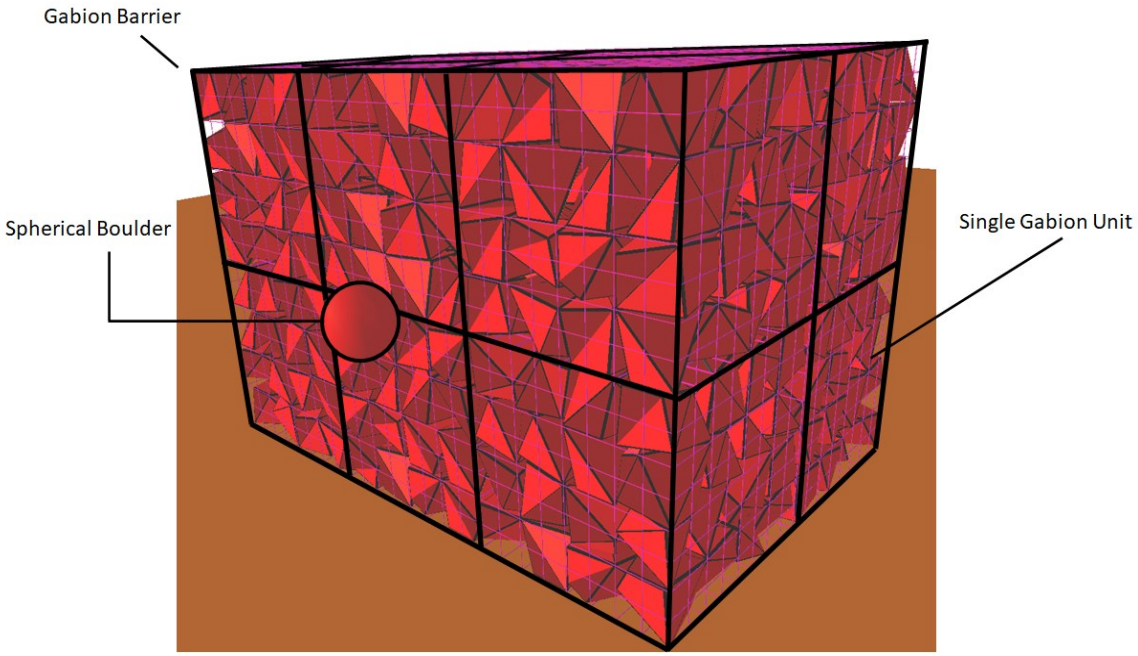

Figure 3.30: Initial conditions for boulder radius of 0.25 ft impacting a gabion barrier constructed from 12 gabion units with dimensions: $3' \times 3' \times 3'$ (rows = 2; columns = 3; stacks = 2).

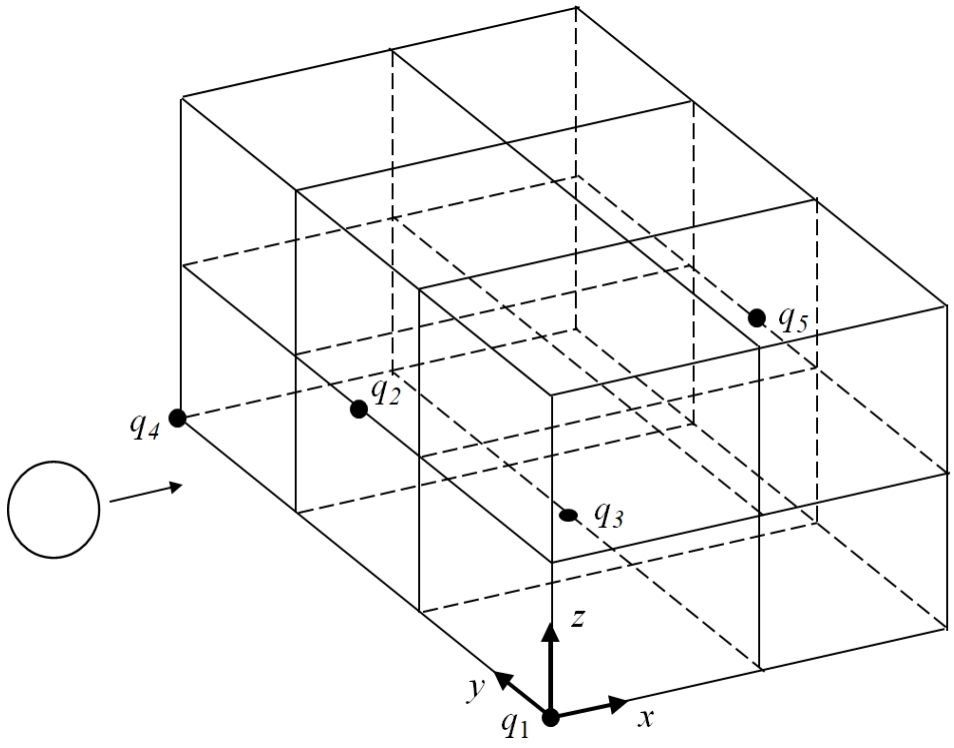

Figure 3.31: Definition sketch for displacement query points on gabion barrier with dimensions: $3' \times 3' \times 3'$ (rows = 2; columns = 3; stacks = 2).

Table 3.5: List of Query Points for Gabion Movement (rows = 2; columns = 3; stacks = 2)

Query Point	Label on Figure 3.31	Coordinates (ft.)
Query 1	q_1	(0, 0, 0)
Query 2	q_2	(0, 4.5, 3)
Query 3	q_3	(3, 4.5, 0)
Query 4	q_4	(0, 9, 0)
Query 5	q_5	(6, 4.5, 3)

The first set of simulations for this gabion barrier configuration involve a boulder of radius 0.25 ft impacting the wall at a velocity of 10 ft/s. After a total of ten consecutive impacts, there was no significant observable damage. Figure 3.32 and Figure 3.33, which are the front and plan views of the gabion barrier, respectively, reveal that the structure has remained essentially intact during the simulation. As expected from previous simulations involving smaller barrier dimensions, the barrier remains structurally sound. The velocity of the boulder is then increased to ascertain if any deformation or wire rupture occurs at a higher energy level of impact.

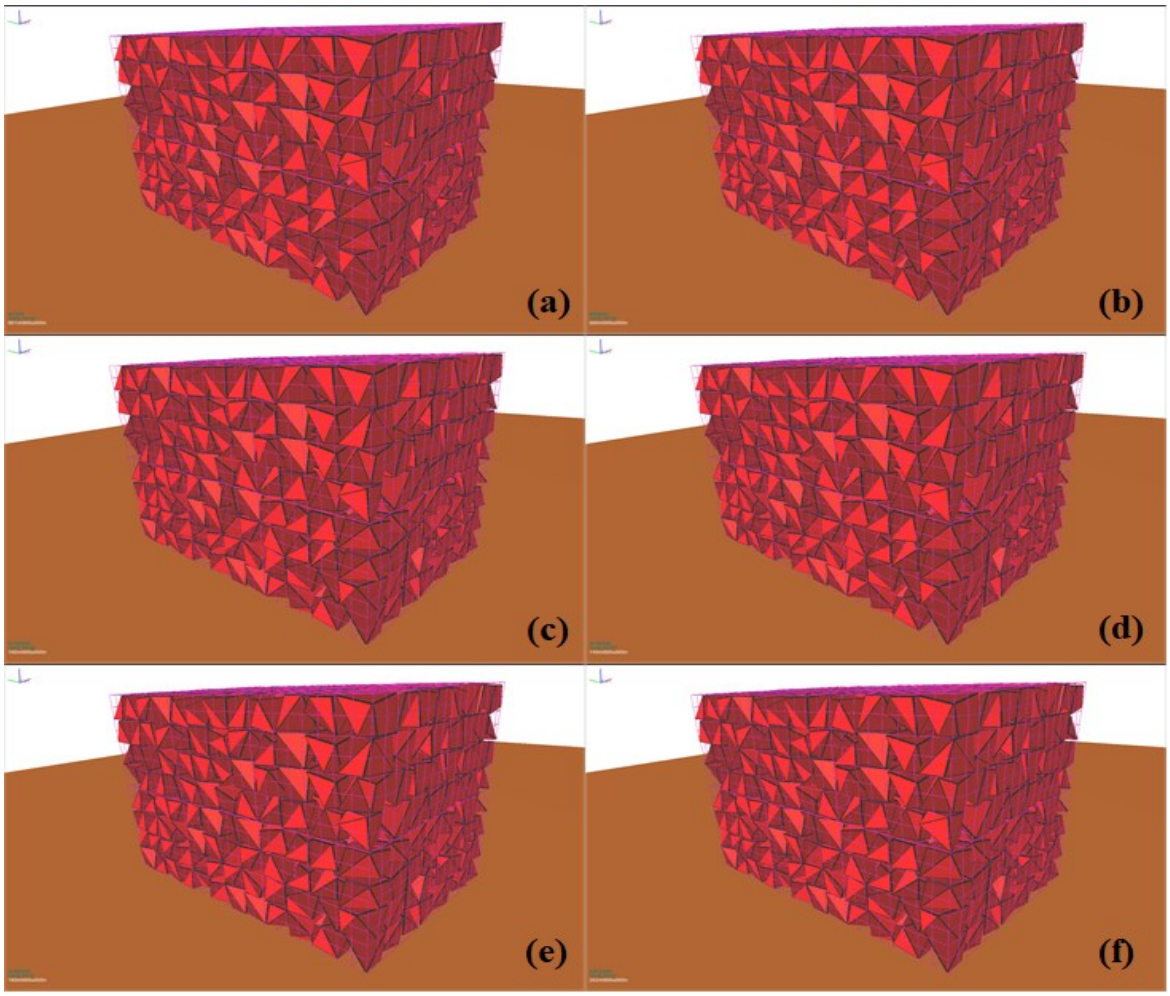

Figure 3.32: Case SBG-IX: Boulder radius of 0.25 ft with initial velocity of 10 ft/s after (front) (a) 0 impacts; (b) 2 impacts; (c) 4 impacts; (d) 6 impacts; (e) 8 impacts; (f) 10 impacts.

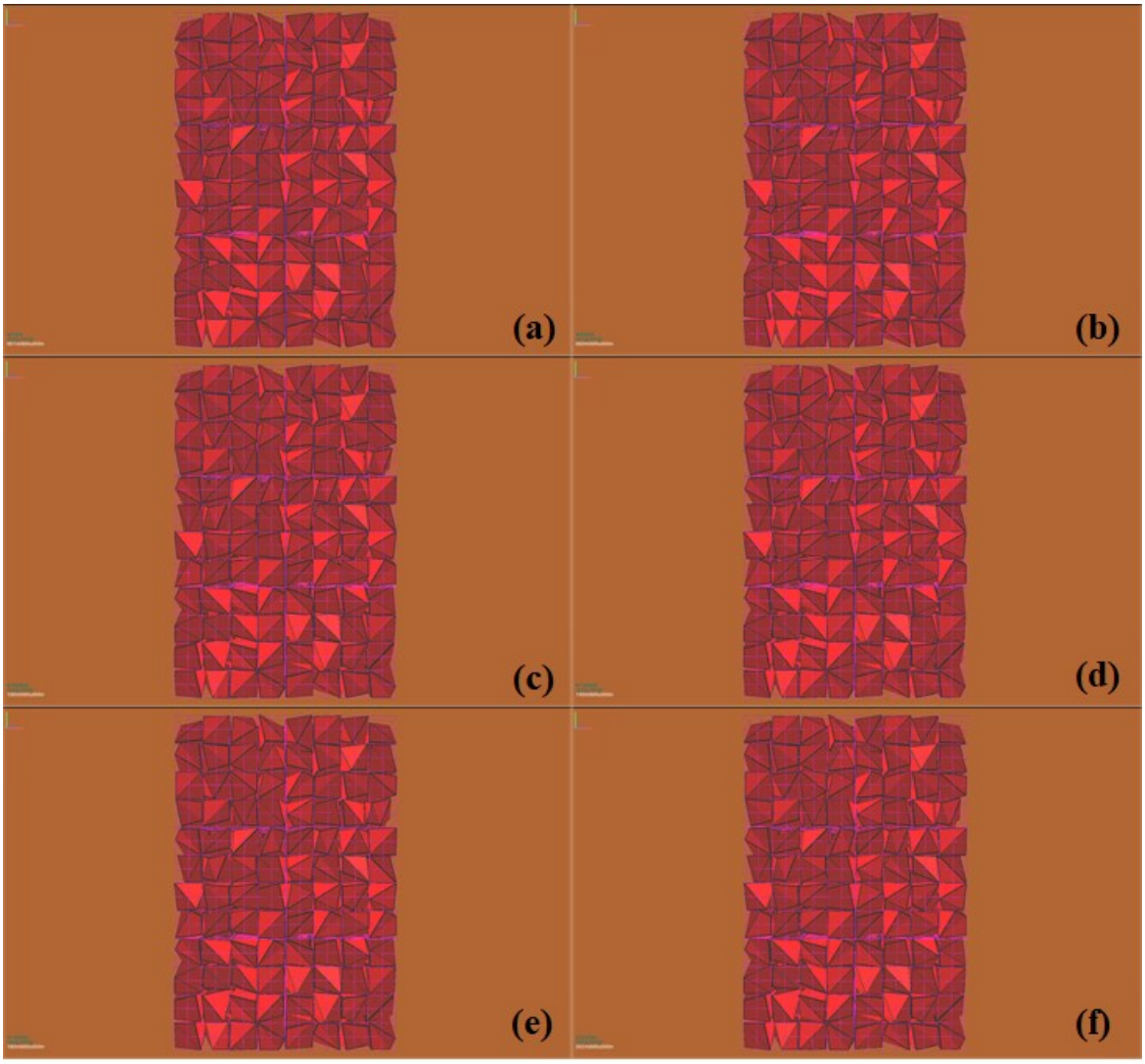

Figure 3.33: Case SBG-IX: Boulder radius of 0.25 ft with initial velocity of 10 ft/s after (plan) (a) 0 impacts; (b) 2 impacts; (c) 4 impacts; (d) 6 impacts; (e) 8 impacts; (f) 10 impacts.

For the next series of simulations, the boulder radius remains at 0.25 feet, but the velocity is increased to 50 ft/s. The deformation after ten impacts is minor and there is no apparent wire rupture (see Figure 3.34 and Figure 3.35). It is concluded from these tests that boulders of this size do negligible damage (over the range of considered velocities: 5 ft/s – 50 ft/s) to a gabion barrier of these dimensions and wire diameter (0.120 in.), and therefore do not likely need to be considered any further.

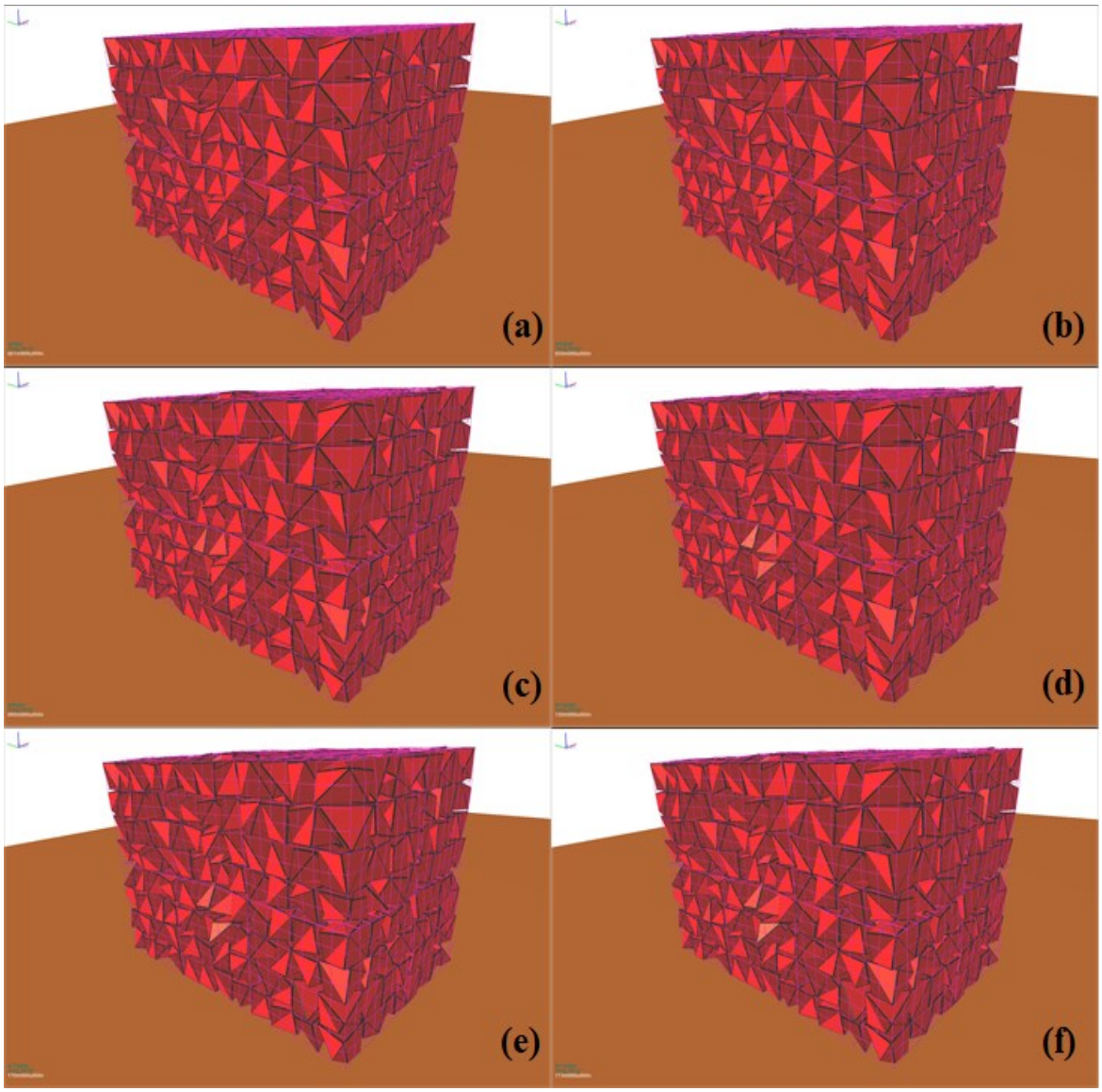

Figure 3.34: Case SBG-X: Boulder radius of 0.25 ft with initial velocity of 50 ft/s after (front) (a) 0 impacts; (b) 2 impacts; (c) 4 impacts; (d) 6 impacts; (e) 8 impacts; (f) 10 impacts.

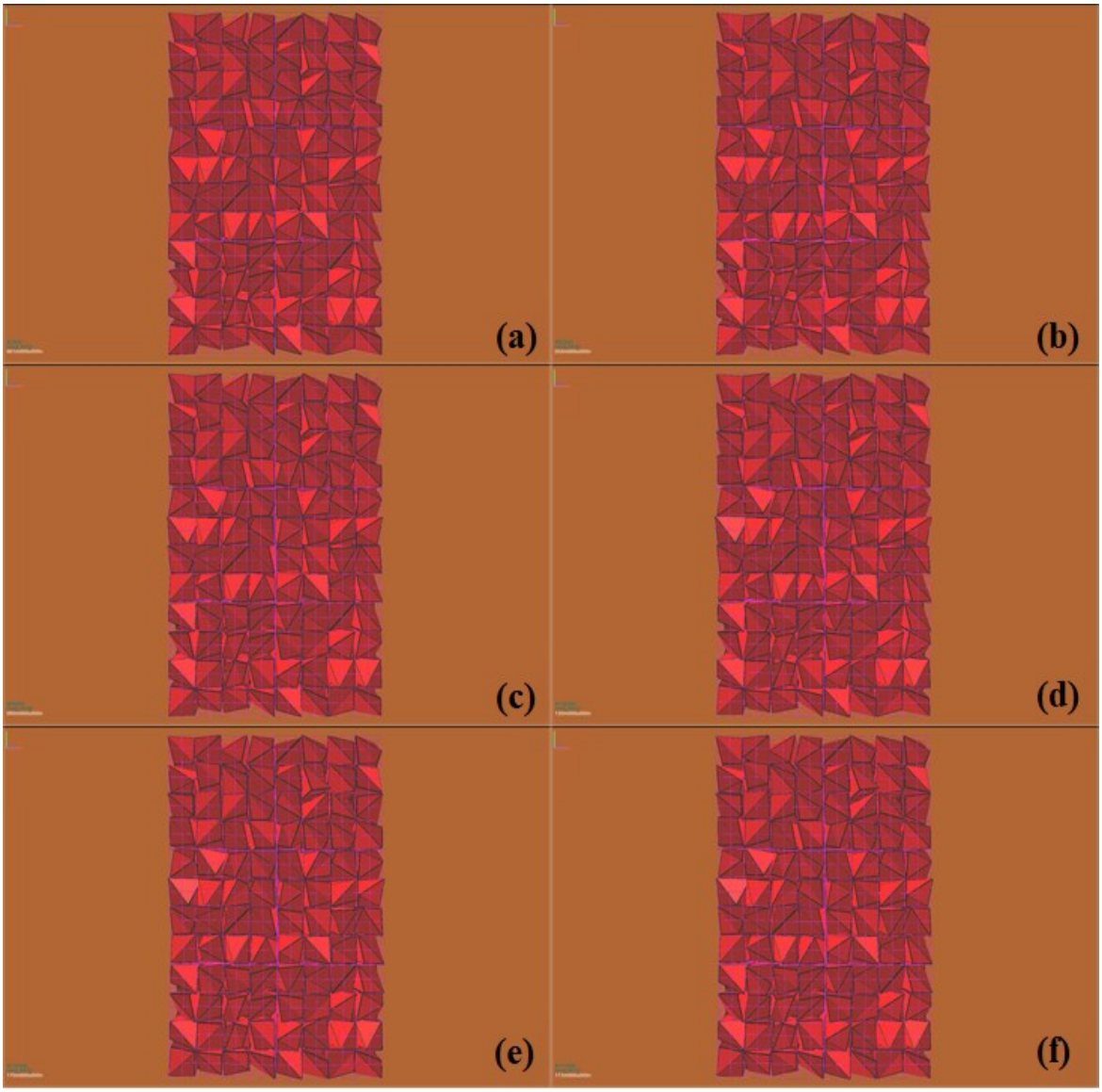

Figure 3.35: Case SBG-X: Boulder radius of 0.25 ft with initial velocity of 50 ft/s after (plan) (a) 0 impacts; (b) 2 impacts; (c) 4 impacts; (d) 6 impacts; (e) 8 impacts; (f) 10 impacts.

The boulder radius is now increased to 0.50 ft in order to test the performance of the gabion under impacts involving a greater momentum. For the test case with a velocity of 10 ft/s, the recorded damage, deformation, and movement are negligible after ten impacts, as is displayed in Figure 3.36 and Figure 3.37. There is some minor wire deformation present, but the exterior and contents of the barrier overall are stable and intact.

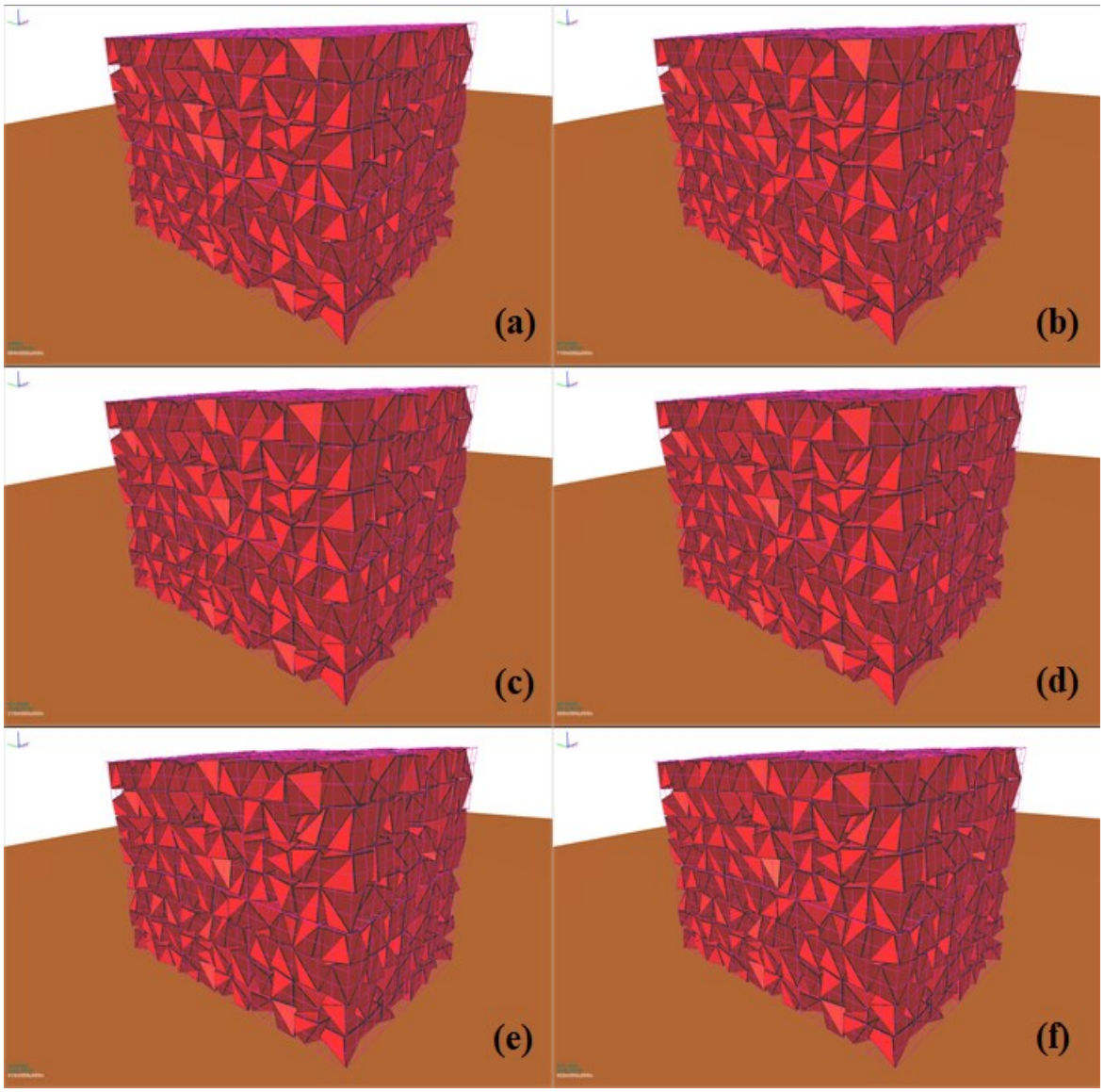

Figure 3.36: Case SBG-XI: Boulder radius of 0.50 ft with initial velocity of 10 ft/s after (front) (a) 0 impacts; (b) 2 impacts; (c) 4 impacts; (d) 6 impacts; (e) 8 impacts; (f) 10 impacts.

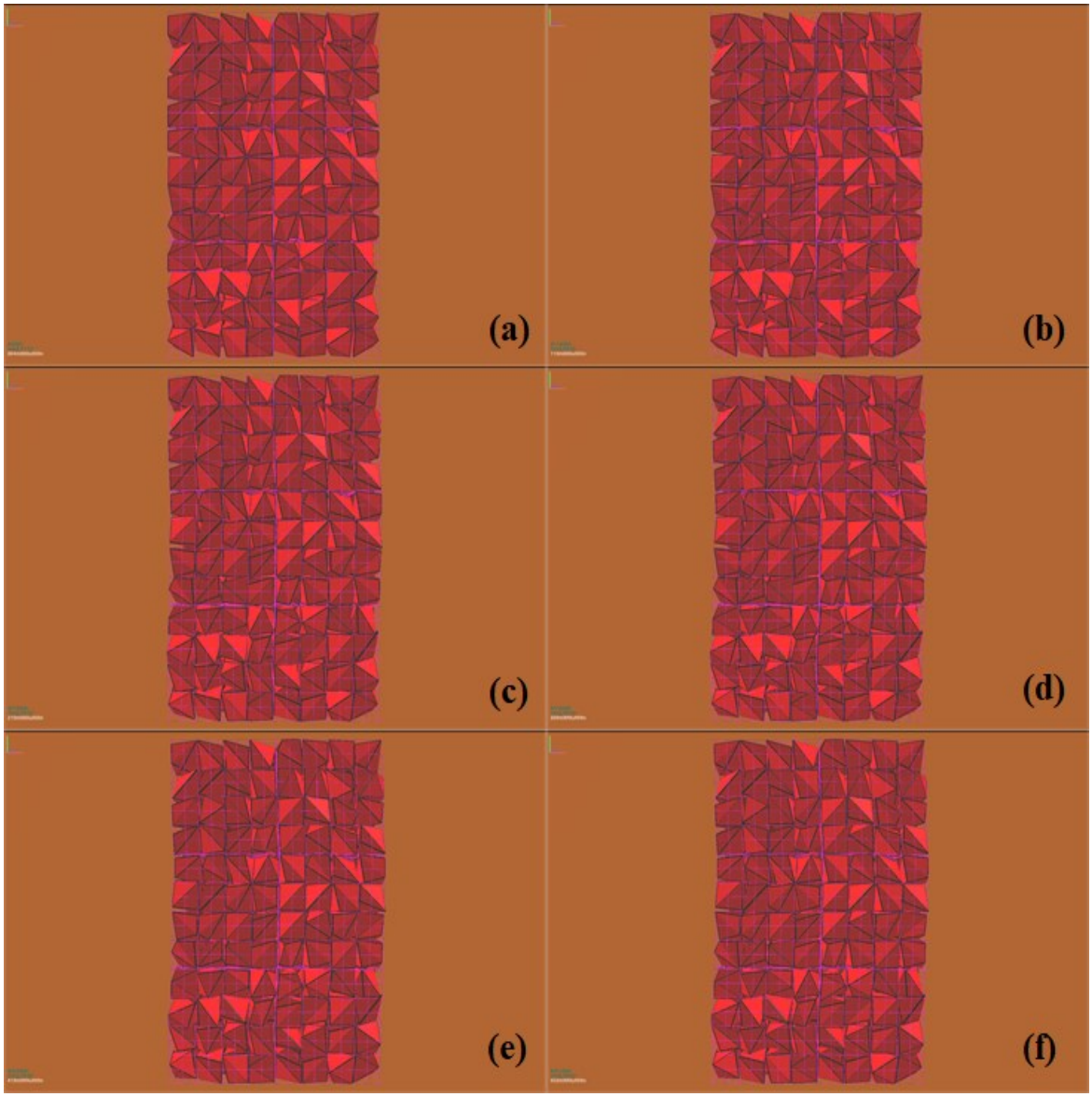

Figure 3.37: Case SBG-XI: Boulder radius of 0.50 ft with initial velocity of 10 ft/s after (plan) (a) 0 impacts; (b) 2 impacts; (c) 4 impacts; (d) 6 impacts; (e) 8 impacts; (f) 10 impacts.

The velocity of the boulder is then increased to 30 ft/s and ten impacts are performed on the gabion barrier. With this velocity, we begin to see some minor deformation on the front and back of the gabion barrier (Figure 3.38). Experiments are then performed where the radius is 0.75 ft which results in moderate displacement as shown in Figure 3.39 and Figure 3.40 after nine impacts at a velocity of 30 ft/s. However, once the boulder radius is increased to 1.0 ft we observe significant damage, primarily in the form of displacement after the middle section of gabion units becomes dislodged from the adjacent modules. This failure is presented in Figure 3.41 and occurs after four impacts at a velocity of 30 ft/s. The damage becomes more pronounced after increasing the boulder radius to 1.5 ft. As shown in Figure 3.42, two of the gabion units become airborne after impacted once by the boulder at a velocity of 30 ft/s. The

severe damage incurred by the gabion barrier suggests that the number of rows of gabion units should be increased to provide more resistance against impacts of this magnitude.

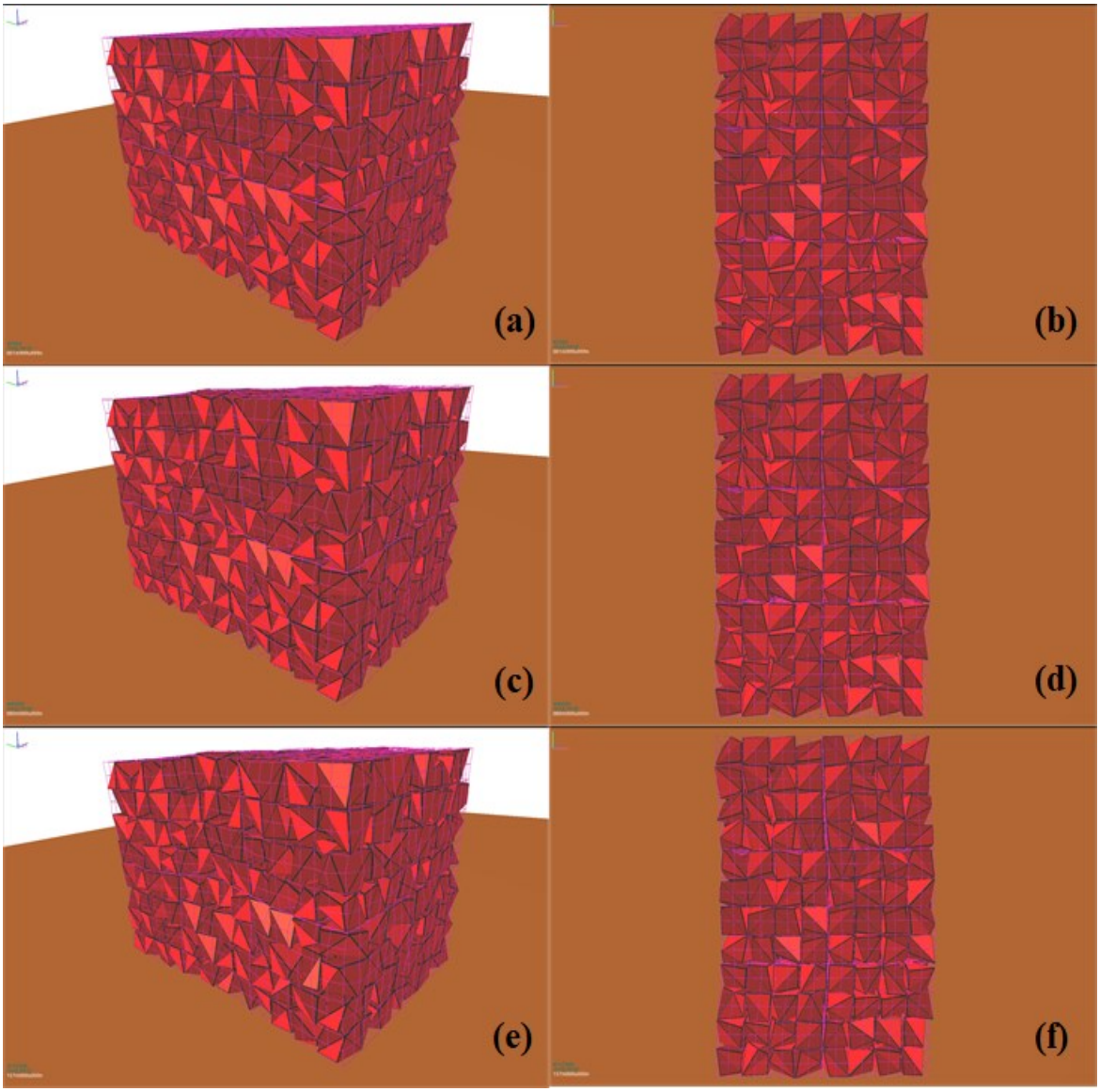

Figure 3.38: Case SBG-XII: Boulder radius of 0.50 ft with initial velocity of 30 ft/s after (plan) (a) 0 impacts; (b) 2 impacts; (c) 4 impacts.

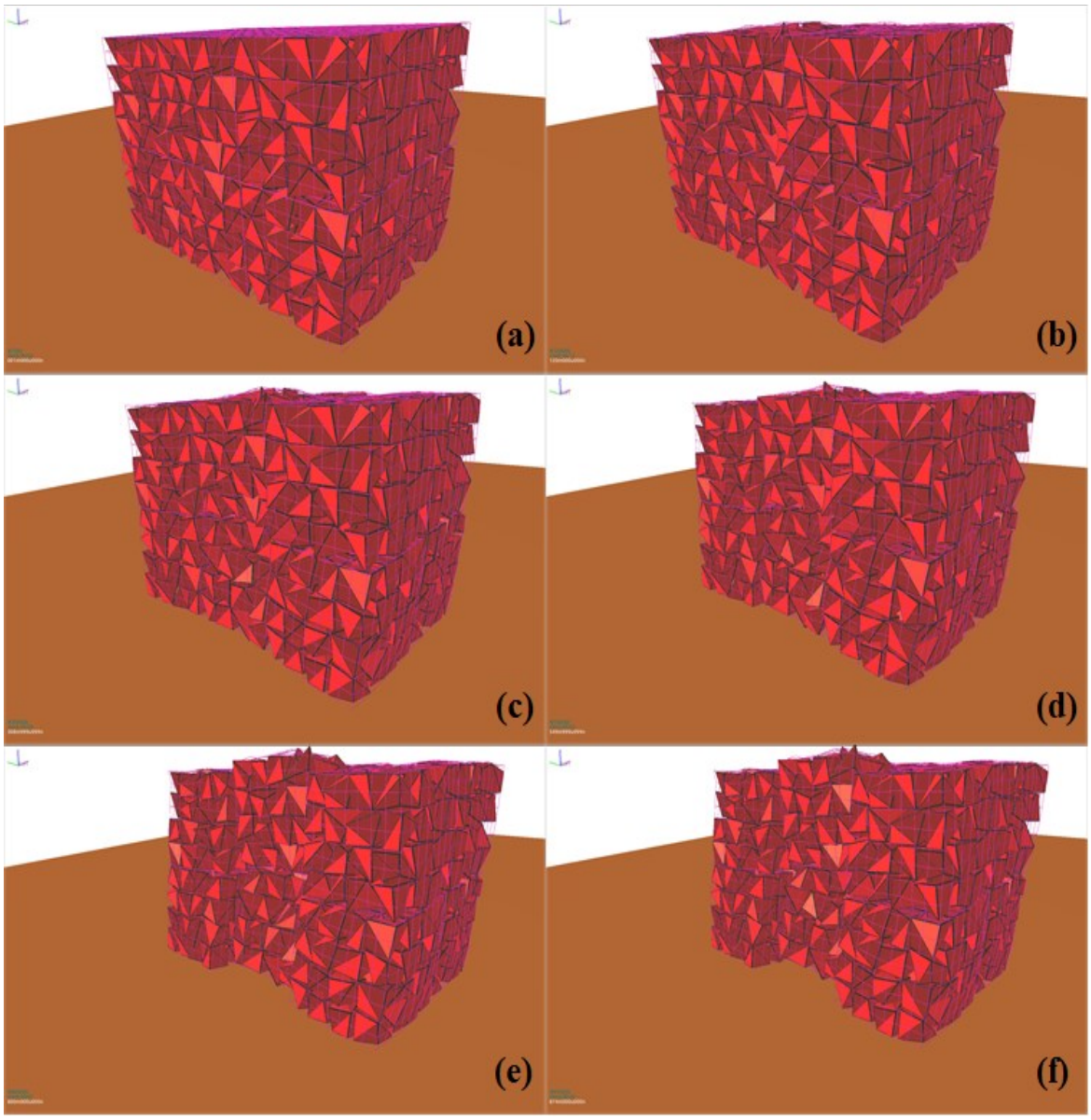

Figure 3.39: Case SBG-XIII: Boulder radius of 0.75 ft with initial velocity of 30 ft/s after (front) (a) 0 impacts; (b) 2 impacts; (c) 4 impacts; (d) 6 impacts; (e) 8 impacts; (f) 9 impacts.

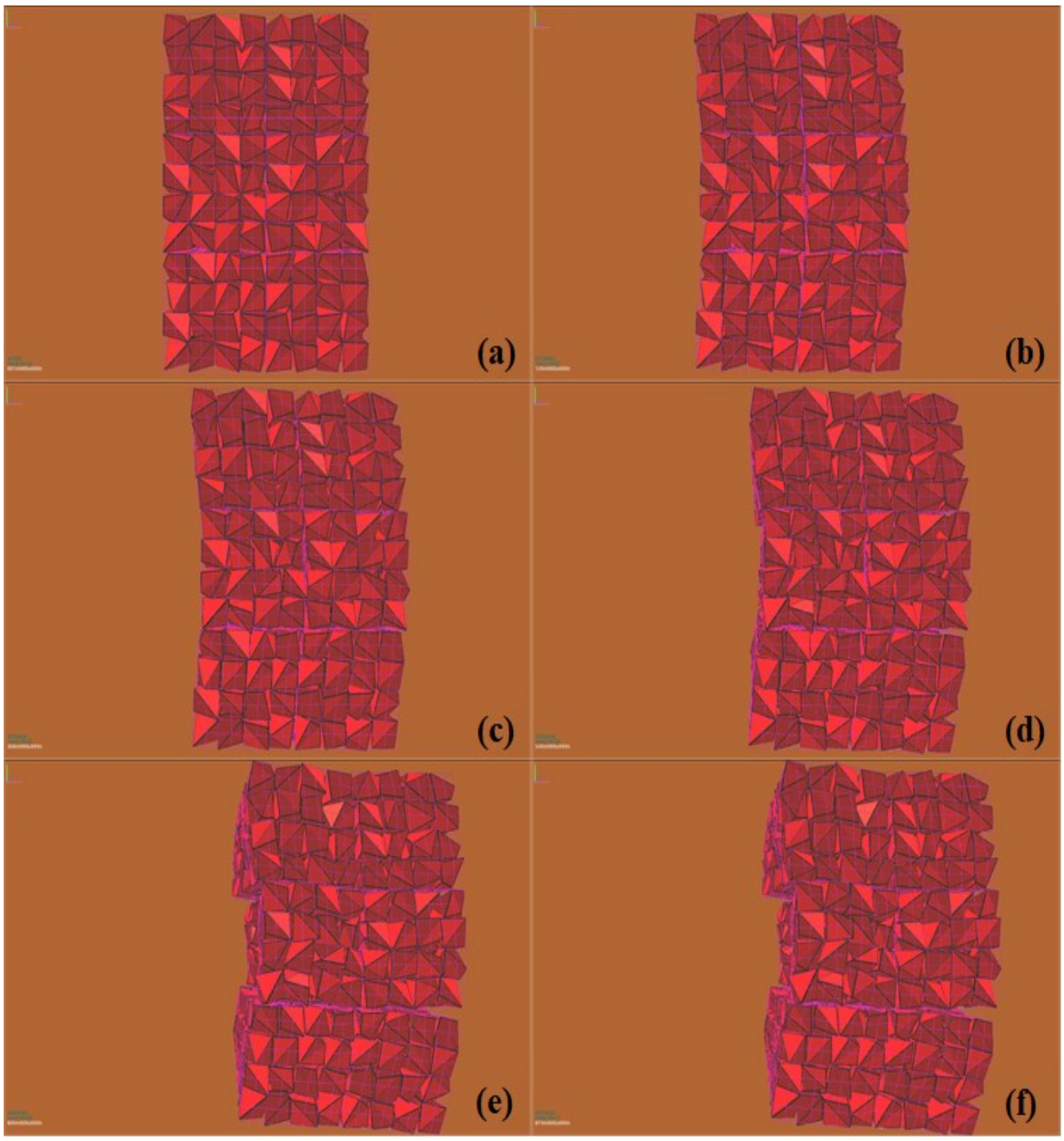

Figure 3.40: Case SBG-XIII: Boulder radius of 0.75 ft with initial velocity of 30 ft/s after (plan) (a) 0 impacts; (b) 2 impacts; (c) 4 impacts; (d) 6 impacts; (e) 8 impacts; (f) 9 impacts.

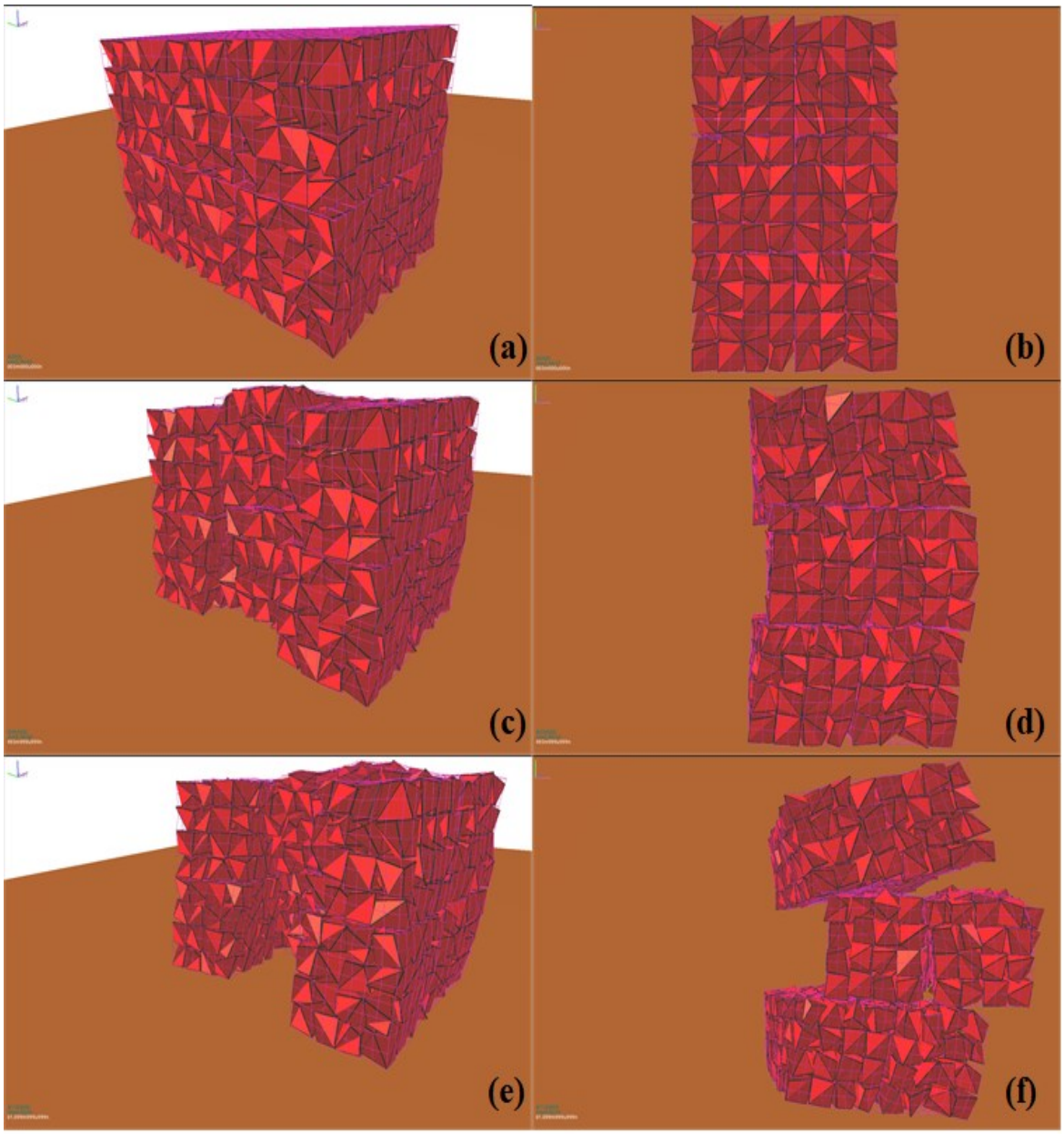

Figure 3.41: Case SBG-XIV: Boulder radius of 1.0 ft with initial velocity of 30 ft/s after (plan) (a) 0 impacts; (c) 2 impacts; (e) 4 impacts.

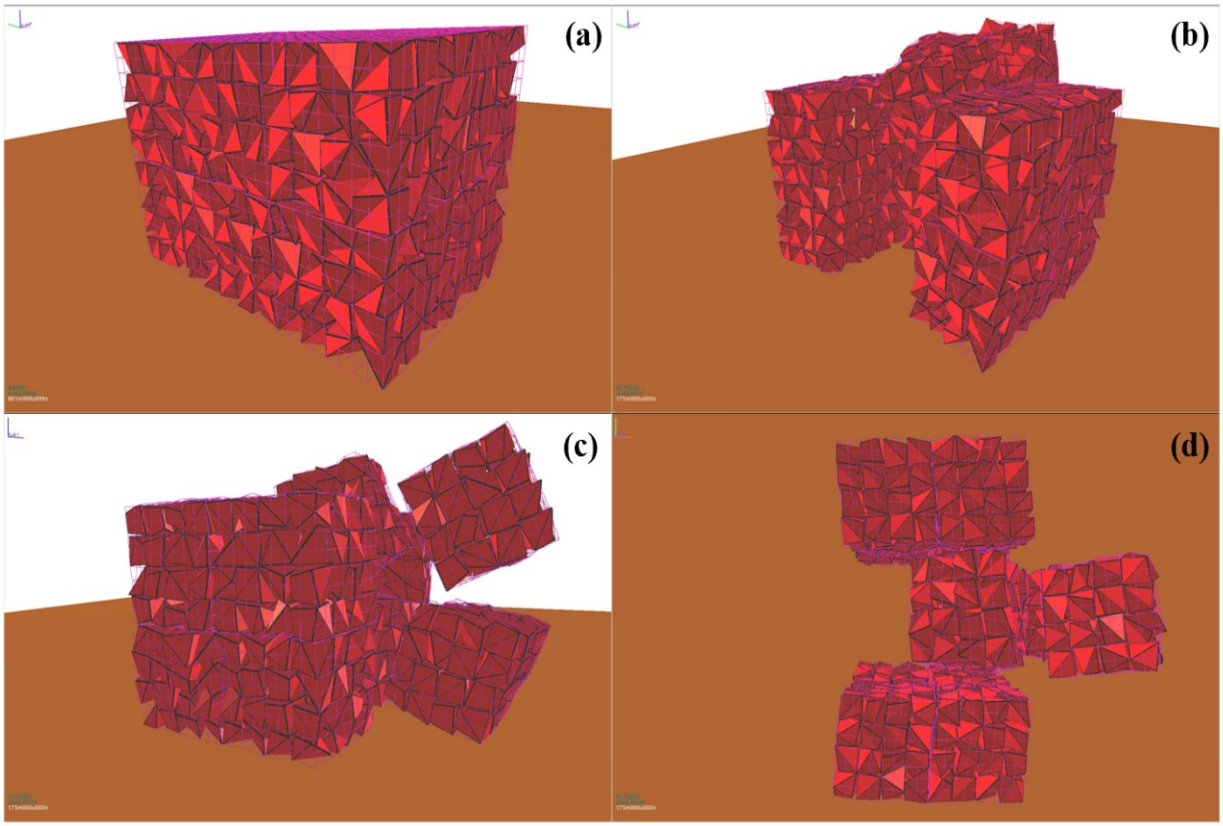

Figure 3.42: Case SBG-XV: Boulder radius of 1.5 ft with initial velocity of 30 ft/s (a) initial front view; (b) front view after one impact; (c) back view after one impact; (d) plan view after one impact.

3.2.4 Test Barrier 4 $(R, C, S) = (3, 3, 2)$

In this set of experiments the gabion barrier is composed of three rows, three columns, and two stacks of $3' \times 3' \times 3'$ gabion units. The barrier is presented in Figure 3.43 and shown schematically in Figure 3.44. Query points are tabulated in Table 3.6. The barrier is subjected to a boulder impact with a radius of 1.5 ft and an initial velocity of 30 ft/s. The center of the barrier dislodges from its adjacent sections and displaces slightly over 3 ft (recorded value of query point q_2), as shown in Figure 3.45. The extra row of gabions in Case SBG-XV appears to reduce the amount of movement compared with Case SBG-XIV, but there is still significant sliding after the dislodgement occurs.

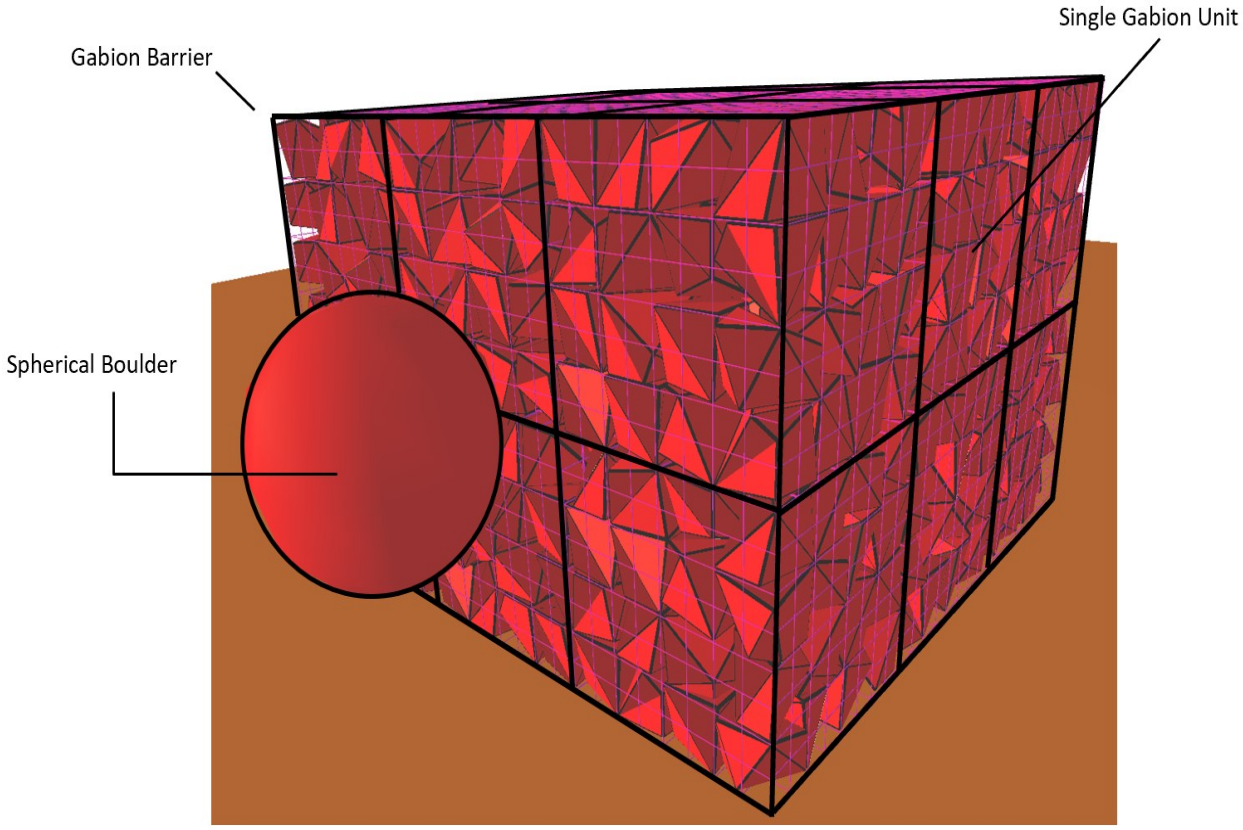

Figure 3.43: Initial conditions for boulder radius of 1.5 ft impacting a gabion barrier constructed from 18 gabion units with dimensions: $3' \times 3' \times 3'$ (rows = 3; columns = 3; stacks = 2).

Table 3.6: List of Query Points for Gabion Movement (rows = 3; columns = 3; stacks = 2)

Query Point	Label on Figure 3.44	Coordinates (ft.)
Query 1	q_1	(0, 0, 0)
Query 2	q_2	(0, 4.5, 3)
Query 3	q_3	(4.5, 4.5, 0)
Query 4	q_4	(0, 9, 0)
Query 5	q_5	(9, 4.5, 3)

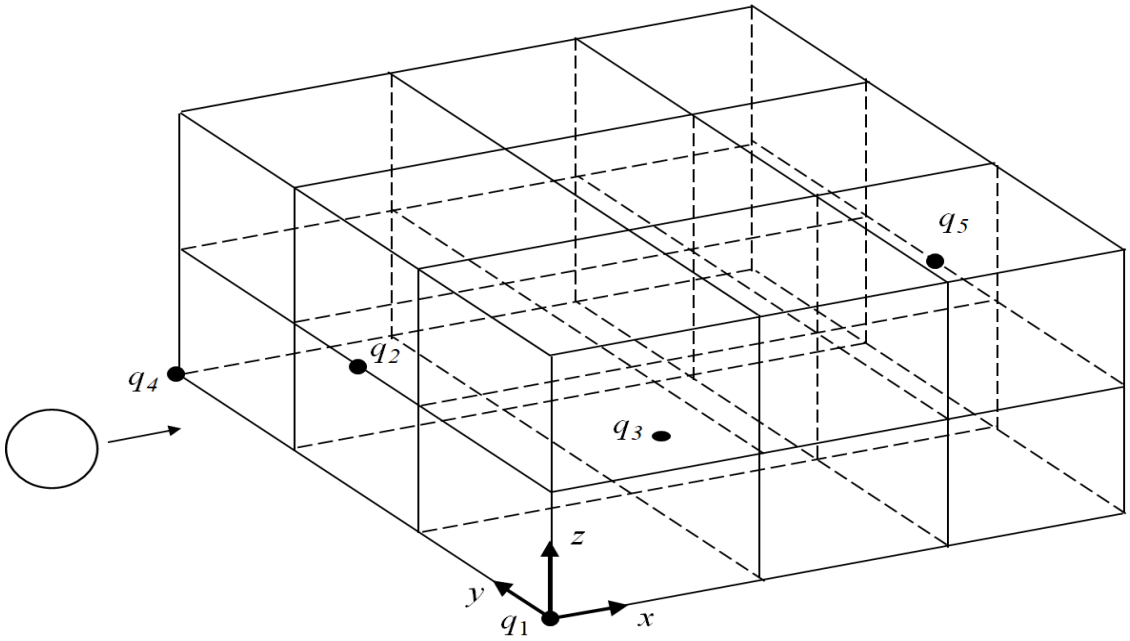

Figure 3.44: Definition sketch for displacement query points on gabion barrier with dimensions: $3' \times 3' \times 3'$ (rows = 3; columns = 3; stacks = 2).

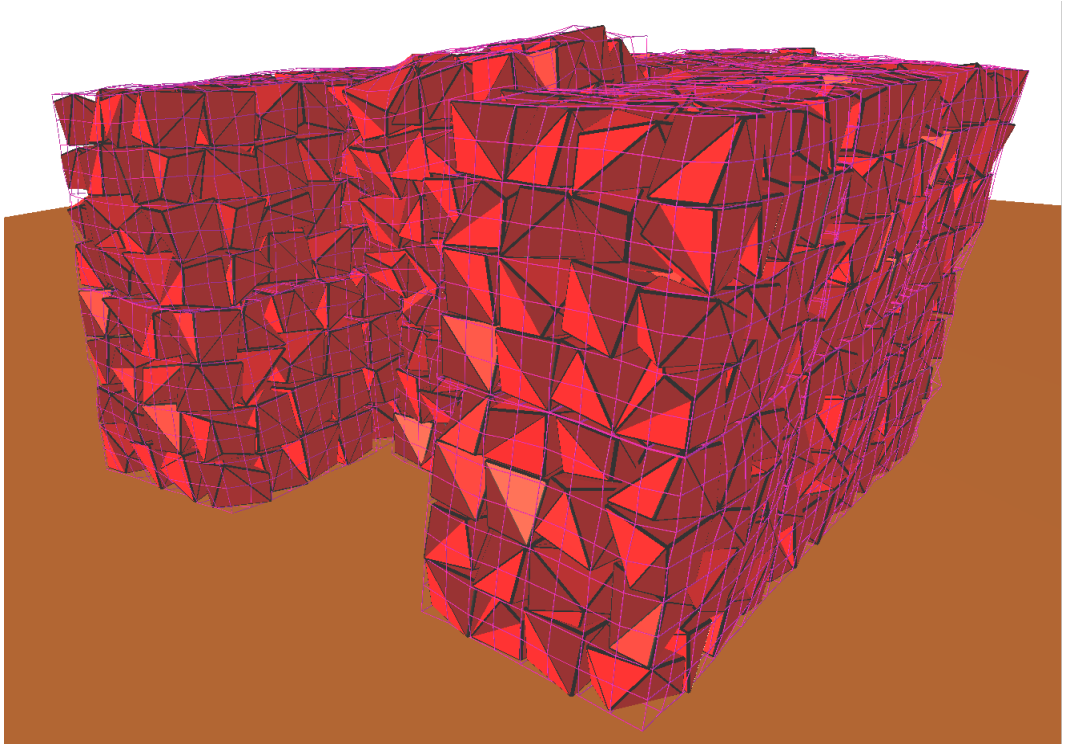

Figure 3.45: Case SBG-XVI: Boulder radius of 1.5 ft with initial velocity of 30 ft/s after 1 impact.

3.3 EFFECTS OF BOULDER GEOMETRY

In the previous section, the boulders were spherical. To explore the effects of variable geometry we now perform numerical experiments with polyhedral boulders. First, we examine the case of stand-alone gabions with hexagonal wire-geometry and then advance to larger barriers with welded wire baskets. Experiments were performed which demonstrated that the performance of welded wire is comparable to the performance of a hexagonal wire mesh. However, these results were not presented for the sake of brevity. Therefore, by observing the performance of welded wire geometry, when subjected to various boulder shapes, we then have a reasonable approximation to the hexagonal wire geometry and vice versa.

3.3.1 Effects of Boulder Geometry on Stand-Alone Gabions

The first experiment consists of a stand-alone gabion unit ($3' \times 3' \times 3'$ with hexagonal wire mesh basket) subjected to an impact by a spherical boulder of radius 1.0 ft with a density of 170 lb./ft^3, corresponding to a weight of 712.3 lb., and an initial velocity of 20 ft/s. In these experiments we are primarily interested in the wire rupture. Figure 3.46 shows that there is deformation and displacement, but no wire rupture.

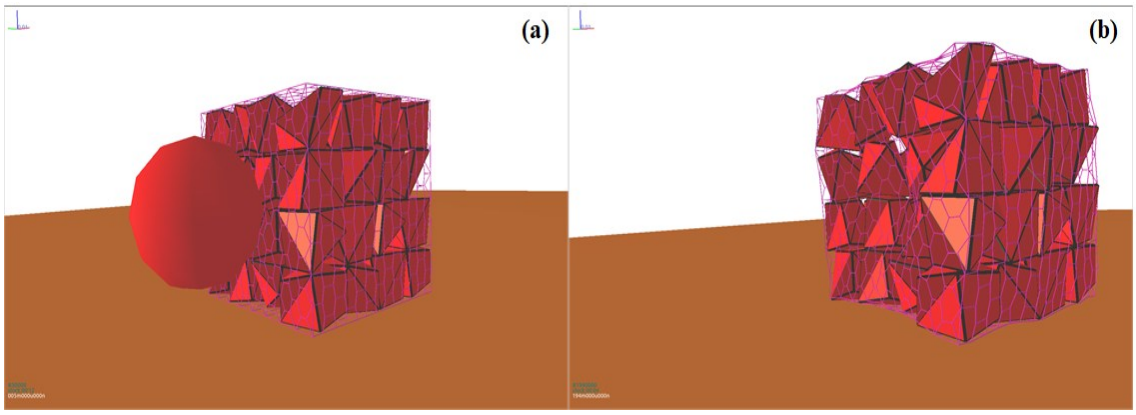

Figure 3.46: Hexagonal wire mesh impacted by spherical boulder (radius = 1.0 ft and initial velocity = 20 ft/s) (a) initial conditions; (b) after one impact.

To determine how boulder geometry may affect the damage done to the wire of the gabion, we use the "sharp" boulder option from *GabBI* in the "polyhedral boulder suite" tab. The boulder is also assigned a weight of 712.3 lb. by scaling the default size by a factor of 3.883. The initial velocity of the boulder is 20 ft/s. Results are presented in Figure 3.47 which demonstrate that severe wire rupture has occurred after the first impact. The damage is sufficient enough for the gabion unit to no longer be functional.

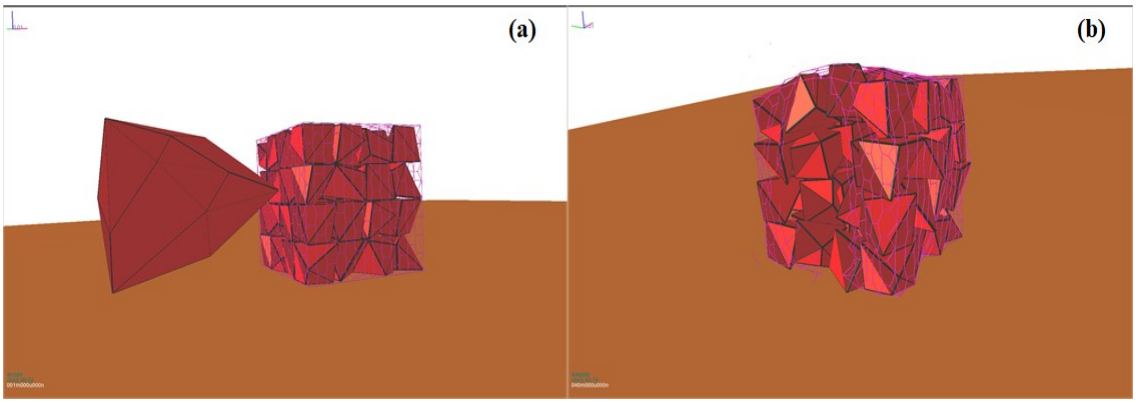

Figure 3.47: Hexagonal wire mesh impacted by sharp boulder (initial velocity = 20 ft/s) after one impact, (a) initial conditions; (b) after one impact.

The "round" boulder geometry was then used to compare wire rupture with the damage done by the spherical boulder. The "round" boulder was scaled by a factor of 2.25, yielding a weight of 710.2 lb. for a density of 170 lb./ft^3. Again, the initial velocity was set at 20 ft/s. The round boulder geometry is presented in Figure 3.48(a) and the resulting wire damage is presented in Figure 3.48(b) and (c). The fortitude of the impact led to significant wire rupture on the front face as well as wire rupture on one of the sides of the gabion unit.

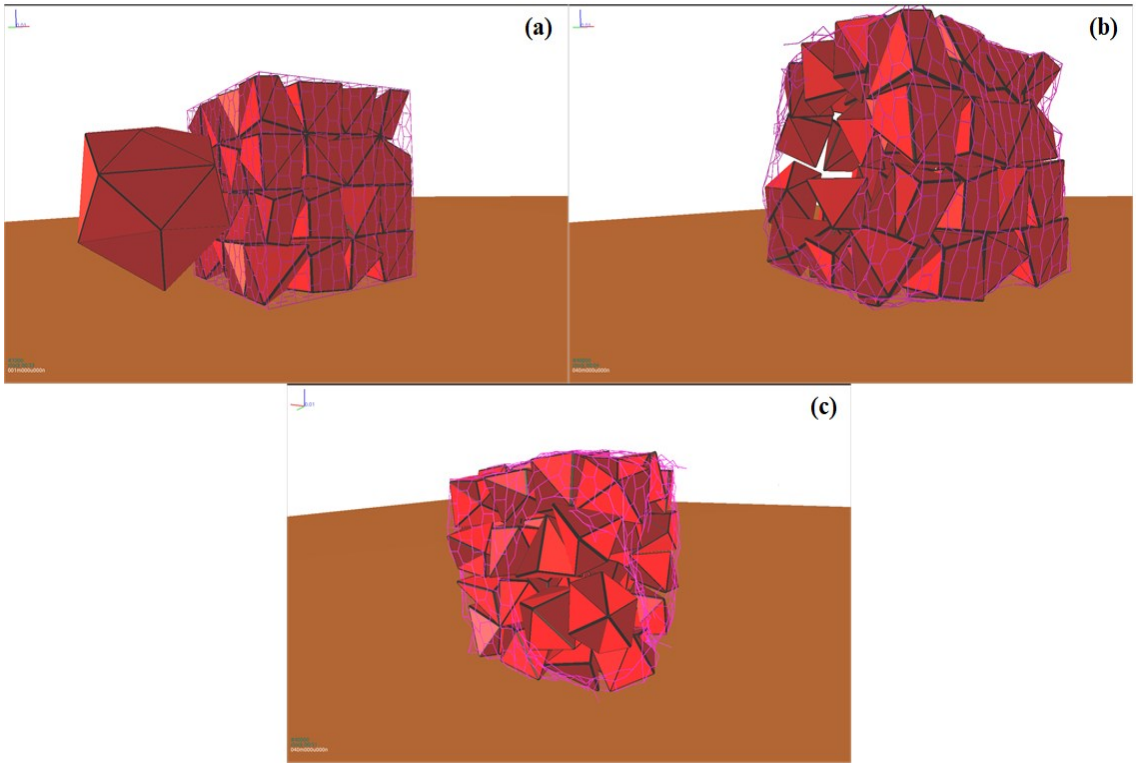

Figure 3.48: Hexagonal wire mesh impacted by round boulder (initial velocity = 20 ft/s) after one impact, (a) initial conditions; (b) after one impact (front view); (c) after one impact (side view).

These numerical experiments suggest that the sharper polyhedral geometries are capable of producing greater amounts of wire damage than the spherical boulder geometry. This can be understood in terms of (1) stresses and (2) the wedging effect of polyhedral boulders. For (1), we have forces of similar magnitude, in the spherical and polyhedral cases, but acting over smaller areas (polyhedral case), thus causing larger stresses and greater amounts of wire rupture. For (2), the polyhedral boulders can penetrate and wedge into the gabion rockfill, pushing the gravel outwards, generating more secondary damage through the expansion which occurs.

3.3.2 Effects of Boulder Geometry on Gabion Barriers

Two series of simulations were performed on gabion barriers made from three rows, three columns, and two stacks of $3' \times 3' \times 3'$ units. The first series used the sharp boulder geometry and the second consisted of an impact from the round boulder geometry. Results for the sharp boulder geometry and round boulder geometry with a velocity of 20 ft/s are presented in Figure 3.49 and Figure 3.50, respectively. Note that the boulders in both experiments weigh approximately 710 lb. The damage patterns for the larger barrier cases are similar to their stand-alone counterpart, where the rounded angular geometry causes the most wire rupture.

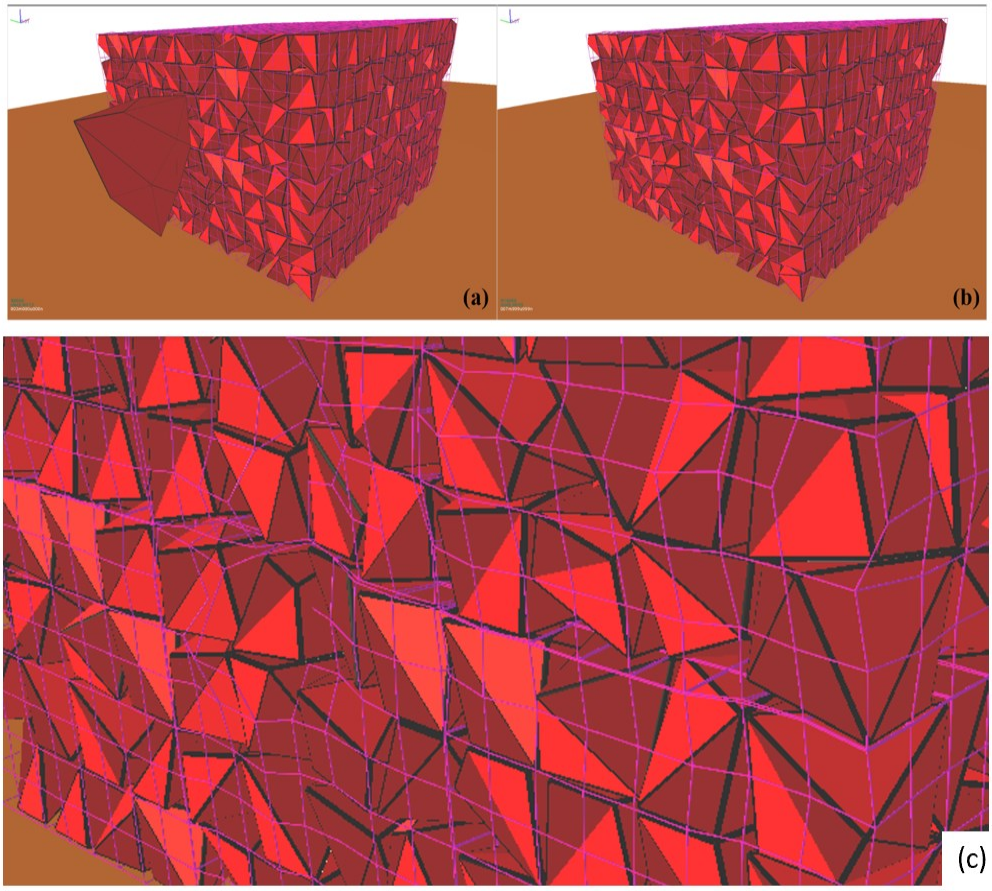

Figure 3.49: Gabion barrier impacted by sharp geometry at 20 ft/s. (a) initial conditions; (b) after one impact; (c) close-up of impacted area.

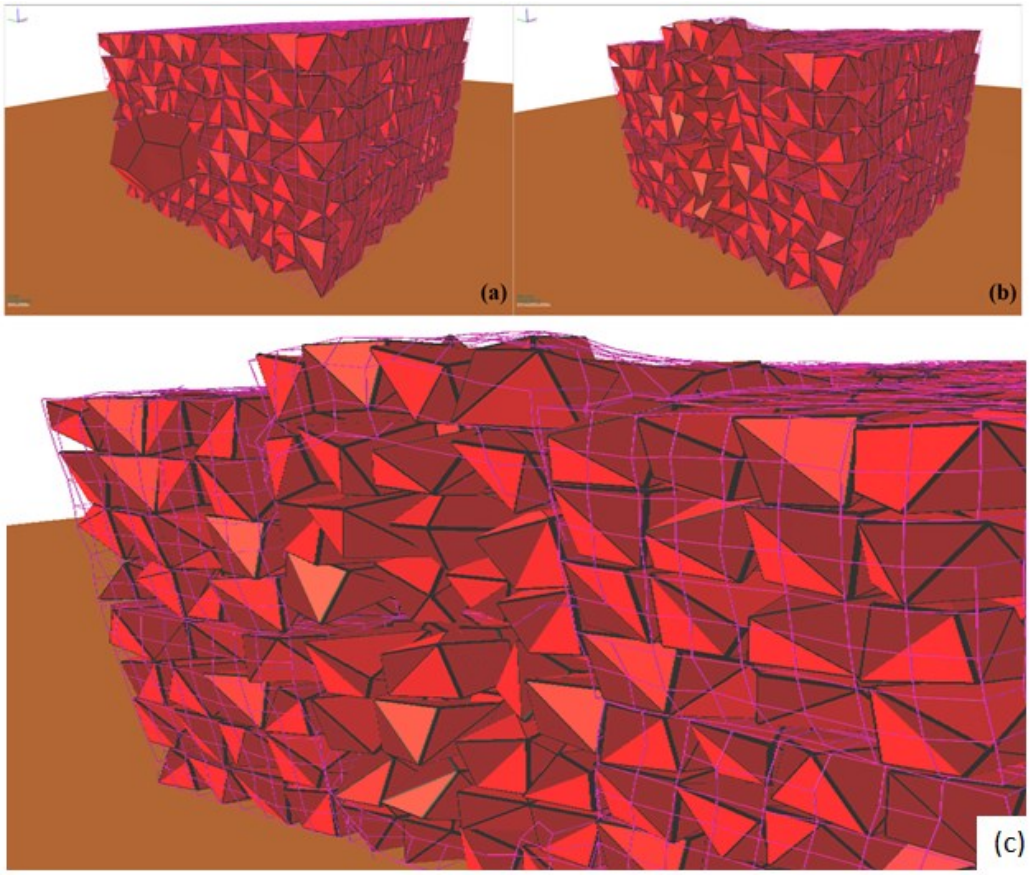

Figure 3.50: Gabion barrier impact with a close-up of the impacted area.

3.4 SIMULTANEOUS IMPACTS

So far, impacts by single boulders have been explored. Now we perform experiments in which there are multiple boulders impacting the gabion barrier almost simultaneously. We perform experiments for a spherical boulder and rounded angular boulder geometry. The weights of each of the six boulders in both experiments are approximately 710 lb. and the initial velocity is 20 ft/s. There is some moderate wire rupture in the spherical case seen in Figure 3.51. However, in the rounded angular boulder case shown in Figure 3.52, there is significant wire rupture. For the spherical boulder case, there is more observed wire rupture for the barrier case as opposed to the stand-alone gabion unit case. This is because the front gabion units now have back support which resist their motion and the boulders experience a larger change in momentum, thus creating a greater force on the face of the barrier.

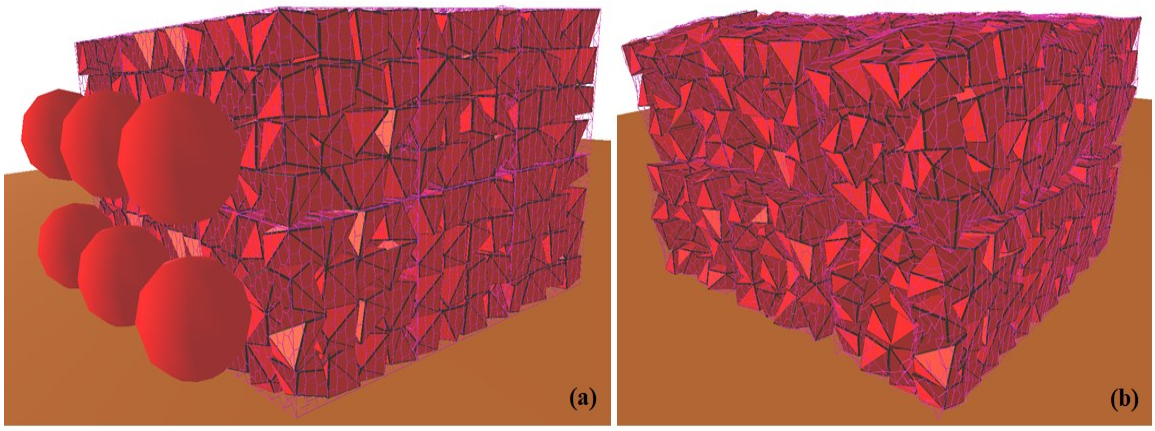

Figure 3.51: Simultaneous impact from six spherical boulders (velocity = 20 ft/s).

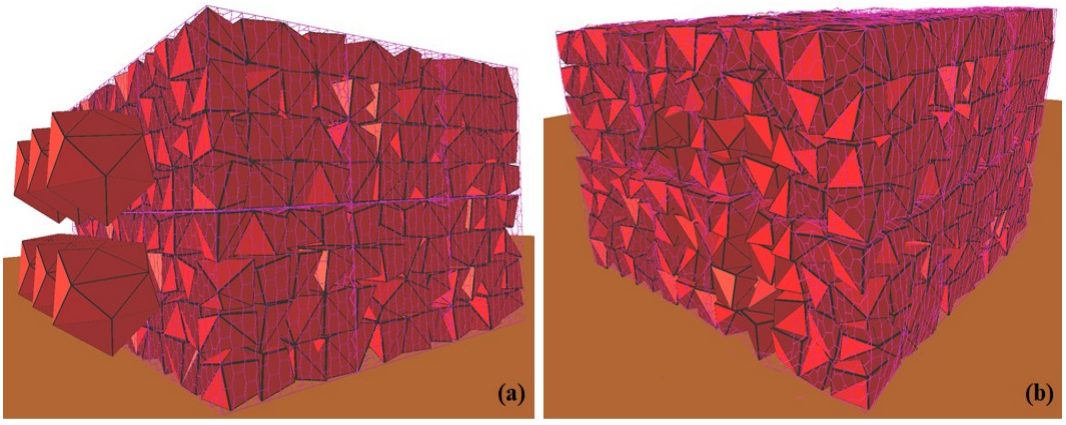

Figure 3.52: Simultaneous impact from six rounded angular boulders (velocity = 20 ft/s).

3.5 SUMMARY OF EXPERIMENTS

Our numerical experiments indicate that gabions made of the $3' \times 3' \times 3'$ units with rows = 2, columns = 3, stacks = 2, are sufficient against boulder impacts with velocities less than 30 ft/s and radii less than 0.75 ft. It is anticipated that larger gabions (in terms of width) will provide more stability due to their greater inertia and ability to resist sliding forces during impact. However, greater resistance to sliding results in larger forces on the face of the gabion barrier during impact, thus creating the potential for larger amounts of wire rupture. For a wire diameter of 0.120 in (still referring to the rows = 2, columns = 3, stacks = 2 case), there appear to be different ranges and combinations of boulder radius and initial velocity that result in different qualitative impact patterns. For radii of 0.25 ft and velocities up to 50 ft/s, and for radii of 0.50 ft and velocities up to 30 ft/s, the radius of influence is negligible (the impact of a local gabion unit does not lead to any significant movement of neighboring gabions). For boulders with radii greater than 0.50 ft and less than or equal to 0.75 ft with velocities of approximately 30 ft/s, there is a significant radius of influence of up to approximately 4.5 ft, with an associated displacement of 1.5 ft. Moderate wire rupture is also observed over this range of boulder radii and velocities. Therefore, from our numerical experiments, we conclude that a section made of the $3' \times 3' \times 3'$ units with rows = 2, columns = 3, stacks = 2, are sufficient against boulder impacts with

velocities less than 30 ft/s and radii less than 0.75 ft. For simulations involving spherical boulders with a radius of 1.5 ft and initial velocity of 30 ft/s impacting barriers (rows = 2, columns = 3, stacks = 2), components of the gabion barrier became airborne projectiles after the impact. When the number of rows was increased to three, the barrier experienced displacement, but no signs of airborne units were observed for an impact of the same momentum. Impacts for a given momentum, but polyhedral geometry, tend to generate larger amounts of wire rupture than their spherical counterparts. For gabion barriers with greater thicknesses (i.e., rows = 3), the displacement and deformation of the structure appears to be significantly reduced. However, wire rupture may increase due to the greater change in momentum of the boulder when impacting the face of one of the gabion units. Characterizations of the damage intensity and the visual descriptions are summarized in Table 3.7 and a damage classification matrix is provided in Table 3.8.

Table 3.7: Results Summary

Case	(R, C, S)	Dimensions	Boulder Radius (ft.)	Impact Velocity (ft./sec)	Number of Impacts	Deformation (ft.)	Wire Rupture (ft.)	Spilled Contents (Y/N)	Dislodgement (Y/N)
SAG-I	(1,1,1)	$3' \times 3' \times 3'$	0.25	5	12	0.17	N/A	N	N/A
SAG-II	(1,1,1)	$3' \times 3' \times 3'$	0.25	20	10	0.82	N/A	N	N/A
SAG-III	(1,1,1)	$3' \times 3' \times 3'$	0.25	50	5	1.98	0.54	N	N/A
SAG-IV	(1,1,1)	$3' \times 3' \times 3'$	0.50	5	7	0.74	N/A	N	N/A
SAG-V	(1,1,1)	$3' \times 3' \times 3'$	0.50	10	9	1.99	0.81	Y	N/A
SAG-VI	(1,1,1)	$3' \times 3' \times 3'$	0.50	20	2	1.85	0.40	N	N/A
SAG-VII	(1,1,1)	$3' \times 3' \times 3'$	0.50	50	1	3.20	0.68*	Y*	N/A
SBG-I	(1,3,1)	$3' \times 9' \times 3'$	0.25	30	10	0.72	0.54	N	N
SBG-II	(1,3,1)	$3' \times 9' \times 3'$	0.25	50	4	0.75	1.08	Y	N
SBG-III	(1,3,1)	$3' \times 9' \times 3'$	0.50	30	1	2.2	1.08	Y	Y
SBG-IV	(2,3,1)	$6' \times 9' \times 3'$	0.25	10	10	0.06	N/A	N	N
SBG-V	(2,3,1)	$6' \times 9' \times 3'$	0.25	30	4	0.1	0.81	Y	N
SBG-VI	(2,3,1)	$6' \times 9' \times 3'$	0.25	40	6	0.5	1.22	Y	N
SBG-VII	(2,3,1)	$6' \times 9' \times 3'$	0.50	40	8	2.5	0.81	Y	N
SBG-VIII	(2,3,1)	$6' \times 9' \times 3'$	0.75	10	10	1.5	0.27	N	N
SBG-IX	(2,3,2)	$6' \times 9' \times 6'$	0.25	10	10	0.09	N/A	N	N
SBG-X	(2,3,2)	$6' \times 9' \times 6'$	0.25	50	10	0.3	N/A	N	N
SBG-XI	(2,3,2)	$6' \times 9' \times 6'$	0.50	10	10	0.2	N/A	N	N
SBG-XII	(2,3,2)	$6' \times 9' \times 6'$	0.50	30	10	0.5	N/A	N	N
SBG-XIII	(2,3,2)	$6' \times 9' \times 6'$	0.75	30	9	3.5	0.54	N	Y
SBG-XIV	(2,3,2)	$6' \times 9' \times 6'$	1.0	30	4	6.6	0.41	N	Y
SBG-XV	(2,3,2)	$6' \times 9' \times 6'$	1.5	30	1	>7	0.54	N	Y
SBG-XVI	(3,3,2)	$9' \times 9' \times 6'$	1.5	30	1	3	0.54	N	Y

*0.68 is approximately 0.70 so it is assumed the gabion contents will spill out from the wire mesh.

Table 3.8: Damage Classification Matrix

Damage Intensity	Description	Examples
Negligible	Some disturbance of rockfill contents, with 1-3 inches of deformation or displacement, and no wire rupture.	SAG-I; SBG-IV; and SBG-IX
Minor	Disturbance of contents, some wire deformation and gabion displacement (3 – 10 in.), no wire rupture	SAG-II; SAG-IV; SBG-I; SBG-X; SBG-XI; and SBG-XII
Moderate	(a) Moderate Rupture: Wire rupture nearly large enough for rockfill to begin to disperse from gabion wire basket, 5 in – 12 in of total displacement; (b) Moderate Deformation: Significant deformation (12 in – 36 in) and sliding without any wire rupture.	SAG-III; SAG-V; SAG-VI; SBG-VII; and SBG-VIII
Major	(a) More than 36 in of deformation or; (b) Wire rupture large enough for rockfill to escape from wire mesh and t least 1 ft of total displacement, possible dislodgement from adjacent gabion units, or airborne units.	SAG-VII; SBG-II; SBG-III; SBG-V; SBG-XIII; SBG-XIV; and SBG-XV

4.0 METHODOLOGY FOR DETERMINING LIFE-CYCLE

4.1 LIFE-CYCLE CALCULATIONS

From the Oregon Magnitude Frequency data, we can approximate how often rockfalls of a given magnitude occur (Figure 4.1). The measure on the ordinate of the graph has units of #/day/ft^2 (i.e., number of rockfalls per day per ft^2). Therefore, we first need to anticipate our region of interest after determining the rockfall intensity (R_I) from Figure 4.1. For the sake of making a conservative calculation, we propose using the "Yellow Jacket" intensity curve given by the blue squares, which is isolated in Figure 4.2.

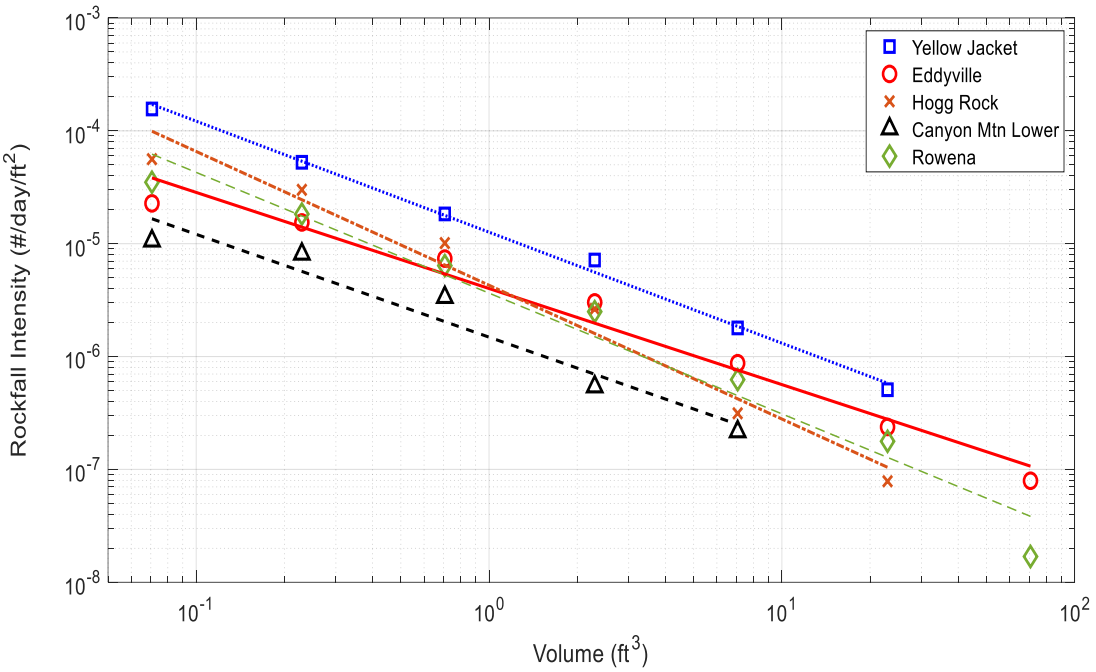

Figure 4.1: Oregon rockfall magnitude frequency chart.

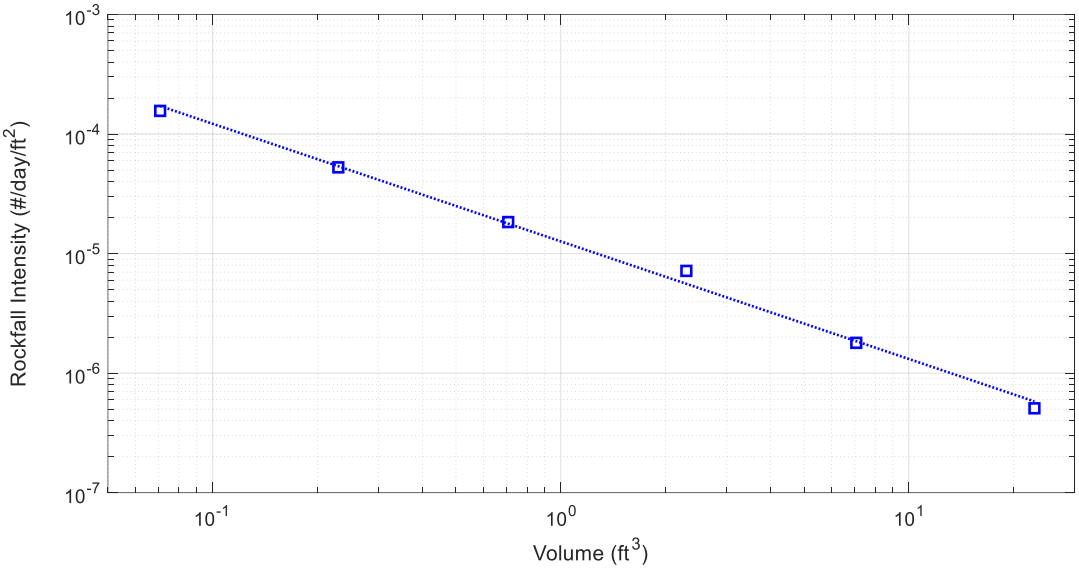

Figure 4.2: Oregon rockfall magnitude frequency chart for Yellow Jacket location.

To estimate the square footage of area where a rockfall event is anticipated, we assume that a boulder or rockfall of boulders occurs from some given vertical location H and that the initial potential energy is 100% converted to horizontal kinetic energy at impact. As a conservative estimate, we assume that the rockfall comes from the highest vertical elevation in the region we are considering. According to Figure 4.3, the area of the region of interest is given as the product of the length of the inclined slope and the length of the barrier $A_s = L_s L_b$. The relationship between the height and inclined length of the slope is given by $L_s = H/\sin\theta$. The elevation H from which the boulder originates may be estimated by equating the final kinetic energy to the initial potential energy: $H = V^2/(2g)$, where V is the impact velocity of the boulder and g is the gravitational acceleration. Therefore, the estimate for the area which may be used in the magnitude frequency charts for calculating the intensity rate is given by:

$$\boldsymbol{A_s = \frac{V^2 L_b}{2g \sin\theta}} \qquad \textbf{(4-1)}$$

for a given slope angle, θ. The dimension L_b is the length of the gabion barrier which is transverse to the anticipated boulder trajectory. Once the area is known, then a rockfall volume may be chosen, which corresponds to a rockfall intensity from Figure 4.4. Geometrical probability is used to estimate the likelihood of a rockfall event impacting a given module of the barrier. To calculate this probability, we look at the area of the back face of an individual gabion section and divide it by the entire surface area of the back of the gabion barrier as follows:

$$\boldsymbol{P = \frac{A_i}{A_T}} \qquad \textbf{(4-2)}$$

From dimensional analysis, we observe that the period T over which N impacts occur at the i^{th} section is then:

$$\boldsymbol{T = \frac{N}{(\Omega)(P)}}$$

(4-3)

In which:

$$\boldsymbol{\Omega = R_I A_s}$$

(4-4)

is the rockfall frequency rate given by multiplying the ordinate of the graph R_I in Figure 4.4 by the inclined area A_s. Note that we are assuming that the probabilistic events are independent of each other and identically distributed.

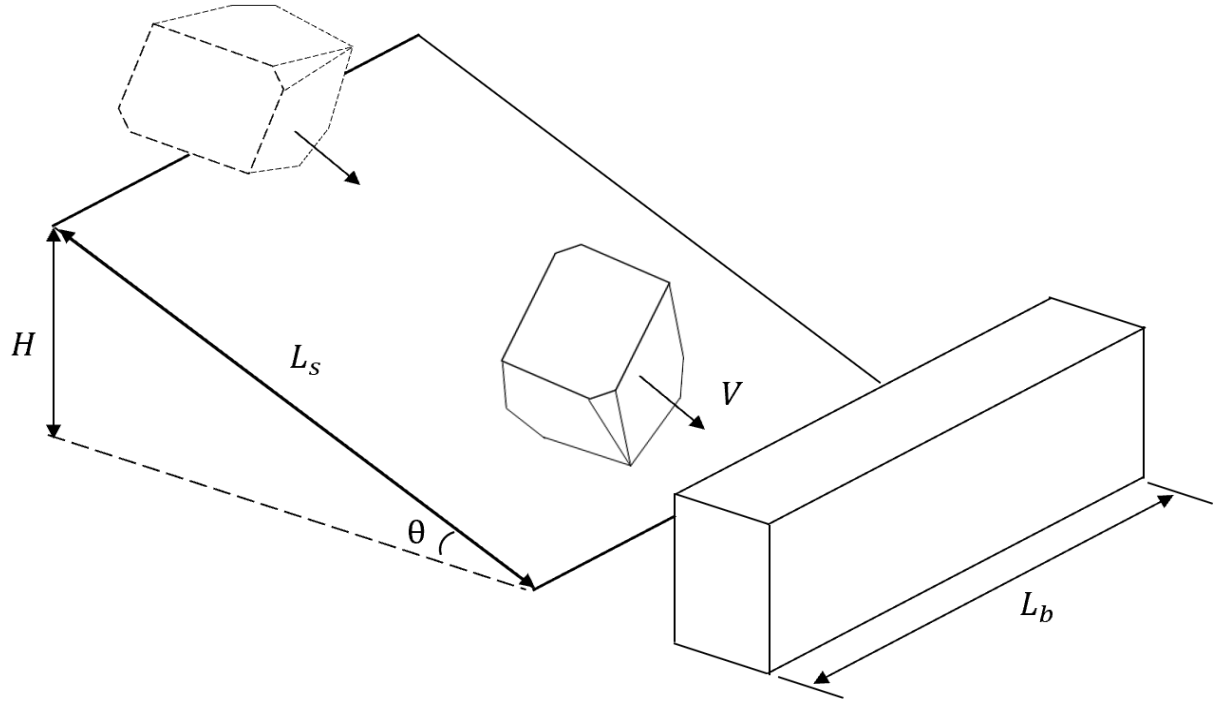

Figure 4.3: Definition sketch for calculating area in magnitude intensity estimate.

As an example, we will consider the following scenario. We want to examine boulder impacts with an expected velocity and volume of 20 ft/s and 0.1 ft^3, respectively, occurring along a barrier which is 99 ft long, by 6 ft high, made out of $3' \times 3' \times 3'$ gabion units. The slope is inclined at an angle of 37^o. Over what period of time will seven impacts strike a given gabion unit?

From our formula for the inclined area over the slope we have:

$$A_s = \frac{\left(20\frac{ft}{s}\right)^2 (99ft)}{2(32.2\ ft/s^2)\sin 37^o} = 1022ft^2$$

(4-5)

From Figure 4.4 we find the rockfall intensity $R_I = 2\text{x}10^{-4}$ #/day/ft^2 (Note: this value is the ordinate of the Magnitude Frequency chart corresponding to a volume of 0.1 ft^3). To find the rockfall frequency rate Ω we simply multiply R_I by the slope area A_s to obtain:

$$\Omega = (1022\ ft^2)(0.0002\ \#/day/ft^2) = 0.20\ \#/day$$

(4-6)

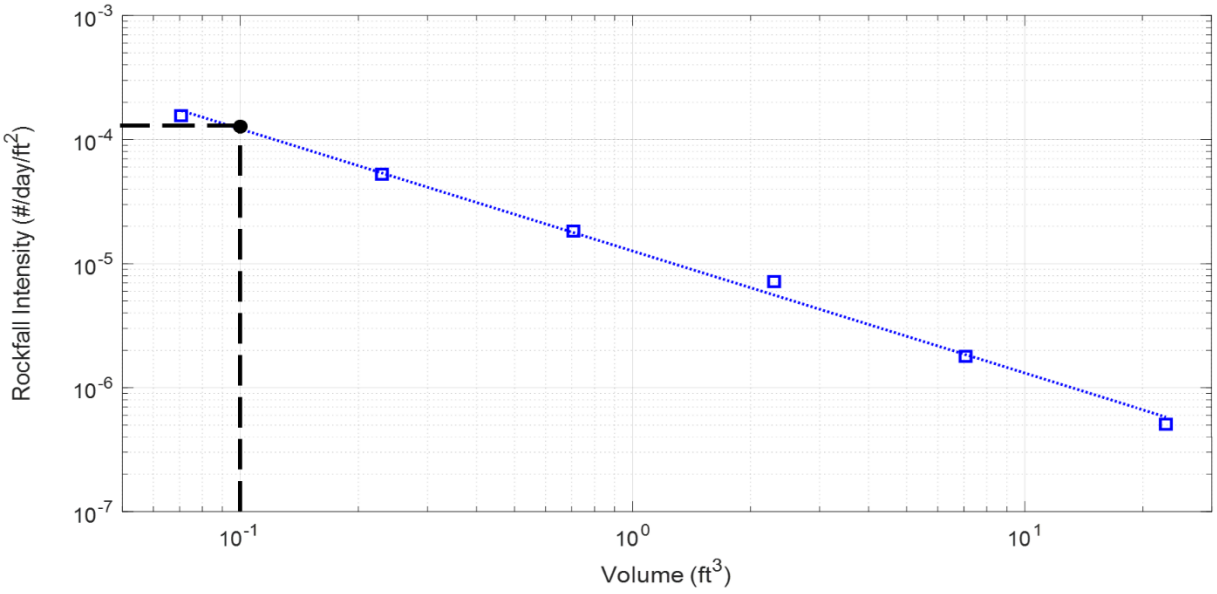

Figure 4.4: Finding intensity rate (IR) from Yellow Jacket magnitude frequency chart.

The probability of a boulder impacting an individual gabion unit is calculated as:

$$P = \frac{A_i}{A_T} = \frac{(3\ ft)(3\ ft)}{(6ft)(99ft)} = 0.015$$

(4-7)

Therefore, the period over which seven impacts will occur can be estimated as:

$$T = \frac{N}{(\Omega)(P)} = \frac{7\ \#}{(0.20\ \#/day)(0.015)} = 2333.3\ days$$

(4-8)

The above example gives an approximation for what span of time T (approximately 6.4 years) must pass before an individual gabion barrier experiences N impacts of a given volume (or boulder size). The second step in determining the life-cycle is then assessing what type of damage may be expected from an impact of a given volume and energy (boulder radius/radii and impact velocity). This is where *GabBI* can be implemented to qualitatively and quantitatively determine what kind of damage (e.g., deformation, total displacement, wire rupture, etc.) may be expected after N consecutive impacts. Engineers can refer to Table 3.8 for the damage classifications. Note that the post-impact images in Section 3 may also be used as a reference for the different damage patterns and intensities that may be observed for various impact radii and velocities. However, it is recommended that simulations in *GabBI* be performed for a given scenario. Therefore, the engineer may estimate how many impacts N are required by a boulder(s) of a given volume and velocity V before a module or section of the gabion barrier fails (or achieves some target damage). Knowing these values allows us to then estimate the period T (or life-cycle) of the gabion unit. Therefore, a proposed systematic approach for estimating the life cycle is as follows:

1. Compute the inclined area A_s from equation **Error! Reference source not found.** for an anticipated boulder velocity V, angle of inclination θ, and barrier length L_b.

2. Estimate the expected rockfall intensity R_I (number of impacts per day per square foot) for a given rockfall volume from the magnitude frequency charts (Figure 4.1 and Figure 4.2).

3. Multiply the value found from step 2) by the inclined area A_s to find the rockfall frequency rate Ω.

4. Calculate the geometric probability P for the given gabion and barrier dimensions.

5. Use *GabBI* to determine how many impacts N it takes for a given velocity $V$and rockfall volume to achieve some level of damage.

6. Use the values of rockfall frequency rate Ω, geometric probability P, and number of impacts N from steps 3), 4), and 5), respectively to calculate the life cycle T of the gabion ($T = N/(\Omega \cdot P)$).

4.2 MASS DISPLACEMENT OF GABIONS CALCULATION

In determining the life-cycle of a gabion barrier, one relevant measure of damage is the displacement. Specifically, the displacement of volume provides information on determining how much of the gabion's weight may be encroaching on a highway and how much work is necessary to mitigate the incident. Therefore, a methodology is presented to approximate the displaced weight of the gabion. This method consists of using query points in *GabBI* to determine the horizontal displacement at various nodes on the back face of the gabion configuration. The points should be evenly distributed over the back face of the gabion in the horizontal and vertical directions. By using a 2D trapezoidal quadrature over the region to which the query points belong, the approximate displaced volume can be calculated as follows:

$$\widetilde{\boldsymbol{V}} = \frac{\boldsymbol{A}\cdot\boldsymbol{B}}{\boldsymbol{4}}\left[\boldsymbol{q}_{\boldsymbol{0,0}} + \boldsymbol{q}_{\boldsymbol{0,M}} + \boldsymbol{q}_{\boldsymbol{N,0}} + \boldsymbol{q}_{\boldsymbol{N,M}}\right] + \frac{\boldsymbol{A}\cdot\boldsymbol{B}}{\boldsymbol{2}}\left[\sum_{\boldsymbol{i=1}}^{\boldsymbol{N-1}} \boldsymbol{q}_{\boldsymbol{i,0}} + \sum_{\boldsymbol{i=1}}^{\boldsymbol{N-1}} \boldsymbol{q}_{\boldsymbol{i,M}} + \sum_{\boldsymbol{j=1}}^{\boldsymbol{M-1}} \boldsymbol{q}_{\boldsymbol{0,j}} + \sum_{\boldsymbol{j=1}}^{\boldsymbol{M-1}} \boldsymbol{q}_{\boldsymbol{N,j}}\right] + \boldsymbol{A}\cdot\boldsymbol{B}\sum_{\boldsymbol{i=1}}^{\boldsymbol{N-1}}\sum_{\boldsymbol{j=1}}^{\boldsymbol{M-1}} \boldsymbol{q}_{\boldsymbol{i,j}}$$

(4-9)

where in this section, the variable $q_{i,j}$ represents the x-component of the displacement at a given query point (refer to Figure 4.5 for indexing). The parameters A and B are the horizontal and vertical wire spacings, respectively. The specific weight of the rockfill in *GabBI* is set at $\gamma = 178\ lb/ft^3$, so the displaced weight may then be calculated as:

$$\widetilde{\boldsymbol{W}} = \boldsymbol{\gamma}\widetilde{\boldsymbol{V}}$$

(4-10)

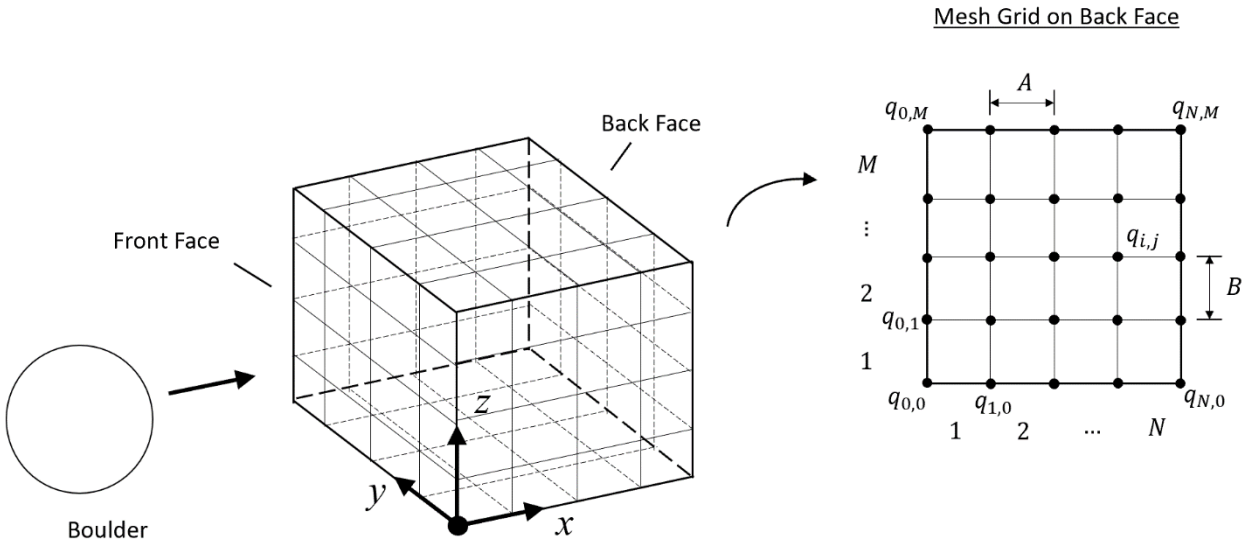

Figure 4.5: Definition sketch for calculation displaced weight and volume from query points and wire mesh spacing.

A simple criterion is developed for determining whether or not the contents (rockfill) of the gabion may exit from the wire basket after a rupture has occurred. This criterion compares the average length scale of the ruptured area $L_{avg} = (L_1 + L_2)/2$ with the average length scale of the rockfill $D_{avg} = (D_1 + D_2 + D_3)/3$, as labeled in Figure 4.6. Note that in *GabBI* $D_{avg} = 0.75\ ft$, so the critical condition at which rockfill may escape corresponds to $L_{avg} \geq 0.75\ ft$.

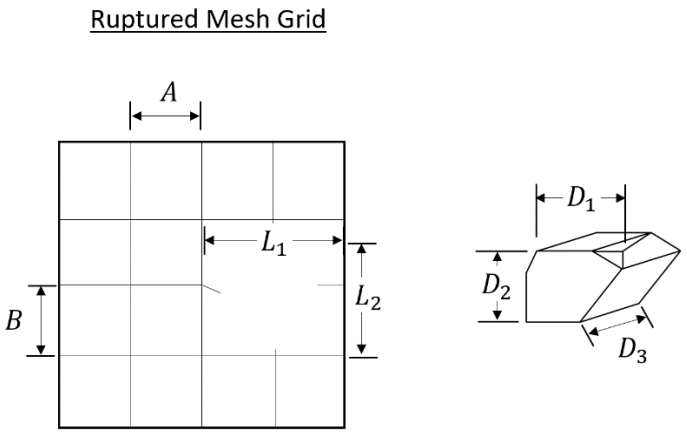

Figure 4.6: Definition sketch for measuring severity of wire rupture.

5.0 PROPOSED DESIGN PROCEDURE FOR GABION BARRIERS

The proposed design standards for gabion barriers are based on the compiled damage matrix (Table 3.8) coupled with the methodology for determining life cycle, as outlined in Section 4. Note that the guidelines developed in the following subsections are derived from combining equations (4-1) – (4-4) to yield:

$$\boldsymbol{T = \frac{2gN}{V^2 R_I} \frac{A_T \sin\theta}{A_i L_b}}$$

(5-1)

Then the period for maintenance or replacement after a number of impacts N for a given velocity V and volumes can be estimated by equation (5-1). Recall that R_I is a function of the rockfall volume, as seen in Figure 4.1. Equation (5-1) can be partitioned into two parts. The first part is the Energy Rate Factor K,

$$\boldsymbol{K = \frac{2gN}{V^2 R_I}}$$

(5-2)

which is related to the impact velocity, volume, and number of impacts. The second part is representative of the geometry of the slope and the gabion barrier, which we shall call the Geometry Factor G,

$$\boldsymbol{G = \frac{A_T \sin\theta}{A_i L_b}}$$

(5-3)

Therefore, the period may be written more concisely as:

$$\boldsymbol{T = KG}$$

(5-4)

The inherent difficulty in this approach is anticipating the impact velocity and or volume of the rockfall event. Therefore, if no other data is available about the site, it is recommended as a best practice to use more conservative values (i.e., assume that the rockfall originates from the highest vertical elevation of the slope).

5.1 FREQUENCY OF MAINTENANCE CHECKS

The following is a guide for determining how frequently maintenance checks should be made on sections of gabion barriers. Note that these maintenance checks are relevant for damage levels that can be classified as negligible to moderate (refer to Table 3.8) and it is up to the discretion of the engineer to determine which level of damage, in the range from negligible to moderate, is worthy of attention. The damage levels correspond to a gabion barrier made of three rows of three columns of three stacks of $3' \times 3' \times 3'$ gabion units. It is valid to focus on the largest barrier dimensions considered, and use this as a benchmark, because we can anticipate the performance of the largest barrier based on the smaller barriers. For example, if a stand-alone (rows = 1, columns = 1, stacks = 1) gabion unit such as SAG-I experiences negligible displacement from an impact of a certain momentum, then it is reasonable to assume that a gabion barrier of larger dimensions (i.e., SBG-XVI) will experience even less displacement.

Range I: V = (0 – 50 ft/s); $Volume$ = (0 – 0.065 ft^3)

As observed from the numerical experiments, volumes of 0.065 ft^3 or less corresponding to velocities less than or equal to 5 ft/s cause negligible damage to individual gabion units, even after twelve consecutive impacts. Therefore, the range of velocities (0 – 5 ft/s) for volumes of (0 – 0.065 ft^3) are considered as low priority for single gabion units with wire diameters of 0.085 in. For larger gabion barriers with wire diameters of 0.120 in., such as in Case SBG-X, velocities of 50 ft/s for boulder volumes of 0.065 ft^3, resulted in negligible damage.

Range II: (5 ft/s < V < 20 ft/s); (0.065 ft^3 < $Volume$ < 0.52 ft^3)

We can estimate the time it takes for minor damage to occur after 10 impacts for a velocity of 20 ft/s and a volume of 0.065 ft^3.

$$\boldsymbol{T\left(N = 10, V = 20\frac{ft}{s}, Volume = 0.065\ ft^3\right) = 167.7G} \tag{5-5}$$

Note that the coefficient of 167.7 has units of ft-days, and G has units of ft^{-1}. Therefore, the units of the maintenance period should be in days. Recall that G is the Geometry Factor which depends on the dimensions of the barrier, an individual gabion unit, and the inclination of the slope upon which the rockfall event occurs. Refer to the Case SAG-II for a visual instance of the damage which is incurred for the upper range of velocities and volumes. Note that the value of $167.7G$ should be taken as an upper limit between intervals of maintenance for a given section of the gabion barrier.

Range III: (10 ft/s < V < 50 ft/s); (0.065 ft^3 < $Volume$ < 1.77 ft^3)

In this range of velocities and volumes, moderate damage is experienced (i.e., SAG-III) after 5 impacts. A sample calculation for the upper limit of time between maintenance checks for the Case SAG-III is approximated as:

$$\boldsymbol{T\left(N=5, V=50\frac{ft}{s}, Volume=0.065\ ft^3\right)=13.4G}$$

(5-6)

To fill in the gaps, or reduce the range in velocities and volumes, it is necessary to perform more numerical experiments to predict the damage patterns and intensities for given boulder impacts.

5.2 ESTIMATE OF LIFE CYCLE

To estimate the life cycle, we perform a similar analysis to the previous section and the section involving "Methodology to determining Life Cycle". The only difference is that we use the Major Damage category to determine how many impacts are necessary at a given velocity and volume for the gabion to reach failure criteria.

5.3 RECOMMENDED GABION DESIGN

From the numerical experiments it is observed that there are different ranges of gabion dimensions for different ranges of momentum and boulder size which result in adequate stability of the structure. **Size (1)**: It is recommended that gabion barriers be made from gabion units of $3' \times 3' \times 3'$ dimensions (at least) with a thickness and depth of two layers are suitable for the following ranges / combinations of boulder velocity and volume: (a) (0 < velocity < 50 ft/s) + (0 < volume < 0.065 ft3); (b) (5 ft/s < velocity < 30 ft/s) + (0.0625 ft^3 < volume < 0.523 ft^3); (c) (0 < velocity < 10 ft/s) + (0 < volume < 1.77 ft^3); and (d) (10 ft/s < velocity < 40 ft/s) + (0.065 ft^3 < volume < 0.523 ft^3). Size (2): Larger dimensioned barriers (rows = 3, stacks = 2 made of $3' \times 3' \times 3'$ gabion units) are recommended for velocities in the range (20 ft/s < velocity < 30 fts/s) + (0.523 ft^3 < volume < 4.19 ft^3). If rockfall events of greater magnitude are anticipated, then larger dimensions are likely necessary for resistance against movement, but the amount of wire rupture primarily seems to be controlled by boulder geometry and momentum independent of whether the gabion basket is made from a welded or hexagonal wire mesh. At any rate, a one-to-one ratio of width to height of the barrier appears to provide adequate stability against overturning during impacts. A wire diameter of 0.120 in. is also recommended.

6.0 CONCLUSIONS AND RECOMMENDATIONS

The goal of the research project is to provide a physics-based multiscale numerical framework for gabion rockfall barrier design. Using state-of-the-art numerical modeling techniques, the research study presents a comprehensive investigation consisting of multi-scale model development, gabion rockfall impact analysis, life-cycle calculation, and gabion design guide. An interactive gabion design software – *GabBI* – with a user-friendly graphical user interface was developed to streamline the gabion model/design process. The numerical models for the gabion basket and in-fill rock are calibrated and validated by performing a series of benchmark simulations, including torque and collision tests. The simulation results are justified by comparing to semi-empirical solutions from the literature or experimental tests. In this study, a damage classification matrix is developed to characterize the integrity of the gabion structure after rockfall impacts. Then a semi-empirical closed-form equation for the life-cycle period is derived to estimate the number of rockfall impacts on the gabion wall.

The performance of gabion rockfall barriers with different dimensions and design considerations (e.g., wire type, rock properties) can be evaluated using *GabBI* for various impact scenarios, such as single boulder or sequential impacts. The outcomes from this research project provide essential numerical evidence to guide gabion barrier design and maintenance decisions along Oregon transportation corridors.

Conclusions based on the numerical and analytical findings, products developed, design recommendations, and additional research discussions are outlined in the following sections.

6.1 CONCLUSIONS

The research project yields a series of deliverables summarized in Table 6.1.

Table 6.1: Deliverable Table

Deliverables	Comments
GabBI	A user-friendly interactive gabion design software
User's Reference Manual	A guide on model setup and execution
PRISM model	A state-of-the-art modeling technique for non-spherical particles
Final Project Report	A document summarizing all research results
Gabion Barrier Design Guide	A general guideline for gabion barrier design procedure, data input, and interpretation of output.
Semi-empirical formula for life-cycle estimation	Combined with the Oregon rockfall magnitude frequency chart, the probability of rockfall impacts can be estimated.

From the numerical simulations, the following general observations and conclusions may be drawn in this work. The Gabion Rockfall Barrier model, along with the life-cycle evaluation, provides a comprehensive basis and numerical evidence for these conclusions.

- The PRISM model can accurately capture non-spherical particle characteristics, with the flexibility to customize the material properties to simulate heterogeneous and anisotropic characteristics.

- Under mild to medium intensity rockfall impacts, the gabion basket will deform elastically until wire fracture occurs.

- The boulder size and impact velocity are the most critical parameters that govern the degree of damage during collisions. In general, a barrier constructed of $3' \times 3' \times 3'$ units with rows = 2 columns = 3 and stacks = 2 is sufficient against boulder impacts with velocities less than 30 ft/s and radii less than 0.75 ft.

- Gabion barriers with large width are more susceptible to wire rupture during impacts due to the concentrated forces on the gabion face as a result of high resistance to sliding.

- Polyhedral boulders will generate more wire damage than spherical ones with similar physical properties (e.g., density, volume, and impact velocity) due to high stress concentration and the wedging effect.

- The effect of boulder geometry on gabion barrier performance is similar, regardless of singular or stacks of baskets.

- Under simultaneous impacts, stacked gabion baskets are more susceptible to wire rupture than single layers because the impact force is aggravated by of the back supports from adjacent barriers.

- The systematic approach for gabion barrier life-cycle estimation can be coupled with the *GabBI* software to qualitatively and quantitatively determine the impact damage.

- Query points in *GabBI* can be used to approximate the displaced weight of the gabion.

- The recommended frequency of maintenance checks can be determined based on the calculated period T value.

- The range of velocities (0 – 5 ft/s) for rock volumes of (0 – 0.065 ft^3) are considered as a low priority for single gabion units with wire diameters of 0.085 in. For larger gabion barriers with wire diameters of 0.120 in., such as in Case SBG-X, velocities of 50 ft/s for boulder volumes of 0.065 ft3, resulted in negligible damage.

- The value of $167.7G$ should be taken as an upper limit between intervals of maintenance for a given section of the gabion barrier.

- Moderate damage is expected after five impacts for 10 ft/s < V < 50 ft/s and 0.065 ft^3 < $Volume$ < 1.77 ft^3.

6.2 RECOMMENDATIONS

- *GabBI* simulations are recommended to estimate how many impacts are required by a boulder of a given volume and velocity before a module or section of the gabion barrier fails.

- To obtain a good estimation in practice for the maintenance frequency, it is recommended to use more conservative values for rockfall mass and velocity, particularly when such data are not available.

- Gabion barriers that are made from gabion units of $3' \times 3' \times 3'$ dimensions (at least) with a thickness and depth of two layers are suitable for the following ranges / combinations of boulder velocity and volume: (a) (0 < velocity < 50 ft/s) + (0 < volume < 0.065 ft^3); (b) (5 ft/s < velocity < 30 ft/s) + (0.0625 ft^3 < volume < 0.523 ft^3); (c) (0 < velocity < 10 ft/s) + (0 < volume < 1.77 ft^3); and (d) (10 ft/s < velocity < 40 ft/s) + (0.065 ft^3 < volume < 0.523 ft^3).

- Larger dimensioned barriers (rows = 3, stacks = 2 made of $3' \times 3' \times 3'$ gabion units) are recommended for velocities in the range (20 ft/s < velocity < 30 fts/s) + (0.523 ft^3 < volume < 4.19 ft^3).

- Large, dimensioned barriers (i.e., rows = 3, stacks = 2 made of $3' \times 3' \times 3'$ gabion units) are recommended for the areas with greater magnitude of rockfall events.

- A one-to-one ratio of width to height of the barrier appears to provide adequate stability against overturning during impacts.

- A wire diameter of 0.120 in. is recommended to significantly reduce wire ruptures during moderate rockfall impacts.

6.3 DISCUSSION AND FUTURE WORK

6.3.1 Discussion of Limitations

- Rock crushing is not considered in the current development of the framework. However, rock crushing dissipates more energy and alleviates collision forces under severe impacts. Ignoring this condition is more conservative for gabion barrier design.

- Momentum conservation is not always maintained during impacts when angular momentum is significant.

- The inertial properties of the polyhedral bodies are accurately calculated exactly from analytic formulas, but resulting torques during collision may carry a certain degree of error.

- When assigning dimensions and geometry for the gabion wire mesh, some rounding is required to create a consistent and uniform wire pattern that avoids particle overlaps.

- When creating polyhedral boulders, it is important to ensure that the boulder dimensions are not too small for a given edge radius.

- The intended purpose of *GabBI* is to simulate gabion barriers with dimensions ranging up to 9 – 12 ft in length, width, and height. While larger barriers may be readily simulated, the limitation is tied to the computational cost associated with domains consisting of a large number of particles.

- The current PRISM method may require a smaller time step for numerical stability due to the small mass values assigned to vertex grid nodes, grid connections, and `pfacets`. Therefore, large inertial values should be assigned to the vertices and then adjust the mass and principal moments of inertia of the centroid accordingly to avoid computational stability issues.

6.3.2 Future Work

The research project Technical Advisory Committee members jointly developed the following list of future research needs to further improve gabion rockfall barrier designs. TAC members are listed in the Acknowledgments section at the beginning of this report.

- Further work should be done with regards to calibrating the model to generate results comparable to physical experiments.

- A particle crushing model could be integrated with PRISM to capture more realistic physics during boulder impacts.

- Conduct experimental tests and compile case studies of in-service gabion barriers and use the results to fine-tune the numerical framework.

- Use field measurements of, for example, boulder rolling energy data, to perform the simulations.

- Couple the numerical simulations with field reconnaissance to develop a series of performance index, which could be used to quantify the degree of damage and urgency of repair.

7.0 REFERENCES

Cornforth Consultants Inc. (2015) *Geotechnical Design* (Report No. K19139 I-84 : MP 61. 2) (unpublished). Portland , Oregon.

Lambert, S., Heymann, A., Gotteland, P., & Nicot, F. (2014). Real-scale investigation of the kinematic response of a rockfall protection embankment. *Natural Hazards and Earth System Sciences*, *14*(5), 1269–1281. https://doi.org/10.5194/nhess-14-1269-2014

Maur, P. (2002). *Delaunay triangulation in 3D* (Doctoral dissertation). Czech Republic: University of West Bohemia in Pilsen. Retrieved from https://www.kiv.zcu.cz/site/documents/verejne/vyzkum/publikace/technicke-zpravy/2002/tr-2002-02.pdf

Ng, C. W. W., Choi, C. E., Su, A., Kwan, J. S. H., & Lam, C. L. (2016). Large-scale successive boulder impacts on a rigid barrier shielded by gabions. *Canadian Geotechnical Journal*, *53*(10), 1688–1699. https://doi.org/10.1139/cgj-2016-0073

Oregon Department of Transportation (ODOT). (2019). *Columbia River Survey Notes* (unpublished).

Peila, D., Oggeri, C., & Castiglia, C. (2007). Ground reinforced embankments for rockfall protection: design and evaluation of full scale tests. *Landslides*, *4*(3), 255–265. https://doi.org/10.1007/s10346-007-0081-4

Simac, M. R., Bathurst, R. J., & Fennessey, T. W. (1997). Case study of a hybrid gabion basket geosynthetic reinforced soil wall. *Proceedings of the Institution of Civil Engineers*, *1*(1), 9–17. https://doi.org/10.1680/gi.1997.010102

Smilauer, V., Catalano, E., Chareyre, B., Dorofeenko, S., Duriez, J., Dyck, N., … Yuan, C. (2015). *Yade documentation* (2nd ed). The Yade Project. https://doi.org/10.5281/zenodo.34073